Calcium carbonate production, growth, and spatial extent of *Lithothamnion glaciale* in a Newfoundland rhodolith bed along environmental gradients

by

Laura L. Teed

A thesis submitted to the
School of Graduate Studies
in partial fulfillment of the
requirements for the degree of
Master of Science

Department of Biology

Memorial University of Newfoundland

October, 2019

St. John's, Newfoundland, Canada

ABSTRACT

Rhodolith beds are highly diverse benthic ecosystems that are distributed worldwide and contribute significantly to global carbon budgets. Discovery of rhodolith beds in Newfoundland has stimulated research on Northwest Atlantic rhodolith (*Lithothamnion glaciale*) $CaCO_3$ production and the factors that influence rhodolith beds. The present study estimated $CaCO_3$ production rate in a rhodolith bed off the coast of St. Philip's, Conception Bay, Newfoundland using compared methodological approaches of extension and weight change. This study also examined bioturbator influence on rhodolith extension and $CaCO_3$ production rate. Applying weight change to rhodolith densities yielded gross and net $CaCO_3$ production rates of approximately 806 and 196 g $CaCO_3$ m^{-2} y^{-1}, respectively. Applying extension to rhodolith biomass yielded a net $CaCO_3$ production rate of 163 g $CaCO_3$ m^{-2} y^{-1}. Bioturbator presence did not impact extension or $CaCO_3$ production. Regarding the spatial distribution and abundance of rhodoliths, one prevalent paradigm is that rhodoliths occur in areas where water motion is strong enough to prevent burial by sediments, but not so strong as to cause fragmentation. A drop camera survey estimated rhodolith abundance in a Newfoundland bed and estimated the influence of several environmental parameters, including water motion. Rhodoliths were found to occur further south in St. Philip's than previously reported. Rhodolith abundance was highly influenced by slope, temperature, and light where abundance increased with light, temperature and decreasing slope. Flow acceleration (water motion) did not vary with depth and remained low, challenging the long-standing paradigm that water motion is a main factor determining rhodolith bed boundaries.

ACKNOWLEDGEMENTS

I thank my supervisors Dr. Patrick Gagnon and Dr. Evan Edinger for their continuous support and encouragement throughout every stage of this project, as well as the other member of my supervisory committee, Dr. Kirk Regular for his support in supplying multibeam bathymetry data and thesis comments. Special thanks to David Bélanger, Sean Hacker-Teper, Logan Zeinert, Anne Provencher St-Pierre, Samantha Trueman, and Julie Jacques for their assistance in field work planning and scientific diving. I would also like to acknowledge Emilie Novaczek, Nick Brown, and Christina Huchuk for their guidance in mapping, URSKI data analyses, and ADCP analyses, respectively. I am also grateful for the support and encouragement of my family and friends. This research was funded by the Natural Sciences and Engineering Research Council of Canada (NSERC Discovery Grants awarded to P. Gagnon and E. Edinger), the Canada Foundation for Innovation (Leaders Opportunity Fund to P. Gagnon), and the Research & Development Corporation of Newfoundland and Labrador (Ignite R&D Grant to P. Gagnon).

TABLE OF CONTENTS

LIST OF TABLES

LIST OF FIGURES

LIST OF APPENDICES

CO-AUTHORSHIP STATEMENT

The work described in the present thesis was conducted by Laura L. Teed with guidance from Patrick Gagnon, Evan Edinger, and David Bélanger. Laura L. Teed and David Bélanger were responsible for field and laboratory data collection and analysis in Chapter II (with assistance by Patrick Gagnon) and contributed to modifications brought to the original design by Patrick Gagnon and Evan Edinger. Laura L. Teed was responsible for the design, field data collection, and analysis in Chapter III, with assistance from Patrick Gagnon and Evan Edinger. Chapters were written by Laura L. Teed with intellectual and editorial input by Evan Edinger and Patrick Gagnon. Chapter II has been submitted to 'Estuarine, Coastal and Shelf Science' (ECSS) under the co-authorship of Laura L. Teed, David Bélanger, Patrick Gagnon and Evan Edinger. Article has been reproduced with permission from co-authors. Chapter III is currently being prepared to submit to 'Marine Ecology Progress Series' (MEPS) under the co-authorship of Laura L. Teed, Patrick Gagnon and Evan Edinger.

Journal references

Estuarine, Coastal and Shelf Science, 2019. Elsevier. Accessed from: https://www.journals.elsevier.com/estuarine-coastal-and-shelf-science/.

Marine Ecology Progress Series, 2019. Inter-Research Science Publisher. Accessed from: https://www.int-res.com/journals/meps/meps-home/.

CHAPTER I

GENERAL INTRODUCTION

1.1 Calcareous algae and rhodoliths

Calcareous algae contribute significant amounts of carbonate to the world's oceans, occurring globally from tropical to polar seas (Amado-Filho et al., 2012; Bracchi and Basso, 2012; Foster et al., 2013). This contribution stems from their ability to sequester carbon in their tissues (Cabioch, 1988; Gamboa et al., 2010; Milliman et al., 1971). As calcified algae develop, they form thin crusts comprised of connected cell filaments (Kerkar and Untawale, 1995; Woelkerling, 1988), in which the cell walls are entirely calcified, where calcite precipitates through the deposition of high-magnesium calcite (Mg-calcite) near the cell surface (Cabioch, 1988; Johansen, 1981). Calcareous alga includes red, green and brown algae that become hard by the addition of calcium. These algae deposit calcium carbonate into the cell walls of living tissue layers (Gamboa et al., 2010; Milliman et al., 1971).

One main group of red calcareous algae is crustose coralline algae. Coralline algae typically encrust rocky surfaces, but also occur as geniculate, and free-living, non-geniculate (i.e., lacking flexible joints) forms, producing Mg-calcite spherical or ellipsoidal nodules known as rhodoliths (Adey et al., 2013; Steneck and Adey, 1976). Rhodoliths reproduce sexually with spores or asexually by fragmentation (Freiwald, 1998). They are slow growing and long-lived, expanding via linear apical extension at rates of 0.1 to 5 mm y^{-1} (Adey et al., 2013; Amado-Filho et al., 2012; Bosence and Wilson, 2003; Jørgensbye and Halfar, 2017). Rhodoliths also contribute significantly to global carbonate production, with the largest known bed off the coast of Brazil (20 900 km^2) reportedly producing 0.025 Gt $CaCO_3$ y^{-1} (Amado-Filho et al., 2012). The purpose of the present study was to estimate calcium carbonate production and spatial variation of a subpolar rhodolith ecosystem under

the influence of several abiotic and biotic factors to gain a better understanding of rhodolith carbonate budgets and the factors that influence them.

All calcareous algae today face the ongoing challenge of climate change in which sea surface temperature is rising, frequency and intensity of storms are increasing, and the oceans are becoming more acidic (Erftemeijer et al., 2012; Harborne et al., 2017; Roth et al., 2018; Wismer et al., 2019). While marine calcifiers such as corals and rhodoliths can adapt to increases in temperature by controlling the pH of calcifying fluids (e.g. McCulloch et al., 2012), or using stored photosynthates (i.e., where growth and production are metabolically driven), there has been little research as to the extent of such adaptations (Cornwall et al., 2017; McCulloch et al., 2012; Williams et al., 2018). As well, while elevated temperatures have been shown to increase rhodolith metabolism, if temperatures exceed local summer maximums, rhodolith sensitivity can increase to the point of mortality due to reduction in calcification rates and photosynthesis (Adey et al., 2013; Schubert et al., 2019; Short et al., 2015). Furthermore, rising sea surface temperatures are not the only side-effect of climate change, possibly interacting with increasing frequency and intensity of storms. Frequent and severe storms can have detrimental effects as wave action is intensified, causing fragmentation of carbonates and sediment resuspension, possibly burying rhodolith beds and removing access to light energy (Barbera et al., 2003; Campos and Dominguez, 2010; Grall and Hall-Spencer, 2003; Sheehan et al., 2015; Villas-Bôas et al., 2014). Sediments can also be resuspended from dredging and trawling to extract economically important species such as scallops (Barbera et al., 2003; Coletti et al., 2017; Grall and Hall-Spencer, 2003). Rhodoliths themselves can be harvested commercially to be used in cosmetics, agriculture, and for their minerals (Grall and Hall-Spencer, 2003).

Continued destruction of rhodolith beds, coupled with the increasing effects of warming seas and intense, frequent storms threaten the structure and function of these biodiverse carbonate habitats.

Perhaps the largest challenge faced by rhodoliths is ocean acidification. Magnesium calcite skeletons of rhodoliths are highly soluble, and thus highly susceptible to ocean acidification (Basso and Granier, 2012; Büdenbender et al., 2011; Erftemeijer et al., 2012; Gamboa et al., 2010; McCoy and Ragazzola, 2014). Rhodoliths form high Mg-calcite skeletons, with high Mg composition that is ~20% more soluble than aragonite (Büdenbender et al., 2011). Dissolution of rhodolith beds will be accelerated in polar and sub-polar waters considering that they have a naturally low calcite saturation state due to cold temperatures (Büdenbender et al., 2011). As such, rhodoliths could begin dissolving by 2040 as the calcite saturation state rapidly declines (Doney et al., 2009; Gunderson et al., 2016). Slow growth of rhodoliths, especially those in colder seas may lead to low resilience and inability to adapt to increasing ocean acidification (Barbera et al., 2003; Büdenbender et al., 2011; Martin and Gattuso, 2009; Noisette et al., 2013). Vulnerability of rhodolith beds further solidifies the need to research processes that influence the build-up of these ecologically and economically important carbonate structures.

1.2 Cold-water carbonate production

Carbonate deposition has been researched extensively in tropical environments including coral reefs and rhodolith beds (Basso, 2012; Lees and Buller, 1972; Perez et al., 2018; Perry et al., 2008). Chave (1967) was the first to report that calcium carbonate production could also take place in temperate and polar areas, predominantly in coastal

areas where terrigenous input can be low. Carbonates occurring in cold-water seas are mostly comprised of heterozoan skeletal remains including those of calcareous algae, molluscs, echinoderms, bryozoans, and cold-water corals (Bracchi and Basso, 2012; James, 1997; James and Lukasik, 2010; Lees and Buller, 1972). Calcareous algae, coral reefs, and bryozoans form extensive and complex structures through deposition of calcium carbonate, creating a habitat that can support high species diversity (Bastos et al., 2018; Chave et al., 1972; Kerkar and Untawale, 1995; Perry et al., 2008; Schäfer et al., 2011). In particular, rhodoliths form dense inter-locking aggregations known as "beds". Rhodolith beds occur worldwide to depths exceeding 250 m, with over 1600 described species associated with such beds (Amado-Filho et al., 2012; Foster, 2001; Riosmena-Rodríguez et al., 2017; Teichert et al., 2012). Rhodoliths act as ecosystem engineers with their complex three-dimensional lattice structure from the formation of their Mg-calcite skeletons (Bracchi et al., 2014; Foster et al., 2013; Tompkins and Steller, 2016). Such a structure houses a high biodiversity of taxa including economically and ecologically important species of fish, invertebrates and other types of algae (Bracchi and Basso, 2012; Coletti et al., 2017; Gagnon et al., 2012; Grall and Hall-Spencer, 2003).

Rhodolith beds act as both a carbon sink and carbon source in the global carbon budget as living tissue layers of rhodoliths uptake CO_2 through photosynthesis by converting HCO_3^- within cells (sink), while releasing CO_2 through calcification and respiration (source) (Martin and Hall-Spencer, 2017). Underlying rhodolith tissue layers and dead rhodoliths also act as a carbon source through the dissolution of their calcified structure (Basso, 2012; Martin and Hall-Spencer, 2017). If dissolution of dead rhodoliths exceeds production of live rhodoliths, net carbonate production becomes negative, resulting

in major marine carbon fluctuations that could expedite ocean acidification (Martin and Hall-Spencer, 2017).

Rhodolith beds are major $CaCO_3$ producers, contributing significantly to the global carbon budget with a production rate per unit area approaching that of coral reefs (Harvey et al., 2017; Stearn et al., 1977). This production varies latitudinally, likely because of differences in abiotic and biotic drivers and the different methods used to estimate $CaCO_3$ production rate (Bahia et al., 2010; Harvey et al., 2017; Jørgensbye and Halfar, 2017; Van Der Heijden and Kamenos, 2015). However, calcium carbonate production of rhodolith beds should be studied more intensively especially considering that rhodoliths are more vulnerable to ocean acidification (because of their high Mg-calcite skeletons) compared to aragonitic corals and other low Mg-calcite counterparts (Martin and Gattuso, 2009; Noisette et al., 2013).

1.3 Spatial variation of rhodoliths and rhodolith beds

Sea temperature and light are the main drivers of the formation and abundance of calcareous algae, often delineating where species colonize on a global scale (Chave et al., 1972; Dutertre et al., 2015; McArthur et al., 2010; Melbourne et al., 2015). Indeed, distribution and abundance of rhodoliths is thought to be predominantly controlled by temperature and light, as well as hydrodynamic forces and sedimentation (Riosmena-Rodríguez et al., 2017; Wilson et al., 2004). Warmer temperatures often accelerate growth and thus, calcium carbonate production of calcareous algae until a threshold is reached (McCoy and Kamenos, 2015; Muñoz et al., 2018; Perez et al., 2018; Short et al., 2015). Indeed, individual rhodoliths can extend and grow up to 5 mm y^{-1} in tropical seas (Steneck

and Adey, 1976), compared to <1 mm y^{-1} in temperate and polar areas (Edyvean and Ford, 1987; Freiwald and Henrich, 1994). A similar trend is seen with light, where abundance and carbonate production often increase with light availability (Coletti et al., 2018; Connor et al., 2003; Sañé et al., 2016). However, too much light, often in coastal areas, can cause UV damage to photosynthetic tissue (Drollet et al., 1993). Rhodoliths in polar environments are tolerant to periods of low light and varying temperature conditions by using stored photosynthates and starch reserves to continuously grow and deposit calcium carbonate year-round (Weykam et al., 1997; Williams et al., 2018).

Hydrodynamic forces also exert considerable influence on the distribution and structure of shallow marine communities, including those dominated by rhodoliths (Blain and Gagnon, 2013; Gaylord, 1999; Joshi et al., 2017a; Kraufvelin et al., 2010). The shallow subtidal zone experiences disturbance of wave action, where species can become dislodged (and carried to deeper depths) or fragmented, thereby driving species zonation (Eckman et al., 2008; Joshi et al., 2017b; Miller et al., 2007). Sediments are resuspended by waves in shallow water and carried to deeper/calmer waters where they settle on the seafloor (Campos and Dominguez, 2010; Griffin et al., 2008; Villas-Bôas et al., 2014). Sedimentation can smother rhodoliths, limiting gas exchange and light availability (Riul et al., 2008; Wilson et al., 2004). These processes may determine rhodolith bed limits, with the upper bed limit driven by wave action, and the lower, deeper limit shaped by sedimentation (Dutertre et al., 2015; Foster, 2001; Steller and Foster, 1995).

Rhodolith beds in the northwest Atlantic were first discovered in the 1960s when Adey (1966) described several beds along the coast of Newfoundland and Labrador. Since then, few studies have investigated species of coralline algae and their distribution (Adey

et al., 2005; Adey and Adey, 1973; Adey and Hayek, 2011). Gagnon et al. (2012), carried out the first quantitative research about Newfoundland rhodolith bed structure and associated fauna. They studied two rhodolith beds in Conception Bay, Newfoundland off the coast of St. Philip's and Holyrood (Figure 1.1), and found that the daisy brittle star (*Ophiopholus aculeata*) and the mottled red chiton (*Tonicella marmorea*) represented 82 and 94% of total invertebrates, respectively. Green sea urchins (*Strongylocentrotus droebachiensis*) and the common sea star (*Asterias rubens*) were also commonly observed on the surface of the rhodolith beds (Gagnon et al., 2012). Millar and Gagnon (2018) continued research in the St. Philip's area (Figure 1.1), challenging the paradigm that moderate hydrodynamic forces are needed to limit sedimentation in rhodolith beds. Instead, bioturbators, in this case, *O. aculeata*, *A. rubens*, and *S. droebachiensis*, facilitated removal of sediment from the rhodolith surface (Millar and Gagnon, 2018). Invertebrate bioturbators present among rhodoliths aid in protecting against sedimentation by mixing and stirring sediments, ventilating rhodoliths and preventing burial (Marrack, 1999; Millar and Gagnon, 2018). Calcium carbonate production and rhodolith abundance in this subpolar bed, as well as the effects of bioturbators on rhodolith proliferation and abundance, are unknown, yet worth studying to gain a better understanding of subpolar rhodolith bed calcium carbonate budgets and the abiotic and biotic factors that influence them.

1.4 Thesis structure

Spatial extent and factors limiting carbonate production and abundance of Newfoundland rhodolith beds has yet to be studied quantitatively. The goal of the present

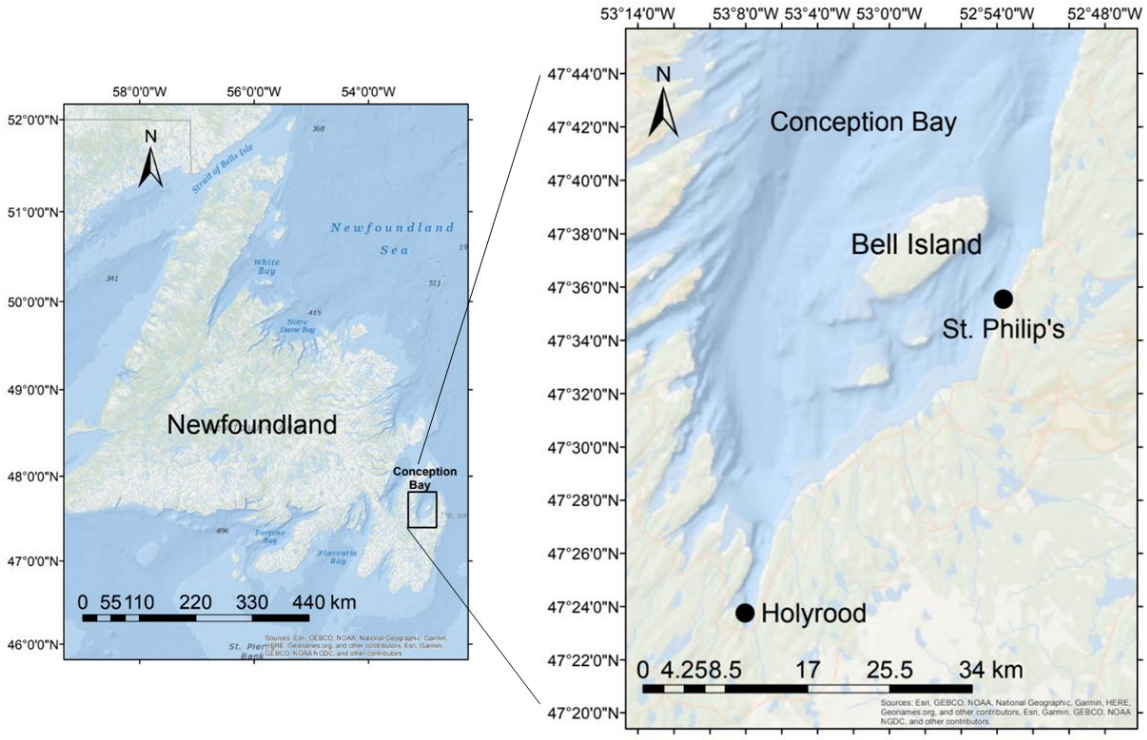

Figure 1.1 Location of the two rhodolith beds previously studied in southeastern Newfoundland. Rhodolith beds are located off the coast of St. Philip's and Holyrood (indicated by black circles) in Conception Bay, Newfoundland. Basemaps obtained from GEBCO.

study is to quantify rhodolith extension, $CaCO_3$ production, as well as explore abiotic and biotic factors driving rhodolith abundance and distribution. Chapter II includes a one-year deployment of rhodoliths in a Newfoundland bed to 1) quantify $CaCO_3$ production using varying methodologies of extension rate and weight change; and 2) assess the influence of bioturbators on rhodolith $CaCO_3$ production rate and extension. Chapter III examines the distribution and abundance of rhodoliths in the same Newfoundland bed, and some of the abiotic (temperature, illuminance, slope, bottom type, and bathymetric position) and biotic (bioturbator and encrusting coralline algae presence) factors that contribute to the observed spatial variation in abundance. Chapter IV presents a summary of the main findings and their contribution to advancing knowledge about factors that drive $CaCO_3$ production and the structure of rhodolith beds. Chapter IV also discusses future research directions in this area.

1.5 LITERATURE CITED

Adey, W.H., 1966. Distribution of saxicolous crustose corallines in the northwestern North Atlantic. J. Phycol. 2, 49–54.

Adey, W.H., Adey, P.J., 1973. Studies on the biosystematics and ecology of the epilithic crustose Corallinaceae of the British Isles. Br. Phycol. J. 8, 343–407. https://doi.org/10.1080/00071617300650381

Adey, W.H., Chamberlain, Y.M., Irvine, L.M., 2005. An SEM-based analysis of the morphology, anatomy, and reproduction of *Lithothamnion tophiforme* (esper) Unger (Corallinales, Rhodophyta), with a comparative study of associated North Atlantic Arctic/Subarctic Melobesioideae. J. Phycol. 41, 1010–1024. https://doi.org/10.1111/j.1529-8817.2005.00123.x

Adey, W.H., Halfar, J., Williams, B., 2013. The Coralline Genus *Clathromorphum* Foslie emend. Adey. Biological, Physiological, and Ecological Factors Controlling Carbonate Production in an Arctic-Subarctic Climate Archive. Washington. 49 pp.

Adey, W.H., Hayek, L.-A.C., 2011. Elucidating marine biogeography with macrophytes: Quantitative analysis of the North Atlantic supports the thermogeographic model and demonstrates a distinct subarctic region in the northwestern Atlantic. Northeast. Nat. 18, 1–128. https://doi.org/10.1656/045.018.m801

Amado-Filho, G.M., Moura, R.L., Bastos, A.C., Salgado, L.T., Sumida, P.Y., Guth, A.Z., Francini-Filho, R.B., Pereira-Filho, G.H., Abrantes, D.P., Brasileiro, P.S., Bahia, R.G., Leal, R.N., Kaufman, L., Kleypas, J.A., Farina, M., Thompson, F.L., 2012. Rhodolith beds are major $CaCO_3$ bio-factories in the tropical south West Atlantic. PLoS One 7. https://doi.org/10.1371/journal.pone.0035171

Bahia, R.G., Abrantes, D.P., Brasileiro, P.S., Pereira-Filho, G.H., Amado-Filho, G.M., 2010. Rhodolith bed structure along a depth gradient on the northern coast of Bahia state, Brazil. Brazilian J. Oceanogr. 58, 323–337.

Barbera, C., Bordehore, C., Borg, J.A., Glémarec, M., Grall, J., Hall-Spencer, J.M., de la Huz, C., Lanfranco, E., Lastra, M., Moore, P.G., Mora, J., Pita, M.E., Ramos-Espla, A.A., Rizzo, M., Sanchez-Mata, A., Seva, A., Schembri, P.J., Valle, C., 2003. Conservation and management of northeast Atlantic and Mediterranean maerl beds. Aquat. Conserv. Mar. Freshw. Ecosyst. 13, S65–S76. https://doi.org/10.1002/aqc.569

Basso, D., 2012. Carbonate production by calcareous red algae and global change. Geodiversitas 34, 13–33. https://doi.org/10.5252/g2012n1a2

Basso, D., Granier, B., 2012. Calcareous algae in changing environments. Geodiversitas 34, 5–11. https://doi.org/10.5252/g2012n1a1

Bastos, A.C., Moura, R.L., Moraes, F.C., Vieira, L.S., Carlos Braga, J., Ramalho, L. V, Amado-Filho, G.M., Magdalena, U.R., Webster, J.M., 2018. Bryozoans are Major Modern Builders of South Atlantic Oddly Shaped Reefs. Sci. Rep. 8, 9638. https://doi.org/10.1038/s41598-018-27961-6

Blain, C., Gagnon, P., 2013. Interactions between thermal and wave environments mediate intracellular acidity (H_2SO_4), growth, and mortality in the annual brown seaweed *Desmarestia viridis*. J. Exp. Mar. Bio. Ecol. 440, 176–184. https://doi.org/10.1016/j.jembe.2012.12.013

Bosence, D., Wilson, J., 2003. Maerl growth, carbonate production rates and accumulation rates in the northeast Atlantic. Aquat. Conserv. Mar. Freshw. Ecosyst. 13, S21–S31. https://doi.org/10.1002/aqc.565

Bracchi, V.A., Basso, D., 2012. The contribution of calcareous algae to the biogenic carbonates of the continental shelf: Pontian Islands, Tyrrhenian Sea, Italy. Geodiversitas 34, 61–76. https://doi.org/10.5252/g2012n1a4

Bracchi, V.A., Nalin, R., Basso, D., 2014. Paleoecology and dynamics of coralline dominated facies during a Pleistocene transgressive-regressive cycle (Capo Colonna marine terrace, Southern Italy). Palaeogeogr. Palaeoclimatol. Palaeoecol. 414, 296–309. https://doi.org/10.1016/j.palaeo.2014.09.016

Büdenbender, J., Riebesell, U., Form, A., 2011. Calcification of the Arctic coralline red algae *Lithothamnion glaciale* in response to elevated CO_2. Mar. Ecol. Prog. Ser. 441, 79–87. https://doi.org/10.3354/meps09405

Cabioch, J., 1988. Morphogenesis and generic concepts in coralline algae — a reappraisal. Helg. Meer. 42, 493–509. https://doi.org/10.1007/BF02365623

Campos, R.H.S., Dominguez, J.M.L., 2010. Mobility of sediments due to wave action on the continental shelf of the Northern coast of the state of Bahia. Brazilian J. Oceanogr. 58, 57–63. https://doi.org/10.1590/S1679-87592010000600007

Chave, K.E., 1967. Recent carbonate sediments – An unconventional view. J. Geol. Education 15(5), 200-204.

Chave, K.E., Smith, S. V, Roy, K.J., 1972. Carbonate production by coral reefs. Mar. Geol. 12, 123–140.

Coletti, G., Basso, D., Corselli, C., 2018. Coralline algae as depth indicators in the Sommières Basin (early Miocene, Southern France). Geobios 51, 15–30. https://doi.org/10.1016/j.geobios.2017.12.002

Coletti, G., Basso, D., Frixa, A., 2017. Economic Importance of Coralline Carbonates, in: Riosmena-Rodriguez, R., Aguirre, J., Nelson, W. (Eds.), Rhodolith/Maerl Beds: A Global Perspective. Springer Nature, Florida, pp. 87–101. https://doi.org/10.1007/978-3-319-29315-8_4

Connor, D., Allen, J., Golding, N., Lieberknecht, L., Northen, K., Reker, J., 2003. The national marine habitat classification for Britain and Ireland. Joint Nature and Conservation Committee. Peterborough. 42 pp.

Cornwall, C.E., Comeau, S., McCulloch, M.T., 2017. Coralline algae elevate pH at the site of calcification under ocean acidification. Glob. Chang. Biol. 23. https://doi.org/10.1111/gcb.13673

Doney, S.C., Fabry, V.J., Feely, R.A., Kleypas, J.A., 2009. Ocean acidification: The other CO_2 problem. Ann. Rev. Mar. Sci. 1, 169–192. https://doi.org/10.1146/annurev.marine.010908.163834

Drollet, J.H., Glaziou, P., Martin, P.M.V., 1993. A study of mucus from the solitary coral *Fungia fungites* (Scleractinia: Fungiidae) in relation to photobiological UV adaptation. Mar. Biol. 115, 263–266. https://doi.org/10.1007/BF00346343

Dutertre, M., Grall, J., Ehrhold, A., Hamon, D., 2015. Environmental factors affecting maerl bed structure in Brittany (France). Eur. J. Phycol. 50, 371–383. https://doi.org/10.1080/09670262.2015.1063698

Eckman, J.E., Andres, M.S., Marinelli, R.L., Bowlin, E., Reid, R.P., Aspden, R.J., Paterson, D.M., 2008. Wave and sediment dynamics along a shallow subtidal sandy beach inhabited by modern stromatolites. Geobiology 6, 21–32. https://doi.org/10.1111/j.1472-4669.2007.00133.x

Edyvean, R.G.J., Ford, H., 1987. Growth Rates of *Lithophyllum incrustans* (Corallinales, Rhodophyta) from South West Wales. Br. Phycol. J. 22, 139–146.

Erftemeijer, P.L.A., Riegl, B., Hoeksema, B.W., Todd, P.A., 2012. Environmental impacts of dredging and other sediment disturbances on corals: A review. Mar. Pollut. Bull. 64, 1737–1765. https://doi.org/10.1016/j.marpolbul.2012.05.008

Foster, M.S., 2001. Rhodoliths: Between rocks and soft places. J. Phycol. 37, 659–667. https://doi.org/10.1046/j.1529-8817.2001.00195.x

Foster, M.S., Filho, G.M.A., Kamenos, N.A., Riosmena-Rodríguez, R., Steller, D.L., 2013. Rhodoliths and Rhodolith Beds. Smithson. Contrib. Mar. Sci. 39, 143–155.

Freiwald, A., 1998. Microbial maceration and carbonate dissolution on cold-temperate shelves. Hist. Biol. 13, 27–35. https://doi.org/10.1080/08912969809386570

Freiwald, A., Henrich, R., 1994. Reefal coralline algal build-ups within the Arctic Circle: morphology and sedimentary dynamics under extreme environmental seasonality. Sedimentology 41, 963–984. https://doi.org/10.1111/j.1365-3091.1994.tb01435.x

Gagnon, P., Matheson, K., Stapleton, M., 2012. Variation in rhodolith morphology and biogenic potential of newly discovered rhodolith beds in Newfoundland and Labrador (Canada). Bot. Mar. 55, 85–99. https://doi.org/10.1515/bot-2011-0064

Gamboa, G., Halfar, J., Hetzinger, S., Adey, W., Zack, T., Kunz, B., Jacob, D.E., 2010. Mg/Ca ratios in coralline algae record northwest Atlantic temperature variations and North Atlantic Oscillation relationships. J. Geophys. Res 115, 12044. https://doi.org/10.1029/2010JC006262

Gaylord, B., 1999. Detailing agents of physical disturbance: wave-induced velocities and accelerations on a rocky shore. J. Exp. Mar. Bio. Ecol. 239, 85–124. https://doi.org/10.1016/S0022-0981(99)00031-3

Grall, J., Hall-Spencer, J.M., 2003. Problems facing maerl conservation in Brittany. Aquat. Conserv. Mar. Freshw. Ecosyst. 13, S55–S64.

https://doi.org/10.1002/aqc.568

Griffin, J.D., Hemer, M.A., Jones, B.G., 2008. Mobility of sediment grain size distributions on a wave dominated continental shelf, southeastern Australia. Mar. Geol. 252, 13–23. https://doi.org/10.1016/J.MARGEO.2008.03.005

Gunderson, A.R., Armstrong, E.J., Stillman, J.H., 2016. Multiple Stressors in a Changing World: The Need for an Improved Perspective on Physiological Responses to the Dynamic Marine Environment. Ann. Rev. Mar. Sci. 8, 357–378. https://doi.org/10.1146/annurev-marine-122414-033953

Harborne, A.R., Rogers, A., Bozec, Y.-M., Mumby, P.J., 2017. Multiple Stressors and the Functioning of Coral Reefs. Ann. Rev. Mar. Sci. 9, 445–468. https://doi.org/10.1146/annurev-marine-010816-060551

Harvey, A.S., Harvey, R.M., Merton, E., 2017. The distribution, significance and vulnerability of Australian rhodolith beds: A review. Mar. Freshw. Res. 68, 411–428. https://doi.org/10.1071/MF15434

James, N.P., 1997. The cold-water carbonate depositional realm, in: James, N.P., Clarke, J.A.D. (Eds.), Cool-Water Carbonates. SEPM Special Publication, pp. 1–20. https://doi.org/10.2110/pec.97.56.0001

James, N.P., Lukasik, J., 2010. Cool- and cold-water neritic carbonates, in: James, N.P., Dalrymple, R.W. (Eds.), Facies Model 4. Geological Association of Canada, St. John's, pp. 371–399.

Johansen, H.W., 1981. Coralline algae, a first synthesis. CRC Press, Boca Raton.

Jørgensbye, H.I.Ø., Halfar, J., 2017. Overview of coralline red algal crusts and rhodolith beds (Corallinales, Rhodophyta) and their possible ecological importance in Greenland. Polar Biol. https://doi.org/10.1007/s00300-016-1975-1

Joshi, S., Duffy, G.P., Brown, C., 2017a. Mobility of maerl-siliciclastic mixtures: Impact of waves, currents and storm events. Estuar. Coast. Shelf Sci. 189, 173–188. https://doi.org/10.1016/j.ecss.2017.03.018

Joshi, S., Duffy, G.P., Brown, C., 2017b. Critical bed shear stress and threshold of motion of maerl biogenic gravel. Estuar. Coast. Shelf Sci. 194, 128–142. https://doi.org/10.1016/j.ecss.2017.06.010

Kerkar, V., Untawale, A.G., 1995. Studies on structure and organization of calcium carbonate deposits in algae. Curr. Sci. 68, 843–845.

Kraufvelin, P., Lindholm, A., Pedersen, M.F., Kirkerud, L.A., Bonsdorff, E., 2010. Biomass, diversity and production of rocky shore macroalgae at two nutrient enrichment and wave action levels. Mar. Biol. 157, 29–47. https://doi.org/10.1007/s00227-009-1293-z

Lees, A., Buller, A.T., 1972. Modern temperate-water and warm-water shelf carbonate sediments contrasted. Mar. Geol. 13, M67–M73. https://doi.org/10.1016/0025-3227(72)90011-4

Marrack, E.C., 1999. The relationship between water motion and living rhodolith beds in the southwestern Gulf of California, Mexico. Palaios 14, 159. https://doi.org/10.2307/3515371

Martin, S., Gattuso, J.P., 2009. Response of Mediterranean coralline algae to ocean acidification and elevated temperature. Glob. Chang. Biol. 15, 2089–2100. https://doi.org/10.1111/j.1365-2486.2009.01874.x

Martin, S., Hall-Spencer, J., 2017. Effects of ocean warming and ocean acidification on rhodolith/maerl beds. In: Rhodolith/ Maërl Beds: A Global Perspective, 1st ed. Springer Nature, Florida. 55-95.

McArthur, M.A., Brooke, B.P., Przeslawski, R., Ryan, D.A., Lucieer, V.L., Nichol, S., McCallum, A.W., Mellin, C., Cresswell, I.D., Radke, L.C., 2010. On the use of abiotic surrogates to describe marine benthic biodiversity. Estuar. Coast. Shelf Sci. https://doi.org/10.1016/j.ecss.2010.03.003

McCoy, S.J., Kamenos, N.A., 2015. Coralline algae (Rhodophyta) in a changing world: integrating ecological, physiological, and geochemical responses to global change. J. Phycol. 51, 6–24. https://doi.org/10.1111/jpy.12262

McCoy, S.J., Ragazzola, F., 2014. Skeletal trade-offs in coralline algae in response to ocean acidification. Nat. Clim. Chang. 4, 719–723. https://doi.org/10.1038/NCLIMATE2273

McCulloch, M., Falter, J., Trotter, J., Montagna, P., 2012. Coral resilience to ocean acidification and global warming through pH up-regulation. Nat. Clim. Chang. 2, 623–627. https://doi.org/10.1038/NCLIMATE1473

Melbourne, L.A., Griffin, J., Schmidt, D.N., Rayfield, E.J., 2015. Potential and limitations of finite element modelling in assessing structural integrity of coralline algae under future global change. Biogeosciences 12, 5871–5883. https://doi.org/10.5194/bg-12-5871-2015

Millar, K.R., Gagnon, P., 2018. Mechanisms of stability of rhodolith beds: sedimentological aspects. Mar. Ecol. Prog. Ser. 594, 65–83. https://doi.org/10.3354/meps12501

Miller, L.P., O'Donnell, M.J., Mach, K.J., 2007. Dislodged but not dead: survivorship of a high intertidal snail following wave dislodgement [WWW Document]. J. Mar. Biol. Assoc. United Kingdom.

Milliman, J.D., Gastner, M., Muller, J., 1971. Utilization of magnesium in coralline algae. Geol. Soc. Am. Bull. 82, 573–580.

Muñoz, P.T., Sáez, C.A., Martínez-Callejas, M.B., Flores-Molina, M.R., Bastos, E., Fonseca, A., Gurgel, C.F.D., Barufi, J.B., Rörig, L., Hall-Spencer, J.M., Horta, P.A., 2018. Short-term interactive effects of increased temperatures and acidification on the calcifying macroalgae *Lithothamnion crispatum* and *Sonderophycus capensis*. Aquat. Bot. 148, 46–52. https://doi.org/10.1016/j.aquabot.2018.04.008

Noisette, F., Duong, G., Six, C., Davoult, D., Martin, S., 2013. Effects of elevated pCO_2 on the metabolism of a temperate rhodolith *Lithothamnion corallioides* grown under different temperatures. J. Phycol. https://doi.org/10.1111/jpy.12085

Perez, D.I., Phinn, S.R., Roelfsema, C.M., Shaw, E., Johnston, L., Iguel, J., 2018. Primary production and calcification rates of algae-dominated reef flat and seagrass communities. J. Geophys. Res. Biogeosciences 123, 2362–2375. https://doi.org/10.1029/2017JG004241

Perry, C.T., Spencer, T., Kench, P.S., 2008. Carbonate budgets and reef production states: a geomorphic perspective on the ecological phase-shift concept. Coral Reefs 27, 853–866. https://doi.org/10.1007/s00338-008-0418-z

Riosmena-Rodríguez, R., Nelson, W., Aguirre, J., 2017. Rhodolith/ Maërl Beds: A Global Perspective, 1st ed. Springer Nature, Florida.

Riul, P., Targino, C.H., Farias, J.D.N., Visscher, P.T., Horta, P.A., 2008. Decrease in *Lithothamnion* sp. (Rhodophyta) primary production due to the deposition of a thin sediment layer. J. Mar. Biol. Assoc. UK 88, 17–19. https://doi.org/10.1017/S0025315408000258

Roth, F., Saalmann, F., Thomson, T., Coker, D.J., Villalobos, R., Jones, B.H., Wild, C., Carvalho, S., 2018. Coral reef degradation affects the potential for reef recovery after disturbance. Mar. Environ. Res. 142, 48–58. https://doi.org/10.1016/j.marenvres.2018.09.022

Sañé, E., Chiocci, F.L., Basso, D., Martorelli, E., 2016. Environmental factors controlling the distribution of rhodoliths: An integrated study based on seafloor sampling, ROV and side scan sonar data, offshore the W-Pontine Archipelago. Cont. Shelf Res. 129, 10–22. https://doi.org/10.1016/j.csr.2016.09.003

Schäfer, P., Fortunato, H., Bader, B., Liebetrau, V., Bauch, T., Reijmer, J.J.G., 2011. Growth rates and carbonate production by coralline red algae in upwelling and non-upwelling settings along the Pacific coast of Panama. PALAIOS 268, 420–432.

Schubert, N., Salazar, V.W., Rich, W.A., Vivanco Bercovich, M., Almeida Saá, A.C., Fadigas, S.D., Silva, J., Horta, P.A., 2019. Rhodolith primary and carbonate production in a changing ocean: The interplay of warming and nutrients. Sci. Total Environ. 676, 455–468. https://doi.org/10.1016/j.scitotenv.2019.04.280

Sheehan, E.V., Bridger, D., Cousens, S., Attrill, M., 2015. Testing the resilience of dead maerl infaunal assemblages to the experimental removal and re-lay of habitat. Mar. Ecol. Prog. Ser. 535, 117–128. https://doi.org/10.3354/meps11400

Short, J., Foster, T., Falter, J., Kendrick, G.A., McCulloch, M.T., 2015. Crustose coralline algal growth, calcification and mortality following a marine heatwave in Western Australia. Cont. Shelf Res. 106. https://doi.org/10.1016/j.csr.2015.07.003

Stearn, C.W., Scoffin, T.P., Martindale, W., 1977. Calcium Carbonate Budget of a Fringing Reef on the West Coast of Barbados Part I—Zonation and Productivity. Bull. Mar. Sci. 27, 479–510.

Steller, D.L., Foster, M.S., 1995. Environmental factors influencing distribution and morphology of rhodoliths in Bahia Concepcion B.C.S., Mexico. J. Exp. Mar. Bio. Ecol. 194, 201–212.

Steneck, R.S., Adey, W.H., 1976. The Role of Environment in Control of Morphology in *Lithophyllum congestum*, a Caribbean Algal Ridge Builder. Bot. Mar. 19, 197–216. https://doi.org/10.1515/botm.1976.19.4.197

Teichert, S., Woelkerling, W., Rüggeberg, A., Wisshak, M., Piepenburg, D., Meyerhöfer, M., Form, A., Büdenbender, J., Freiwald, A., 2012. Rhodolith beds (Corallinales, Rhodophyta) and their physical and biological environment at 80°31′N in Nordkappbukta (Nordaustlandet, Svalbard Archipelago, Norway). Phycologia 51, 371–390. https://doi.org/10.2216/11-76.1

Tompkins, P.A., Steller, D.L., 2016. Living carbonate habitats in temperate California (USA) waters: distribution, growth, and disturbance of Santa Catalina Island rhodoliths. Mar. Ecol. Prog. Ser. 560, 135–145. https://doi.org/10.3354/meps11919

Van Der Heijden, L.H., Kamenos, N.A., 2015. Reviews and syntheses: Calculating the global contribution of coralline algae to total carbon burial. Biogeosciences 12, 6429–6441. https://doi.org/10.5194/bg-12-6429-2015

Villas-Bôas, A.B., Tâmega, F.T.D.S., Andrade, M., Coutinho, R., Figueiredo, M.A.D.O., 2014. Experimental Effects of Sediment Burial and Light Attenuation on Two Coralline Algae of a Deep Water Rhodolith Bed in Rio de Janeiro, Brazil. Cryptogam. Algol. 35, 67–76. https://doi.org/10.7872/crya.v35.iss1.2014.67

Weykam, G., Thomas, D.N., Wiencke, C., 1997. Growth and photosynthesis of the Antarctic red algae *Palmaria decipiens* (Palmariales) and *Iridaea cordata* (Gigartinales) during and following extended periods of darkness. Phycologia 36, 395–405. https://doi.org/10.2216/i0031-8884-36-5-395.1

Williams, S., Adey, W., Halfar, J., Kronz, A., Gagnon, P., Bélanger, D., Nash, M., 2018. Effects of light and temperature on Mg uptake, growth, and calcification in the proxy climate archive *Clathromorphum compactum*. Biogeosciences 15, 5745–5759. https://doi.org/10.5194/bg-15-5745-2018

Wilson, S., Blake, C., Berges, J.A., Maggs, C.A., 2004. Environmental tolerances of free-living coralline algae (maerl): implications for European marine conservation. Biol. Conserv. 120, 279–289. https://doi.org/10.1016/J.BIOCON.2004.03.001

Wismer, S., Tebbett, S.B., Streit, R.P., Bellwood, D.R., 2019. Spatial mismatch in fish and coral loss following 2016 mass coral bleaching. Sci. Total Environ. 650, 1487–1498. https://doi.org/10.1016/J.SCITOTENV.2018.09.114

Woelkerling, W.J., 1988. The coralline red algae : an analysis of the genera and subfamilies of nongeniculate Corallinaceae. British Museum (Natural History), London; Oxford; New York.

CHAPTER II

CALCIUM CARBONATE ($CaCO_3$) PRODUCTION OF A SUBPOLAR RHODOLITH BED: EFFECTS OF BIOTURBATORS, METHODS OF ESTIMATE, AND GLOBAL COMPARISONS

ABSTRACT

Present estimates suggest that rhodolith beds are major $CaCO_3$ producers, with production rates similar to those of coral reefs. Production rates vary latitudinally because of differences in abiotic and biotic drivers and, presumably, the different methods used to estimate $CaCO_3$ production rate. We used a 378-d manipulative experiment in a subpolar rhodolith bed to test the hypothesis that bioturbators increase rhodolith apical extension (growth) and $CaCO_3$ production, as well as to quantify and compare gross and net rhodolith $CaCO_3$ production rates with the apical extension and weight change methods. We also reviewed published estimates of $CaCO_3$ production rates in rhodolith-forming, red coralline algae from polar to tropical realms to situate the present study's findings, while assessing global variability in production rates. Bioturbators did not affect apical extension (0.541 mm y^{-1}) and weight change (1.64 g y^{-1}; as averaged across sizes) rates of live, stained or unstained rhodoliths. Rhodolith age estimates ranged from 38 y (based on use of the gross weight change method) to 72 y (apical extension), to 115 y (net weight change), indicating that different methods can under- or over-estimate age by up to three times. Gross (806.1 g $CaCO_3$ m^{-2} y^{-1}) and net (196.2 g $CaCO_3$ m^{-2} y^{-1}) rhodolith $CaCO_3$ production rates estimated from rhodolith weight change and rhodolith abundance (density) in the bed were similar to those in European beds and lower than in sub-tropical and tropical beds. The latter net production rate was also similar to that estimated from rhodolith age (calculated from apical extension rate and physical dimensions) and rhodolith abundance (biomass) in the bed (163 g $CaCO_3$ m^{-2} y^{-1}). Our results imply that gross $CaCO_3$ production by living rhodoliths is far greater than net estimates, in which dry weight loss by dead rhodoliths may account for as much as 75% of gross production. $CaCO_3$ production rates

reported in the present study are similar to other polar and subpolar rhodolith beds, however, there is a clear discrepancy across studies due to the use of varying methods in estimation.

2.1 INTRODUCTION

Marine calcifiers such as hermatypic and cold-water corals, bryozoans, and calcareous algae are important to the oceans and atmosphere, playing a key role in the global carbon cycle (Kleypas et al., 2006; Perez et al., 2018; Perry et al., 2018). Corals and calcareous algae produce calcium carbonate ($CaCO_3$) skeletons and build structurally complex habitats supporting high biodiversity (Basso, 2012; Harvey et al., 2017; Hibino and Van Woesik, 2000). Marine calcifiers face the mounting challenge of ocean acidification, which interferes with key basic life functions, including the deposition of $CaCO_3$ in their tissues (Kleypas et al., 2006). This phenomenon and its synergistic effect with ocean warming are largely unexplored in rhodoliths (Basso, 2012; Cavalcanti et al., 2014; dos Reis et al., 2016; Foster, 2001; James and Lukasik, 2010; Martin and Hall-Spencer, 2017; Stearn et al., 1977).

Rhodoliths are non-geniculate red coralline algae that form extensive, biodiverse communities known as “beds” in tropical to polar seas at depths down to several hundreds of meters (Amado-Filho et al., 2012; Bahia et al., 2010; Foster, 2001; Gagnon et al., 2012; Harvey et al., 2017; Matsuda and Iryu, 2011). Rhodolith bed size varies geographically, with the largest known bed (~20 900 km^2) located off the coast of Brazil (Amado-Filho et al., 2012; Brasileiro et al., 2016; Pereira-Filho et al., 2012; Villas-Boas et al., 2014). Given their wide distribution, importance to biodiversity, and likely vulnerability to ocean

acidification and warming, it is important to measure and understand the contribution of rhodolith beds to global carbonate production (Basso, 2012; Kleypas et al., 2006; Perez et al., 2018; Perry et al., 2018). Yet, the diversity of approaches used to estimate $CaCO_3$ production in rhodolith beds, combined with geographic variation, yield significant intra- and inter-regional differences, making it difficult to compare rhodolith beds' global carbonate production among global carbonate realms (Bahia et al., 2010; Jørgensbye and Halfar, 2017; Van Der Heijden and Kamenos, 2015; the present study).

Present estimates suggest that rhodolith beds are major $CaCO_3$ producers, with production rates similar to those of coral reefs (Harvey et al., 2017). Production rate varies latitudinally, likely because of differences in abiotic and biotic drivers, but possibly also due to different methods used to estimate $CaCO_3$ production rate. Tropical beds, like those in Brazil, produce large amounts of $CaCO_3$, with net rates ranging from 300 to 2700 g m^{-2} y^{-1} (Amado-Filho et al., 2012). Temperate beds exhibit lower $CaCO_3$ production rates, from 200 to 1200 g m^{-2} y^{-1} (Bosence and Wilson, 2003). For example, rhodolith (*Lithothamnion coralloides*) beds in Europe have net and gross $CaCO_3$ production rates from 84 to 876 g m^{-2} y^{-1} (Bosence, 1983; Potin et al., 1990). The latter rates mirror those of subpolar beds: in Norway, production rates of rhodolith (*Lithothamnion glaciale*) beds range from 420 to 1430 g m^{-2} y^{-1} (Freiwald and Henrich, 1994).

Gross $CaCO_3$ production rate refers to the amount (mass) of new carbonate skeleton produced and added to the bed by rhodoliths, whereas net $CaCO_3$ production rate accounts for carbonate skeleton losses to bioerosion, dissolution, and maceration (the process by which microbes break down a rhodolith's organic matrix via enzymatic degradation of starch; Freiwald, 1998) (Chave, 1972; Schonberg et al., 2017). Effects of bioerosion,

dissolution, and maceration together with intra-bed variation in dead versus live rhodolith abundance, should be considered because 1) the rate of loss of calcified tissues in dead rhodoliths may approach or temporarily exceed the rate of $CaCO_3$ production in live rhodoliths, with net estimates of production rate potentially below zero (i.e. a net loss, equivalent to a temporary state of net reef erosion in coral reefs [Perry et a., 2008]); and 2) the proportion of dead versus live rhodoliths can vary spatially within a bed (Canals and Ballesteros, 1997; Savini et al., 2012; Schwarz et al., 2005).

There are three methods used in estimating $CaCO_3$ production rate of rhodoliths. The first method is the most common, relying on measurement of extension rates of rhodolith apices (Figure 2.1; Blake and Maggs, 2003; Caragnano et al., 2016; Figueiredo et al., 2012; Frantz et al., 2000; Noisette et al., 2013). Apical extension rates are often measured by staining rhodoliths with Alizarin Red, then measuring new tissue added beyond the stained layer over a known period of time (Blake and Maggs, 2003; Bosence and Wilson, 2003; Bosence, 1983; Freiwald, 1998). In general, extension rates of rhodoliths for the North Atlantic are between 0.2 and 3 mm y^{-1} (Blake and Maggs, 2003; Bosence and Wilson, 2003; Figueiredo et al., 2012), which is lower than the 0.8 to 5 mm y^{-1} range in tropical seas (Amado-Filho et al., 2012; Steller et al., 2007). Extension rate has been used to estimate net rhodolith $CaCO_3$ production rate by incorporating rhodolith age and mass (Figure 2.1) (Amado-Filho et al., 2012; Bosence and Wilson, 2003; Nelson et al., 2012). The second method used less frequently is the weight change method (Figure 2.1), where rhodoliths are weighed before and after deployment in a rhodolith bed, measuring weight gain (in live rhodoliths) and/or loss (in dead rhodoliths) over time. This method often yields similar $CaCO_3$ production rates to those obtained from apical extension rates (Potin et al.,

1990). The third method is observing changes in total alkalinity (measuring the concentration of alkaline substances in seawater – namely carbonates) (Chisholm, 2000; Martin et al., 2006, 2007). This method sometimes yields higher $CaCO_3$ production rate estimates than the weight change and extension methods, up to 10 300 g $CaCO_3$ m^{-2} y^{-1} (Chisholm, 2000; El Haikali et al., 2004). These three methods have not been used simultaneously to calculate and compare $CaCO_3$ production rates for the same rhodolith bed, therefore limiting the ability to compare their accuracy and consistency (Potin et al., 1990).

Rhodolith beds generally develop in habitats with moderate hydrodynamic forces, presumably because such forces limit the accumulation of sediment and move rhodoliths around, therefore exposing their surface to adequate levels of light for photosynthesis (Foster, 2001; Joshi et al., 2017; Marrack, 1999). Millar and Gagnon (2018) challenged this paradigm with a study of sedimentation patterns in a coastal rhodolith (*Lithothamnion glaciale*) bed located off the coast of St. Philip's in Conception Bay, southeastern Newfoundland (Canada) that contains macroinvertebrate suspension feeders (e.g. the brittle stars *Ophiopholis aculeata* and *Ophiura robusta*), grazers (e.g. mottled red chiton, *Tonicella marmorea*; green sea urchin, *Stronglyocentrotus droebachiensis*), and predators (e.g. common sea star, *Asterias rubens*) (Gagnon et al., 2012). They concluded that hydrodynamic forces were insufficient to move rhodoliths and that resident bioturbators, in this case, *O. aculeata*, *A. rubens*, and *S. droebachiensis*, contributed to movement and dislodgement of sediment from the rhodoliths, and hence to the overall growth of the bed (Millar and Gagnon, 2018). $CaCO_3$ production rate in this subpolar bed, and the effects of bioturbators on this production rate, are unknown, yet worth studying to gain a better

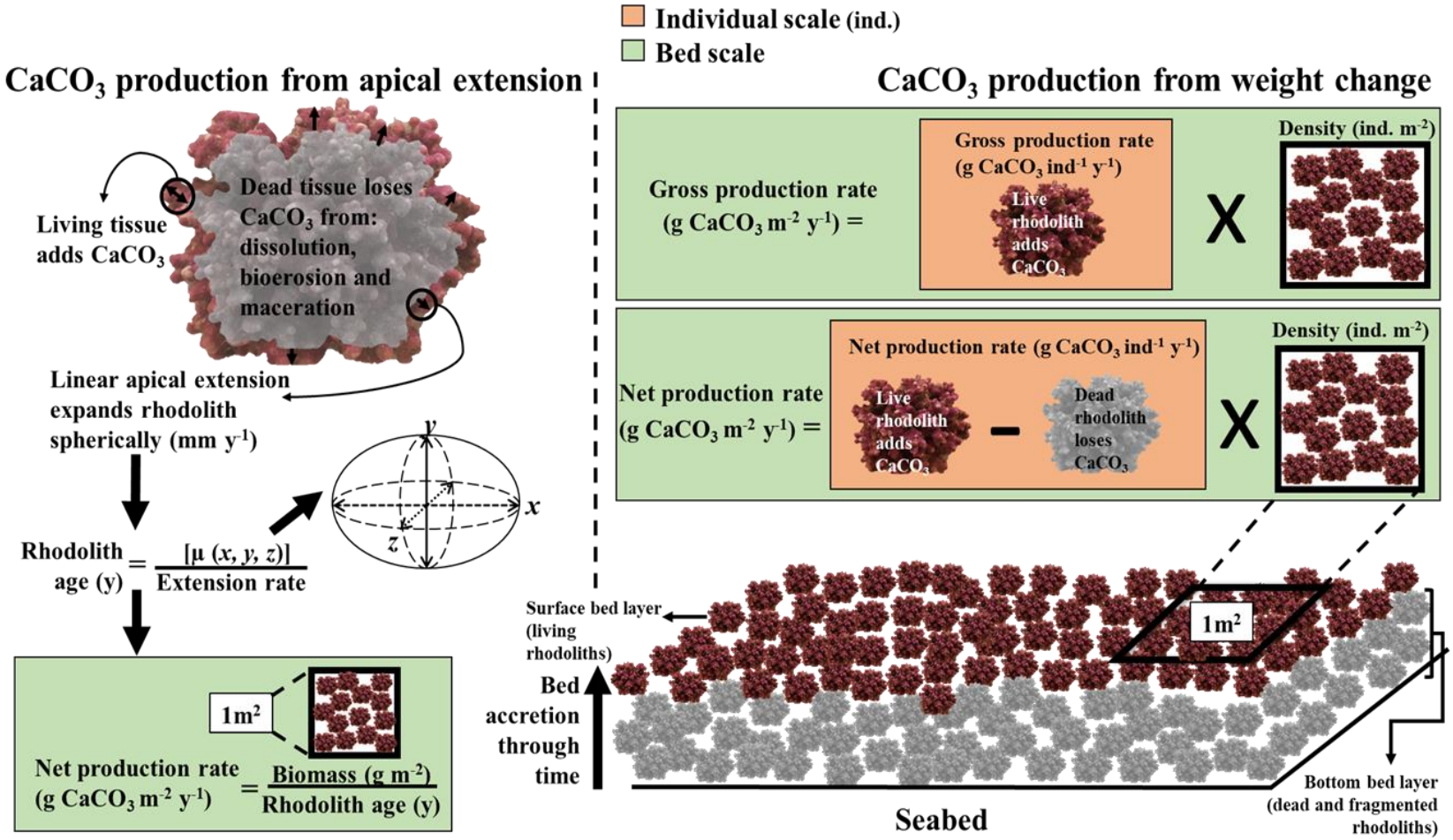
Individual scale (ind.)
Bed scale
CaCO3 production from apical extension
Living tissue adds CaCO3
Dead tissue loses CaCO3 from: dissolution, bioerosion and maceration
Linear apical extension expands rhodolith spherically (mm y-1)
Rhodolith age (y) = [μ (x, y, z)] / Extension rate
y
x
z
1m2
Net production rate (g CaCO3 m-2 y-1) = Biomass (g m-2) / Rhodolith age (y)
CaCO3 production from weight change
Gross production rate (g CaCO3 m-2 y-1) =
Gross production rate (g CaCO3 ind-1 y-1)
Live rhodolith adds CaCO3
X
Density (ind. m-2)
Net production rate (g CaCO3 m-2 y-1) =
Net production rate (g CaCO3 ind-1 y-1)
Live rhodolith adds CaCO3
–
Dead rhodolith loses CaCO3
X
Density (ind. m-2)
Surface bed layer (living rhodoliths)
Bed accretion through time
1m2
Bottom bed layer (dead and fragmented rhodoliths)
Seabed

Figure 2.1 Schematic of methods used to estimate $CaCO_3$ production rates in an *in situ* rhodolith bed (*sensu* Bosence, 1976) like that in the present study. Lower right-hand portion: live, un-attached rhodoliths form a top layer underneath which dead or dying rhodoliths fragment and accumulate over time, forming a compact foundation of fine-grained, possibly anoxic sediment. Left vertical portion: $CaCO_3$ production rates are most commonly estimated from rhodoliths' apical extension rates. Rhodoliths grow predominantly spherically, adding a thin (millimeter scale) layer of new living tissue and $CaCO_3$ matrix at their surface every year. Some of the inner $CaCO_3$ matrix is also lost yearly to dissolution, bioerosion, and maceration, which is accounted for in measuring rhodolith biomass (in g m^{-2}: bed scale – green rectangle). With this method, a bed's net $CaCO_3$ production rate is estimated by dividing rhodolith biomass by mean rhodolith age. A single rhodolith's age is determined by measuring its longest (*x*), intermediate (*y*), and shortest (*z*) axes, then dividing mean axes length by extension rate (mm y^{-1}). Right vertical portion: one less common method to estimate $CaCO_3$ production rates is based on rhodolith weight change, which allows for the separation of gross and net estimates when both live and dead rhodoliths are considered. Gross $CaCO_3$ production rate of an individual rhodolith (orange rectangle) is estimated by measuring the gain in weight over time caused mainly by the growth of the $CaCO_3$ matrix. Net individual $CaCO_3$ production rate (orange rectangle) is estimated by subtracting the mean loss of $CaCO_3$ of dead rhodoliths from new $CaCO_3$ added by live rhodoliths. On a rhodolith bed scale (green rectangles), $CaCO_3$ production rates are estimated by multiplying individual gross or net $CaCO_3$ production rates by the density of rhodoliths in the bed (in individuals m^{-2}).

understanding of local and global rhodolith bed carbonate budgets and the biological factors that influence them.

The present study uses a 378-d manipulative experiment in the rhodolith bed in St. Philip's to (1) test the hypothesis that bioturbators increase rhodolith apical extension [growth] and $CaCO_3$ production; and (2) quantify and compare gross and net rhodolith $CaCO_3$ production rates with the apical extension and weight change methods. It also (3) reviews published estimates of $CaCO_3$ production rates in rhodolith-forming, red coralline algae from polar to tropical realms obtained with the three methods outlined above to situate the present study's findings, while assessing global variability.

2.2 MATERIALS AND METHODS

2.2.1 Study site

The present study was carried out in a rhodolith bed located off the coast of St. Philip's (47.592° N, 52.893° W), on the southeast shore of Conception Bay in Newfoundland, Canada (Figure 2.2A). The bed extends from depths of 8 to >25 m and is predominantly composed of largely spheroidal rhodoliths with an average diameter of ~6 ± 2 cm (Figure 2.3A) (Gagnon et al., 2012). Green sea urchins (*Stronglyocentrotus droebachiensis*), brittle stars (*Ophiopholus aculeata* and *Ophiura robusta*), common sea stars (*Asterias rubens*), and mottled red chitons (*Tonicella marmorea*) are common across the surface of the bed (Gagnon et al., 2012). Millar and Gagnon (2018) showed that this bed is exposed to chronic low hydrodynamic forces, which appear insufficient to overturn the rhodoliths.

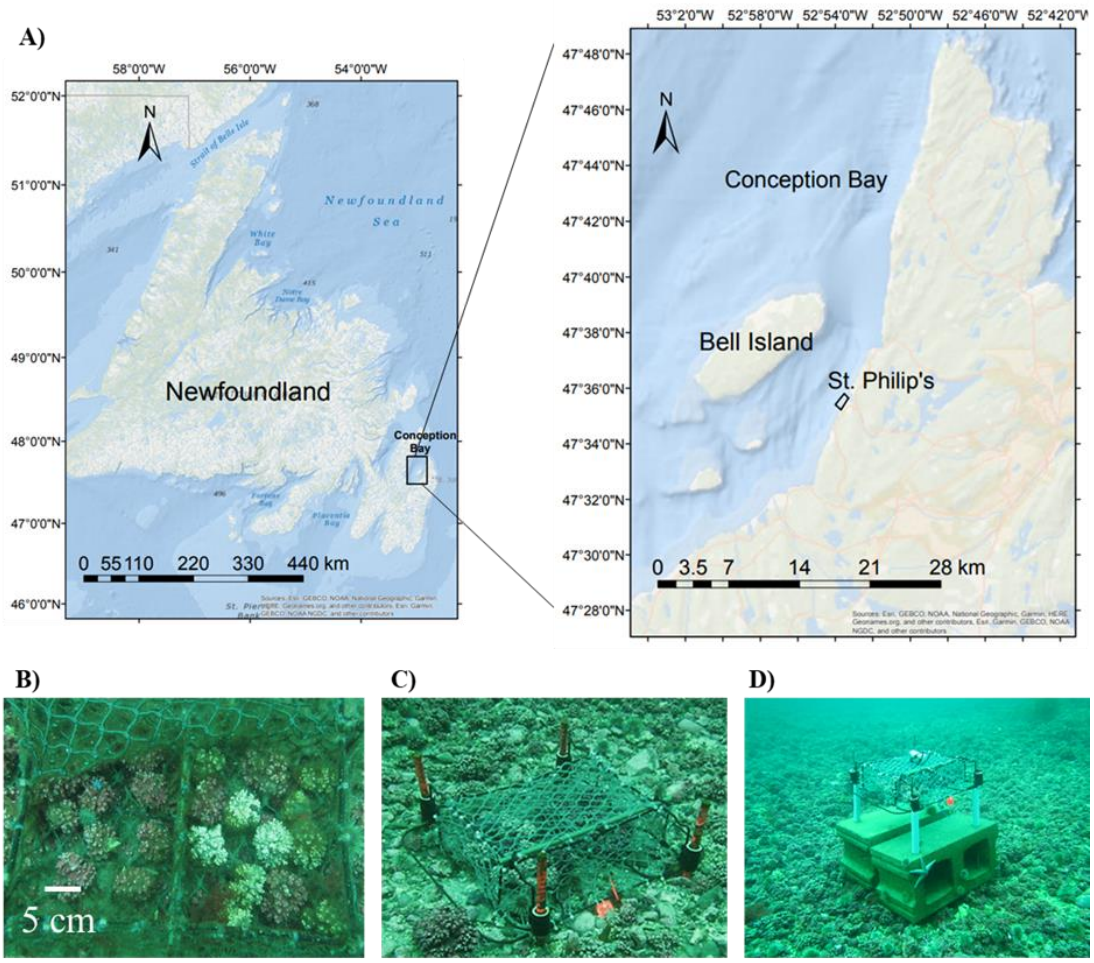

Figure 2.2 Location of the rhodolith bed studied near St. Philip's, Newfoundland (**A**) and experimental setup showing enclosures, each containing live-stained (n=3), live-unstained (n=10) and dead (n=10) rhodoliths (**B**) directly on the seabed (**C**) or raised 50 cm above it (**D**). One temperature and light (Lux) logger attached to the top of one of the enclosures (**D**).

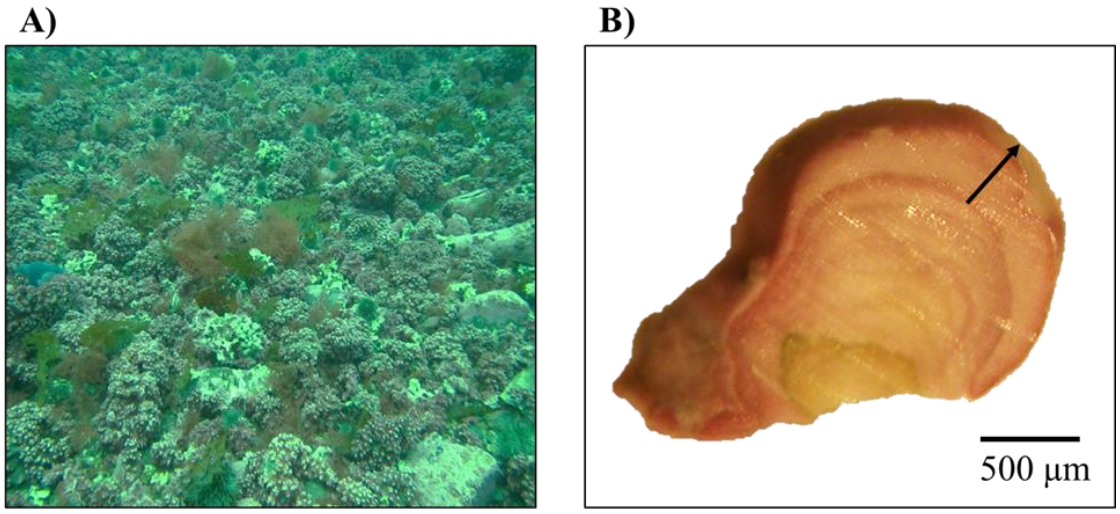

Figure 2.3 View of the rhodolith (*Lithothamnion glaciale*) bed in St. Philip's showing primarily spheroidal rhodoliths (**A**), image courtesy of David Bélanger. Portion of a rhodolith thallus where apical extension was measured from the purple coloured Alizarin Red stain line to the edge of the branch tip (**B**).

2.2.2 Rhodolith collection and staining

On 15 April, 2016, 276 spheroidal, *L. glaciale* rhodoliths (~4-6 cm in diameter) were hand collected by divers at a depth of ~16 m in the middle section of the bed where they are evenly distributed. Rhodoliths were transported to Memorial University of Newfoundland's Ocean Science Centre (OSC) in plastic containers filled with seawater (see Appendix A for a complete timeline of the experiment). Upon arrival at the OSC, rhodoliths were dispatched equally into four 180-L glass aquaria supplied with flow-through (1 L min^{-1}) seawater. Seawater was pumped in from the adjacent embayment, Logy Bay, at a depth of ~5 m, and exposed to the natural photoperiod of sunlight entering the laboratory through three 1-m diameter circular windows. Rhodoliths were exposed to these environmental conditions until the onset of the field experiment.

On 3 June, 2016, rhodoliths were individually inspected and cleaned of all visible epibionts with forceps and a smooth nylon brush. Small cryptofauna (e.g. amphipods, gastropods, chitons) and boring organisms (e.g. polychaetes, bivalves) located inside the rhodoliths were too difficult to remove without breaking some rhodolith tissue, and hence were not removed. Epibionts removed from rhodoliths before and after the field experiment (see below) were not quantified. On 14 June, 2016, each rhodolith was individually blotted, and weighed (initial wet weight) with a balance with a precision of 0.001 g (Mettler Toledo Classic plus PB503-S). Each rhodolith was identified with small plastic tags (~1 cm^2) attached with fishing line. Rhodoliths were divided into three groups based on their biological status: 120 live-unstained rhodoliths, 120 dead rhodoliths, and 36 live-stained rhodoliths. Dead rhodoliths were live rhodoliths haphazardly selected from the aquaria, killed by exposing them to ambient air (~20°C) for seven days, and dry weighed (initial

dead dry weight: $DDW_{initial}$). Complete bleaching of rhodolith tissue caused by loss of photosynthetic pigments indicated that no live tissue remained at the surface of the dried thalli.

For live-staining, rhodoliths were transferred to a separate tank filled with a solution of 8.5 g of Alizarin Red dissolved in 10 L (85 mg L^{-1}) of seawater and stained for 48 h. Temperature was gradually increased from ~2°C to ~7°C over the first six hours and maintained at the latter temperature during the remainder of the staining period (Blakes and Maggs, 2003; Kamenos et al., 2008; Ragazzola et al., 2012). During staining, rhodoliths were exposed to artificial light from 61-cm long, actinic fluorescent tubes (Marine-GO T8, 20W; Rolf C. Hagen) placed ~30 cm above the water surface and emitting ~20 µmol photons m^{-2} s^{-1} from 05:00 to 21:00 to mimic the natural photoperiod. Staining solution was aerated with a pump (Elite802; Rolf C. Hagen) delivering 1500 cm^3 of air min^{-1} and maintained at ~7°C with one immersion probe cooler (IP-35RCL; PolyScience) throughout the staining process. At the end of the 48 h, a low seawater flow (250 ml min^{-1}) was re-established in the aquarium to flush the stain and gradually bring the temperature back to ambient (~4°C) over the course of 1 h (see Figure 2.3B for an example of a stained rhodolith). Water flow was increased to 1 L min^{-1} once ambient temperature was reached.

2.2.3 Field experiment

Two main objectives of the present study were to (1) test the hypothesis that bioturbators increase rhodolith apical extension [growth] and $CaCO_3$ production; and (2) quantify and compare gross and net rhodolith $CaCO_3$ production rates with the apical extension and weight change methods. These objectives were addressed with a field

experiment during which apical extension and weight change of live (stained or not) and dead rhodoliths placed in enclosures in the rhodolith bed in St. Philip's (Figure 2.2B-D) were monitored over 365 d in the presence or absence of bioturbators, mainly *S. droebachiensis* and *A. rubens*. Live-unstained rhodoliths represented rhodoliths producing carbon in gross $CaCO_3$ rate estimates (using the weight change method), and were used in conjunction with dead rhodoliths to estimate net $CaCO_3$ production rate. Dead rhodoliths were used for net estimates, accounting for natural rhodolith weight loss. $CaCO_3$ production rate depends on rhodolith tissue growth, which is in large part conditioned by the physical environment, including water temperature and irradiance (Adey, 1970, Blake and Maggs, 2003, Kamenos and Law, 2010). Five branch tips from each of the live-stained rhodoliths were used to measure apical extension and apply this to net $CaCO_3$ production rate estimates (Figure 2.3B). Live-stained rhodoliths were weighed to determine if $CaCO_3$ accumulation rate was comparable in stained and non-stained rhodoliths (i.e. to verify that there was no staining effect).

On 22 June, 2016, rhodoliths held in laboratory conditions were transported to the bed and manually introduced by divers inside 12 enclosures, each made of a rectangular metal frame (L x W x H: 26 x 18 x 7 cm) covered with 2-cm nylon polyester mesh. These enclosures were divided in two adjacent sections of equal size (Figure 2.2B) that were installed at the initial rhodolith collection site, ~5 m apart in a 6 x 2 grid. Six randomly chosen enclosures were installed directly on the seabed (Seabed enclosures) to allow free access of benthic fauna (namely *O. aculeata, O. robusta, A. rubens,* and *T. marmorea* that can enter the 2-cm mesh) are common across the surface of the bed to the rhodoliths inside the enclosures (Figure 2.2C). The other six enclosures (Raised enclosures) were anchored

to cinder blocks, at ~50 cm above the seabed by four stainless steel rods attached to each corner to limit access by benthic fauna (Figure 2.2D).

Rhodoliths were transported by divers, from containers in a boat to the enclosures, inside pre-labeled, sealed plastic bags. There were three bags for each enclosure; one bag for each rhodolith biological state (dead, live-unstained, and live-stained). Bags contained either 10 (dead and live-unstained) or three (live-stained) specimens to allow fragment retrieval in case of thalli breakage during deployment. The 10 live-unstained rhodoliths were introduced in one section of each enclosure through a small aperture located on the top, whereas the 10 dead and three live-stained rhodoliths were introduced in the other section, for a total of 23 rhodoliths per enclosure. Live-stained rhodoliths were placed among the dead (bleached) ones to allow easy discrimination between the two in case identification tags were lost or damaged during the experiment. Each side of the enclosure could only accommodate a certain number of rhodoliths to ensure equal space for growth (10 live-stained rhodoliths would not fit with 10 live-unstained and 10 dead rhodoliths), and five branch tips from each of the three live-stained rhodoliths per enclosure was deemed sufficient to estimate apical growth (Teichert and Freiwald, 2014).

Initial wet weight of each group of dead ($DWW_{initial}$), live-unstained ($L_UWW_{initial}$), and live-stained ($L_SWW_{initial}$) rhodoliths inside each enclosure was calculated by averaging the individual wet weight of each rhodolith prior to field deployment. In the three cases where fragmentation occurred during deployment (one group of each dead, live-unstained, and live-stained rhodoliths), initial wet weight was calculated by subtracting the weight of the fragments retrieved from the plastic bags from total rhodolith weight measured in the lab.

On 22 June, 2017, each rhodolith was manually removed from the enclosures by divers and placed into individual, pre-labelled sealed plastic bags to avoid loss of rhodolith fragments during manipulation. Bags were transported to the OSC, and rhodoliths were individually cleaned over the next five days from all visible epibionts with forceps and a smooth nylon brush. During cleaning, rhodoliths were exposed to near darkness to limit growth, and the water inside the bags was changed twice daily to limit the accumulation of CO_2, a respiration by-product which can potentially cause $CaCO_3$ dissolution. Final wet weight of each rhodolith was measured on 27 June, 2017, 378 d after measuring initial weight. Rhodoliths were oven dried at 40°C for 48 h and their final dry weight measured. The same balance was used to measure initial and final wet and dry weights. Measurement of both dry and wet weights were used to convert initial wet weights for live rhodoliths into dry weights for calculation purposes (eq. 3). Wet and dry weights of dead rhodoliths at depths of ~15-17 m were highly correlated (Dry weight = 0.83 x Wet weight; R^2=0.99; $p<0.001$), therefore enabling estimation of initial dry weight in live-unstained and live-stained rhodoliths.

2.2.4 Temperature and light environment

Sea temperature and illuminance were measured every five minutes throughout the 365-d St. Philip's deployment with one temperature and light logger (HOBO Pendant, Onset Computer Corporation) attached to the top of one randomly chosen enclosure (Figure 2.2D). Daily mean temperature was calculated by averaging the 288 temperature values taken every day. Illuminance is a measure of the total light energy that hits a surface area. The sensor's configuration determines the portion of the electromagnetic spectrum over

which the energy is measured; in the present study, 150 to 1200 nm. Photosynthetically active radiation (PAR), on the other hand, designates the range of the electromagnetic spectrum between 400 and 700 nm used by primary producers to carry out photosynthesis (McCree, 1973). PAR (in µmol photons m^{-2} s^{-1}) is more appropriate than illuminance to characterize the light environment when addressing growth of photosynthetic tissue, like in the present study. Accordingly, illuminance values recorded on the top of the enclosure were converted to their PAR equivalents with the following equation (Long et al., 2012):

$$PAR = I/CF \quad (1)$$

where PAR is the photosynthetically active radiation in µmol photons m^{-2} s^{-1}, I is the illuminance in lux (lx) recorded by the logger, and CF is a lux to PAR conversion factor (23.5) in lx/µmol photons m^{-2} s^{-1} obtained from simultaneous measurement of illuminance and irradiance of sunlight at a depth of 15 m (Appendix B). Daily light integral (DLI) is a time integrated index of the total amount of PAR received by a surface of one square meter over 24 h. Assuming constant irradiance in between successive PAR readings, DLI was calculated for each of the 365 d with the following equation (from Korczynski et al., 2002):

$$DLI = \sum_{i=1}^{288} \frac{300 x_i}{10^6} \quad (2)$$

where DLI is daily light integral in mol photons m^{-2} d^{-1}, 288 is the number of PAR readings over 24 h, x_i is the i^{th} PAR value in µmol photons m^{-2} s^{-1}, 300 is the number of seconds

separating two consecutive readings (one reading every 5 min), and 10^6 is the µmol to mol scaling factor.

2.2.5 Rhodolith apical extension

At the end of the 365-d field deployment, rhodolith apical extension was calculated by averaging the tissue growth of five branch tips chosen haphazardly from each of the three live-stained rhodoliths from each enclosure (for a total of 15 branch tips per enclosure). Live-stained branch tips were sanded and chipped off manually with a speed rotary tool (Dremel 3000) equipped with fine sanding discs. Only branch tips with a clearly visible band of Alizarin Red stain were used to estimate extension (Figure 2.3B), which sometimes required sampling additional branch tips to obtain 15 tips of acceptable quality. Branch tips were magnified at 20X and imaged with a Nikon SMZ1000 stereomicroscope connected to a Nikon Coolpix 4500 camera. Branch tips were then placed individually in plastic bags labelled with proper information to trace back their biological state and enclosure from which they came. ImageJ was used to measure, on each image, the thickness of new rhodolith tissue added (i.e. the new growth) between the stain line and edge of branch tip, along the longest axis possible (Figure 2.3B). The longest axis was chosen from 15 to 20 measurements per branch tip.

2.2.6 Calcium carbonate production rate

$CaCO_3$ production rate estimates are typically reported in g $CaCO_3$ m^{-2} y^{-1} (Perry et al., 2018; Schafer et al., 2011; Stearn et al., 1977; Teichert and Freiwald, 2014). Estimates of rhodolith density and biomass for the bed in St. Philip's were obtained from a companion study of the bed's structure and biodiversity carried out in 2013 (Bélanger and Gagnon,

unpublished data). In the latter study, average rhodolith density (d; 768 ± 61.6 [95% CI, unless otherwise stated] individuals m^{-2}) and biomass (B; 11.7 ± 0.9 kg rhodoliths m^{-2}) were estimated in winter, spring, summer, and fall from rhodoliths in 30 x 30-cm quadrats placed by divers every 5 m along one 40-m transect (9 quadrats per transect) at each of two depths, 15 and 17 m (roughly the centre of the rhodolith bed), for a total of 72 quadrats (9 quadrats x 2 transects x 4 collections). The present study estimates rhodolith carbonate production under the methodologies of weight change and extension rate. Total alkalinity was not included due inaccessibility of incubation chambers to measure short term alkalinity changes.

2.2.6.1 Gross $CaCO_3$ production rate based on rhodolith weight change

Gross calcium carbonate production rate based on the weight change method was first calculated in live-unstained rhodoliths from seabed cages. Live-unstained rhodoliths were chosen because they reflect natural rhodolith bed conditions with: 1) possible tissue loss from bioturbation/grazers, and 2) no possible biological alteration by the Alizarin Red stain. Given the short timescale of the experiment comparing live and dead rhodoliths, the potential unmeasured weight loss in live rhodoliths (from microbioerosion and dissolution) is negligible compared to measured weight loss in dead rhodoliths. This experimental design and terminology is analogous to the use of the terms gross and net carbonate production within tropical reef carbonate budget research (Perry et al., 2012, 2013). Because rhodolith wet and dry weights were measured on day 1 and day 378 respectively, absolute dry weight change (ADWC) was converted into a yearly rate with the following equation:

$$\text{ADWC (g rhodolith y}^{-1}) = [(L_UDW_{final} - L_UDW_{initial})/378 \text{ d}] \text{ x } 365 \text{ d y}^{-1} \quad (3)$$

Mean annual percent dry weight change (PDWC) in each enclosure was calculated with the following equation (adapted from Potin et al., 1990):

$$\text{PDWC (\% weight change y}^{-1}) = \text{ADWC x } 100\% / L_UDW_{initial} \quad (4)$$

where L_UDW_{final} and $L_UDW_{initial}$ are respectively the final and initial dry weights of live-unstained rhodoliths, in g. Mean gross calcification rate (GC) was then estimated with the following equation:

$$\text{GC (g CaCO}_3 \text{ rhodolith}^{-1} \text{ y}^{-1}) = \text{PDWC x } L_UDW_{initial} \quad (5)$$

Gross $CaCO_3$ production rate was further estimated by multiplying GC by average rhodolith density across all seasons (d, reported above):

$$\text{Gross CaCO}_3 \text{ production rate (g CaCO}_3 \text{ m}^{-2} \text{ y}^{-1}) = \text{GC x d} \quad (6)$$

2.2.6.2 Net $CaCO_3$ production rate based on rhodolith weight change

Net $CaCO_3$ production rate is the difference between gross carbonate deposition and carbonate loss from dissolution, bioerosion and maceration. Net $CaCO_3$ production rate based on weight change was calculated using live-unstained and dead rhodoliths from

seabed cages. Live-unstained rhodoliths in seabed enclosures reflected natural rhodolith bed surface layer conditions, while dead rhodoliths (also in seabed enclosures) represented natural bed carbonate loss of thallus tissue in underlying dead rhodolith bed layers. Dry weight change was first converted into a yearly rate. Then PDWC was calculated based on yearly rate (g y^{-1}) for both live-unstained and dead rhodoliths (% rhodolith weight change y^{-1}) (see above). PDWC of dead rhodoliths (DDW_{final}) in seabed enclosures (n=60) was subtracted from live-unstained rhodolith PDWC over the course of one year (L-D). Net PDWC was then multiplied by the net final mean dry weight of the same rhodoliths ($L_UDW_{initial} - DDW_{initial}$: divided by 2 to account for both the live-unstained and dead rhodoliths) to estimate net calcification rate. Net calcification rate (NC) was determined with the following equation:

$$NC\ (g\ CaCO_3\ rhodolith^{-1}\ y^{-1}) = PDWC_{\ L\text{-}D} \times [(L_UDW_{initial} - DDW_{initial}) / 2] \qquad (7)$$

Net calcification rate was then multiplied by previously measured rhodolith density (d, reported above) to estimate net $CaCO_3$ production rate, in g m^{-2} y^{-1}.

2.2.6.3 Net $CaCO_3$ production rate based on rhodolith extension rate

Net $CaCO_3$ production rate based on the extension rate method was calculated on the live-stained rhodoliths in all enclosures since enclosure location had no effect on apical extension rate (see results). Live-stained rhodoliths were chosen as thallus extension could easily be quantified by the distance between the Alizarin Red stain and the branch tip.

Extension, quantified on day 376, was converted to a yearly extension rate (ER) with the following equation:

$$\text{ER (mm rhodolith y}^{-1}) = (\text{E}/376\text{ d}) \times 365\text{ d y}^{-1} \quad (8)$$

where E is the apical extension, in mm. The age of each rhodolith was estimated from its ER and longest (*x*), intermediate (*y*), and shortest (*z*) axes measured to the nearest mm with calipers, after Edyvean and Ford (1987) and Nelson et al. (2012). Longest, intermediate, and shortest axes lengths were measured in all live-stained rhodoliths and averaged for each axis across all enclosures. There is only one layer of living tissue on the surface of a rhodolith, as the underlying layers undergo degradation through bioerosion, dissolution and maceration. Apical extension measures the addition of new hard ($CaCO_3$ matrix) and soft (photosynthetic) rhodolith tissue at the surface. Measuring the total biomass (g m^{-2}) of rhodoliths then accounts for the addition of living tissue on the surface layer, and the loss in internal tissue. By dividing rhodolith biomass by estimated rhodolith age, we can generate a net rate of carbonate deposition. Net $CaCO_3$ production rate was obtained with the following equation:

$$\text{Net } CaCO_3 \text{ production rate (g } CaCO_3\text{ m}^{-2}\text{ y}^{-1}) = \text{B / Age} \quad (9)$$

where B is the biomass of rhodoliths in the bed (reported above), in g m^{-2}, and Age is the estimated age of rhodoliths, in year. Average age of rhodoliths was estimated first based on extension rate with the following equation:

$$\text{Age (y)} = [\mu(x, y, z)] / \text{ER} \quad (10)$$

where μ is the mean length of all the live-stained rhodoliths along the longest (*x*), intermediate (*y*) and shortest (*z*) axes (in mm), ER is the mean extension rate of live-stained rhodoliths; in the present study, 0.541 mm y^{-1} (see results), which, as per Edyvean and Ford (1987) and Teichert and Freiwald (2014), was assumed to be constant throughout rhodoliths' lifespan.

For comparison purposes, rhodolith weight change data were also used to estimate rhodolith age. Because live rhodoliths grow more or less radially by adding new tissue superficially on all sides (with each rhodolith branch extending at a constant, linear rate), their weight should increase exponentially with age. Accordingly, rhodolith age based on weight change can be determined by rearranging the following equation to solve for age (adapted from Yong et al., 2013):

$$\text{Weight (g)} = (1 + \text{PDWC}_{\text{L-D}})^{\text{Age(y)}} \quad (11)$$

where weight is the average weight of live rhodoliths, across all enclosures; in the present study, 15.65 g, and net $\text{PDWC}_{\text{L-D}}$ is the percent dry weight change of deposition of tissue by live rhodoliths minus the dissolution, bioerosion and maceration of dead rhodoliths; in the present study, 2.42 % (gross PDWC was 7.53 %). Gross and net PDWC were pooled across raised and bottom enclosures because weight change was similar among enclosure type (see results). Then the equation was rearranged to solve for age:

$$\text{Age (y)} = (\ln [\text{Weight}_{(g)}]) / (\ln [1 + \text{PDWC}_{\text{L-D}}]) \quad (12)$$

2.2.7 Statistical analysis

Four split-plot ANOVAs (Quinn and Keough, 2002) with the fixed between-plot factor enclosure Location (the two locations where enclosures were installed: on the seabed or raised above it), random factor Enclosure (the 12 enclosures used) nested within Location (six enclosures per Location), and fixed within-plot factor rhodolith State (the three rhodolith biological states examined: live-unstained, dead, and live-stained) were used to test individual and interactive effects of enclosure location and rhodolith biological state on rhodolith: 1) percent wet weight change; and 2) percent dry weight change. The expected mean square was used for the error term of mixed models (containing both fixed and random factors); i.e., adjusted p-values were determined from the corrected F-ratios based on expected mean squares as per Quinn and Keough (2002). One bag with three live-stained rhodoliths was lost underwater before they could be introduced to one of the raised enclosures. This enclosure therefore contained 20 rhodoliths (10 live-unstained and 10 dead) instead of 23 as in the other enclosures, reducing the overall sample size to n=35. The analysis was applied to the raw data.

A two-way ANOVA with the fixed factor enclosure Location (the two locations where enclosures were installed: on the seabed or raised above it) and the random factor Enclosure (the 12 enclosures used) nested within Location (six enclosures per location), was used to test the effect of enclosure location on rhodolith apical extension rate (n=11; 12 enclosures, with one live-stained group lost). The analysis was applied to the raw data.

Two Pearson's correlation analyses were used to determine if mean extension rates of live-stained rhodoliths in seabed (n=6) and raised (n=5) enclosures were good predictors of dry weight gain (ADWC) and percent weight change.

In all ANOVAs, homogeneity of the variance and normality of the residuals were verified by examining the distribution of the residuals and the normal probability plot of the residuals (Snedecor and Cochran, 1994). In ANOVAs, Tukey HSD multiple comparison tests (comparisons based on least-square means; Sokal & Rohlf, 2012) were used to detect differences among levels within a factor. A significance level of 0.05 was used in all analyses. All analyses were carried out in RStudio Desktop 1.2 (R Core Team, 2014). All means are presented with 95% confidence intervals (means ± 95% CI), unless otherwise stated.

2.3 RESULTS

Sea temperature and irradiance at the experimental site varied seasonally peaking respectively to ~16°C in late summer (August and September 2016), and to ~2.7 mol photons m^{-2} day^{-1} in early summer (July 2016 and June 2017) (Figure 2.4). In fall and winter, water temperature and irradiance dropped to nearly -1°C (February to mid-April, 2017) and 0 mol m^{-2} day^{-1} (October 2016 to April 2017), respectively (Figure 2.4).

2.3.1 Bioturbation and $CaCO_3$ production rate

Absolute and percent rhodolith wet weight increased for all rhodolith biological states (Figure 2.5). However, dead rhodoliths exhibited a dry weight loss of 0.73 (± 0.05 [95% CI, unless otherwise stated]) g y^{-1} and 5.1 (± 0.33) % y^{-1}. Wet weight change in live-unstained and live-stained rhodoliths was respectively two and three times higher than in

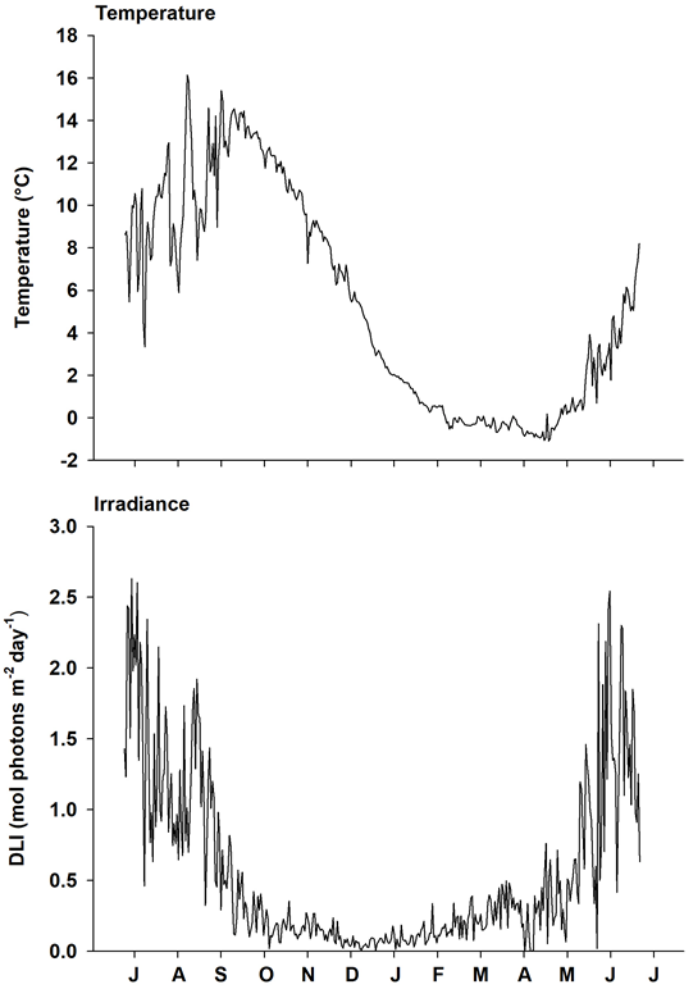

Figure 2.4 Daily mean sea temperature (top panel) and daily light integral (DLI) of photosynthetically active radiation (PAR) at the surface of the rhodolith bed throughout the 365-d field experiment.

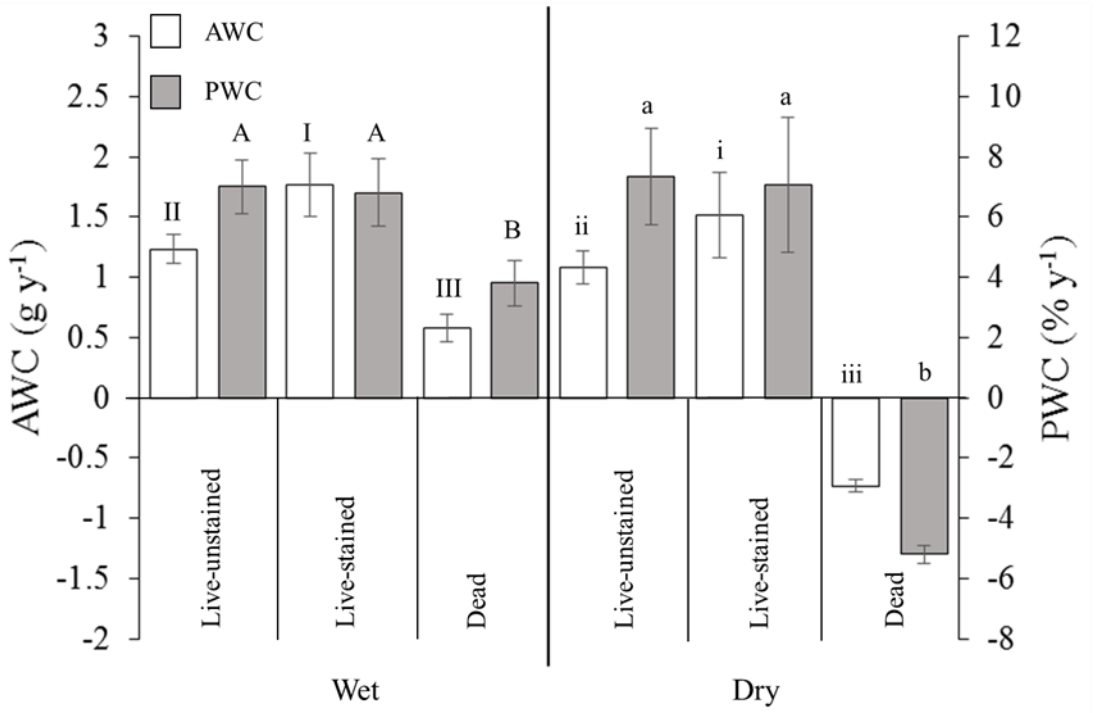

Figure 2.5 Mean (±95% CI) absolute (AWC) and percent (PWC) wet or dry weight change of live-unstained (n=120), live-stained (n=33), and dead (n=120) rhodoliths (averaged per treatment and divided by number of rhodoliths per treatment; 10 live-unstained and dead rhodoliths and 3 live-stained rhodoliths) over the 365-d field experiment. Data are pooled across locations (seabed and raised enclosures). Bars not sharing the same letters or roman numerals are statistically different.

dead rhodoliths (Figure 2.5). Live-stained rhodoliths exhibited the highest increase in absolute wet (1.76 [± 0.27] g y^{-1}) and dry (1.51 [± 0.36] g y^{-1}) weight change, as well as in percent wet (7.03 [± 0.81] % y^{-1}) and dry (7.1 [± 1.69] % y^{-1}) weight change (Figure 2.5). Absolute wet ($p=0.049$) and dry ($p=0.003$) weight changes were both ~1.5 times greater in live-stained than live-unstained rhodoliths. However, there was no significant difference in percent dry weight change of live-stained and live-unstained, only in absolute dry weight change. There was no significant interaction between rhodolith biological state (live-stained, live-unstained, and dead) and location (seabed and raised enclosures) on percent wet and dry weight change (Table 2.1A and B). Hence, percent wet and dry weight change did not differ between seabed (5.8 ± 2.0 % y^{-1} and 2.7 ± 5.9 % y^{-1}) and raised (6.1 ± 2.1 % y^{-1} and 3.5 ± 6.7 % y^{-1}) enclosures (Table 2.1B).

2.3.2 Apical extension rate

Apical extension rate of live-stained rhodoliths did not differ between seabed (0.536 ± 0.076 mm y^{-1}) and raised (0.548 ± 0.062 mm y^{-1}) enclosures (Table 2.2), averaging 0.541 ± 0.069 mm y^{-1} overall. There was also no significant relationship between extension rate of live-stained rhodoliths (pooled across seabed and raised enclosures) and their absolute or percent dry weight change (Figure 2.6).

2.3.3 Carbonate production rate estimates

Gross individual weight gain of live-unstained rhodoliths based on ADWC and PDWC was 1.08 ± 0.15 g $CaCO_3$ y^{-1} and 7.53 ± 2.37 % $CaCO_3$ y^{-1}, respectively (Figure 2.7A), translating into a gross bed scale production rate of 806.13 ± 25.05 g $CaCO_3$ m^{-2} y^{-1} (Figure 2.7B). Net individual weight change of live-unstained rhodoliths based on ADWC

Table 2.1 Summary of split-plot ANOVA (applied to percent dry weight change data), testing the effects of rhodolith biological state (live-unstained, live-stained and dead), location (in seabed or raised enclosures) and enclosure on percent rhodolith wet weight (**A**) and dry weight (**B**) change over the 365-d field experiment.

A. Wet weight

Source	df	SS	MS	F	p-value
State	2	100.972	50.486	78.151	**<0.001**
Location	1	1.109	1.109	0.3597	0.557
Enclosure(Location)	10	30.835	3.083	NR*	
State*Location	2	1.990	0.995	1.540	0.240
State(Enclosure(Location))	19	12.266	0.646	NR*	

B. Dry weight

Source	df	SS	MS	F	p-value
State	2	1326.63	663.31	398.519	**<0.001**
Location	1	4.83	4.83	1.043	0.331
Enclosure(Location)	10	46.31	4.63	NR*	
State*Location	2	6.43	3.21	3.0420	0.250
State(Enclosure(Location))	19	40.79	2.15	NR*	

*NR = value is not relevant to the present study.

Table 2.2 Summary of two-way ANOVA (applied to raw data), testing the effects of rhodolith location (seabed or raised enclosures) and enclosure on apical extension rate of live-stained rhodoliths over the 365-d field experiment.

Source	df	SS	MS	F	p-value
Location	1	0.005	0.005	1.718	0.219
Enclosure (Location)	10	0.030	0.003	NR*	

*NR = value is not relevant to the present study.

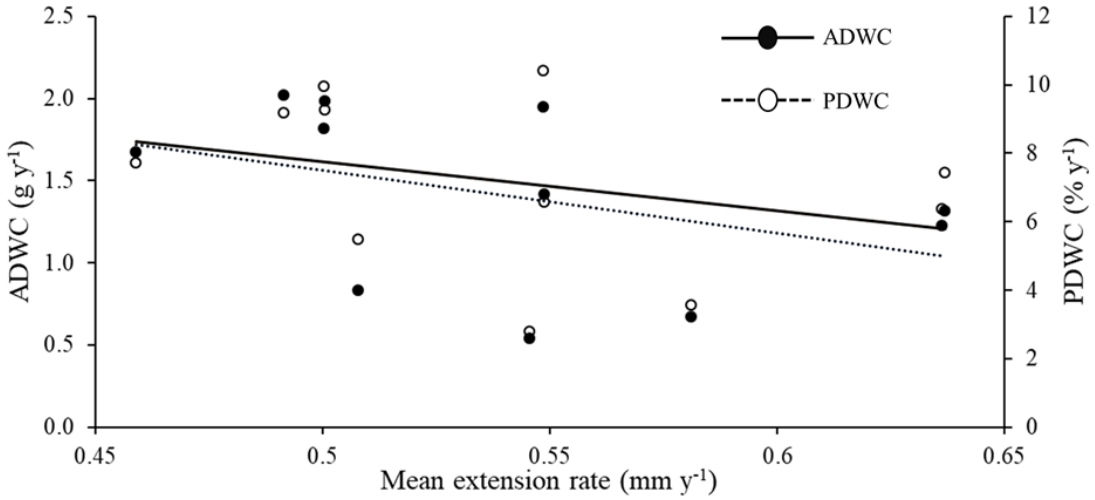

Figure 3.6 Relationship between absolute (ADWC: y = -3.818x + 3.472; R2 = 0.169; p=0.185) or percent (PDWC: y = -14.371x + 14.493; R2 = 0.109; p=0.292) dry weight change and mean extension rate of live-stained rhodoliths. Data are pooled across seabed and raised enclosures (n=11 for each type of enclosure).

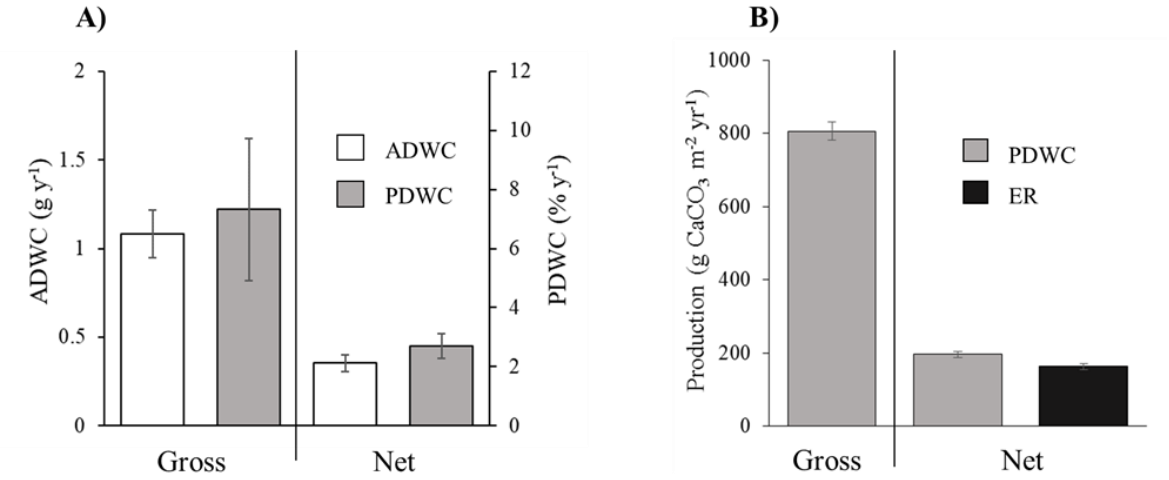

Figure 3.7 Mean (±95% CI) gross and net absolute (ADWC) and percent (PDWC) dry weight change of live-unstained (gross and net) and dead (net) rhodoliths at the individual scale over the 365-d field experiment (**A**), and corresponding rhodolith bed $CaCO_3$ production rate estimates based on gross or net PDWC and extension rate (ER) (**B**).

and PDWC was 0.35 ± 0.05 g $CaCO_3$ y^{-1} and 2.42 ± 0.29 % $CaCO_3$ y^{-1}, respectively (Figure 2.7A), yielding a net bed scale production rate of 196.16 ± 7.31 g $CaCO_3$ m^{-2} y^{-1} (Figure 2.7B).

Mean rhodolith age based on mean physical dimensions of live-stained rhodoliths (x = 45.15 ± 5.27 mm, y = 38.72 ± 3.77 mm, z = 38.10 ± 4.06 mm) and mean extension rate of 0.541 mm y^{-1} (see above) was 71.6 ± 10.1 y. Age based on gross and net PDWC (exponential growth function, see section 2.2.6.3) was 37.9 ± 8.4 y and 115.0 ± 21.7 y, respectively. Net $CaCO_3$ production rate based on rhodolith biomass in the bed and age estimates from extension rate (71.6 y) was 162.83 ± 8.40 g $CaCO_3$ m^{-2} y^{-1} (Figure 2.7B).

2.4 DISCUSSION

Our study aimed to (1) determine bioturbator effect on rhodolith [*Lithothamnion glaciale*] apical extension [growth] and $CaCO_3$ production in a subpolar rhodolith bed; (2) quantify and compare gross and net $CaCO_3$ production rates in that same bed with the apical extension and weight change methods; and (3) compare these $CaCO_3$ production rates to those of rhodolith-forming, red coralline algae reported worldwide. Overall, location of enclosures (raised [deterring bioturbators] and seabed) had no effect on rhodolith apical extension and weight change. Our results imply that gross $CaCO_3$ production by living rhodoliths is far greater than net estimates, in which dry weight loss by dead rhodoliths may account for as much as 75% of gross production. $CaCO_3$ production rates reported in the present study are similar to other polar and subpolar rhodolith beds, however, there is a clear discrepancy across studies due to the use of varying methods in estimation.

2.4.1 Bioturbation effects, rhodolith extension rate, and weight change

Bioturbation can remove sediment and debris from rhodolith surfaces, providing greater access to light for photosynthesis, and hence may facilitate rhodolith growth (Marrack, 1999; Millar and Gagnon, 2018; Rebelo et al., 2018). Interestingly, in the present study, extension rate (growth) and weight change of rhodoliths over one year was similar between seabed and raised enclosures. This finding suggests that the lack of bioturbator effect likely stems from similar abundances of benthic invertebrates inside seabed and raised enclosures noted on monthly site visits, including known bioturbators such as the common sea star (*Asterias rubens*), and green sea urchin (*Strongylocentrotus droebachiensis*) (Millar and Gagnon, 2018). The lack of a difference in rhodolith extension rate could also result from higher hydrodynamic forces in raised than seabed enclosures because of the former's higher placement in the water column (Denny, 1988). Continuous exposure to higher water circulation may have contributed to clearing sediment off the surface of rhodoliths in raised enclosures (Joshi et al., 2017; Riul et al., 2008; Wilson et al., 2004). Moreover, low sedimentation in this bed, with a maximum of ~2 mg cm^{-2} d^{-1} throughout most of the year, may have been insufficient to affect rhodolith growth and weight change despite the presence or absence of bioturbators (Millar and Gagnon, 2018).

Regardless of bioturbator effect, a rhodolith extension rate of 0.541 mm y^{-1} in the present study is low, reflecting the predominantly cold-water systems in which Newfoundland rhodolith beds develop. Sub-zero sea temperatures during winter and early spring, when irradiance was also lowest (Blain and Gagnon, 2013; Han et al., 2019), likely depress rhodolith metabolism, limiting growth to the energy available in stored photosynthates (Hofmann et al., 2018; Williams et al., 2018). Rhodolith apical extension is

therefore higher in summer and fall (Williams et al., 2018), when sea temperature and irradiance both increase to annual peaks. Likewise, seasonal variation in temperature and light regimes are common across the polar and subpolar realms, and there too rhodolith extension rates are similarly low, ranging for example from 0.5 to 2.7 mm y^{-1} in Northern Europe (Bosence and Wilson, 2003; Büdenbender et al., 2011; Schäfer et al., 2011; Steneck and Adey, 1976). In comparison to the present study, Freiwald and Henrich (1994) showed a slightly higher extension rate of 0.6 to 1 mm y^{-1} in rhodolith-forming *L. glaciale* in Norway, whereas Kamenos et al. (2008) found an even lower rate of 0.146 to 0.156 mm y^{-1} in *L. glaciale* in Scotland. These interregional differences might be because of different environmental conditions or methods used to quantify growth. In tropical and sub-tropical seas, temperature and irradiance are typically much higher and more stable year round (Amado-Filho et al., 2012; Darrenougue et al., 2013; Foster, 2001; Frantz et al., 2000; Schäfer et al., 2011), resulting in higher rhodolith extension rates than in polar and subpolar beds (Freiwald and Henrich, 1994). For example, *L. congestum* in Bermuda (Steneck and Adey, 1976) and *L. margaritae* in the Gulf of California (Steller et al., 2007) can grow as fast as 5 mm y^{-1}.

Interregional differences are also observed in reported rhodolith weight change, directly related to the amount of rhodolith tissue added or lost. Weight loss in polar and subpolar systems can occur at a faster rate than in temperate and tropical ones because cold water can accelerate dissolution of carbonate skeleton or usage of starch reserves by rhodoliths (Foster, 2001; Freiwald and Heinrich, 1994). Without chemical composition analyses, we cannot distinguish loss from $CaCO_3$ or organic components. Accordingly, rhodolith carbonate production rate typically decreases during winter, likely as a result of

seasonal decline in photoperiod and sea temperature (Freiwald and Heinrich, 1994; Han et al., 2019; Schafer et al., 2011). As predicted, in our study dry weight increased similarly in live-stained and live-unstained rhodoliths, by 1.64 g y^{-1}, but decreased in dead rhodoliths, by 0.73 g y^{-1}. Processes causing weight loss were not investigated but likely included microbioerosion, dissolution of carbonates, degradation of starch granules, and maceration of proteins by microorganisms as seen in other rhodolith beds (Bosence, 1983; Canals and Ballesteros, 1997; Freiwald, 1998; Halfar and Riegl, 2013; Krayesky-Self et al., 2016; Nitsch et al., 2015; Riosmena-Rodríguez et al., 2012; Schonberg et al., 2017). Abrasion and fragmentation of rhodolith tissue from wave- and current-induced displacement or rhodoliths can also cause weight loss (Nelson et al., 2012; New Zealand Department of Conservation, 2011). However, the bed studied is characterized by chronic low flow speeds of 0.001 to 0.301 m s^{-1} under normal sea conditions, which is insufficient to move rhodoliths (Millar and Gagnon, 2018). No rhodoliths in seabed or raised cages exhibited significant breakage, indicating that the bulk of observed weight loss in dead rhodoliths was caused by a combination of the biological and chemical processes mentioned above.

2.4.2 Comparing $CaCO_3$ production of St. Philip's rhodoliths to worldwide estimates

Gross and net rhodolith $CaCO_3$ production rates in the present study are estimated to be 806.13 ± 25.05 and 196.16 ± 7.31 g $CaCO_3$ m^{-2} y^{-1}, respectively, similar to those reported in European beds (Norway, UK, France) ranging from 84 to 1430 g m^{-2} y^{-1} (Bosence, 1983; Freiwald and Henrich, 1994; Potin et al., 1990), and lower than reported sub-tropical and tropical beds (Table 2.3, Figure 2.8) (Amado-Filho et al., 2012; Edyvean and Ford, 1987; El Haïkali et al., 2004; Schäfer et al., 2011; Stearn et al., 1977; Teichert

Table 2.3 Comparison of gross and net $CaCO_3$ production rates of rhodolith-forming, red coralline algae from polar to tropical realms as estimated with three different methods: apical extension, weight change, and total alkalinity. Carbonate realms are based on minimum local sea surface temperature (SST) as per James (1997) and James and Lukasik (2010). Temperatures with an asterisk (*) were not available from the study. They were calculated with ArcGIS 10.5 from AVHRR Pathfinder SST data extracted from NOAA's World Ocean Database (https://www.arcgis.com/home/webmap/viewer.html?webmap=bb7d1f1163724cdeae71fc2cb665fdab&fbclid) for the year in which the study was carried out. Pathfinder SST reports monthly SST averages across the year that each study took place. In such cases, minimum and maximum SST represent the lowest and highest monthly averages over the year.

Study	Location	Latitude	Minimum SST (°C)	Maximum SST (°C)	Carbonate realm	$CaCO_3$ production rate ($g\ m^{-2}\ y^{-1}$)	Method	Species	Gross/Net
1.[1] Teichert and Freiwald, 2014	Floskjeret, Svalbard	78.31°N	-0.8*	7*	Polar	757	Extension + density	*Lithothamnion glaciale*	Net
1.[2] Teichert and Freiwald, 2014	Krossfjorden, Svalbard	79.09°N	-1.2*	6.7*	Polar	637-652	Extension + density	*Lithothamnion glaciale*	Net
1.[3] Teichert and Freiwald, 2014	Mosselbukta, Svalbard	79.89°N	-1.6*	6.4*	Polar	684	Extension + density	*Lithothamnion glaciale*	Net
1.[4] Teichert and Freiwald, 2014	Nordkappbukta, Svalbard	80.53°N	-0.8*	5.4*	Polar	701-714	Extension + density	*Lithothamnion glaciale*	Net
2.[1] Freiwald and Henrich, 1994	Straumen Bioherm, Norway	69.67°N	3	16	Subpolar	420-630	Extension + weight of thalli	*Lithothamnion glaciale*	Net
2.[2] Freiwald and Henrich, 1994	Storvoll Reef, Norway	70.00°N	3	16	Subpolar	895-1432	Extension + weight of thalli	*Lithothamnion glaciale*	Net
3.[1] Present study	Newfoundland, Canada	47.59°N	-1	16	Subpolar	196	Weight change	*Lithothamnion glaciale*	Net
3.[2] Present study	Newfoundland, Canada	47.59°N	-1	16	Subpolar	806	Weight change	*Lithothamnion glaciale*	Gross
3.[3] Present study	Newfoundland, Canada	47.59°N	-1	16	Subpolar	163	Extension + biomass	*Lithothamnion glaciale*	Net
4. Bélanger and Gagnon (unpublished data)	Newfoundland, Canada	47.59°N	-1	16	Subpolar	170-495	Extension + biomass	*Lithothamnion glaciale*	Net
5.[1] Bosence, 1980	Mannin Bay, Ireland	53.46°N	8.1*	13.3*	Cold-temperate	29-164	Extension + weight of thalli	*Lithothamnion coralloides*	Net
5.[2] Bosence, 1980	Mannin Bay, Ireland	53.46°N	8.1*	13.3*	Cold-temperate	7-249	Extension + weight of thalli	*Lithothamnion calcareum*	Net
6. Bosence and Wilson, 2003	Mannin Bay, Ireland	53.46°N	8.1*	13.3*	Cold-temperate	200-1200	Extension + weight of thalli	*Lithothamnion coralloides*	Net
7.[1] Edyvean and Ford, 1987	Manorbier, Wales	51.64°N	6.3*	15.3*	Cold-temperate	380	Extension + density	*Lithophyllum incrustans*	Net
7.[2] Edyvean and Ford, 1987	West Angle Bay, Wales	51.69°N	7.1*	14*	Cold-temperate	60	Extension + density	*Lithophyllum incrustans*	Net
8. Martin et al., 2006	Bay of Brest, France	48.33°N	9.6	17.6	Cold-temperate	145-3100	Total alkalinity	*Lithothamnion coralloides*	Net
9. Martin et al., 2007	Bay of Brest, France	48.33°N	9.6	17.6	Cold-temperate	487	Total alkalinity	*Lithothamnion coralloides*	Net
10. Potin et al., 1990	Bay of Brest, France	48.35°N	8.4*	17.9*	Cold-temperate	876	Weight change	*Lithothamnion coralloides*	Gross
11. El Haikali et al., 2004	Marseille, France	43.28°N	13	17	Warm-temperate	5037	Total alkalinity	*Corallina elongata*	Net
12. Canals and Ballesteros, 1997	Mallorca-Menorca, Spain	40.50°N	13.2*	26.4*	Warm-temperate	210-289	Weight change	*Lithophyllum* sp.	Gross
13. Savini et al., 2012	Tyrrhenian Sea, Italy	40.30°N	15	27	Warm-temperate	90	Weight + density	*Lithothamnion coralloides*	Gross
14. Amado-Filho et al., 2012	Abrolhos Shelf, Brazil	19.75°S	18	24	Warm-temperate	300-2700	Extension + density	Various rhodolith species	Gross
15. Gherardi, 2004	Arvoredo Island, Brazil	27.25°S	17	21	Warm-temperate	55-136	Extension + weight of nodules in grabs	*Lithophyllum* sp.	Net
16.[1] Walker and Woelkerling, 1988	Shark Bay, Australia	25.50°S	20.4*	27.5*	Sub-tropical/Tropical	35-295	Total alkalinity	*Fosliella* sp.	Net
16.[2] Walker and Woelkerling, 1988	Shark Bay, Australia	25.50°S	20.4*	27.5*	Sub-tropical/Tropical	50-526	Weight change	*Fosliella* sp.	Gross
17.[1] Schafer et al., 2011	Gulf of Panama	07.60°N	21.2*	29.4*	Sub-tropical/Tropical	23	Extension + weight of nodules in grabs	*Lithothamnion* sp.	Net
17.[2] Schafer et al., 2011	Gulf of Chiriqui	08.00°N	28.2*	30*	Sub-tropical/Tropical	81	Extension + weight of nodules in grabs	*Lithothamnion* sp.	Net
18.[1] Stearn et al., 1977	Barbados, Lesser Antilles	13.25°N	25.5*	28.8*	Sub-tropical/Tropical	1355	Extension + density	*Lithophyllum* sp.	Net
18.[2] Stearn et al., 1977	Barbados, Lesser Antilles	13.25°N	25.5*	28.8*	Sub-tropical/Tropical	1225	Extension + density	*Neogoniolithon* sp.	Net
18.[3] Stearn et al., 1977	Barbados, Lesser Antilles	13.25°N	25.5*	28.8*	Sub-tropical/Tropical	2378	Extension + density	*Porolithon* sp.	Net
18.[4] Stearn et al., 1977	Barbados, Lesser Antilles	13.25°N	25.5*	28.8*	Sub-tropical/Tropical	167	Extension + density	*Mesophyllum* sp.	Net
19. Agegian et al., 1988	Penguin Bank, Hawaii	21.13°N	23	26	Sub-tropical/Tropical	2100	Extension + density	*Porolithon onkodes*	Net
20.[1] Chisholm, 2000	Lizard Island, Australia	14.67°S	23	30	Sub-tropical/Tropical	1500	Total alkalinity	*Neogoniolithon conicum*	Net
20.[2] Chisholm, 2000	Lizard Island, Australia	14.67°S	23	30	Sub-tropical/Tropical	10 300	Total alkalinity	*Hydrolithon onkodes*	Net

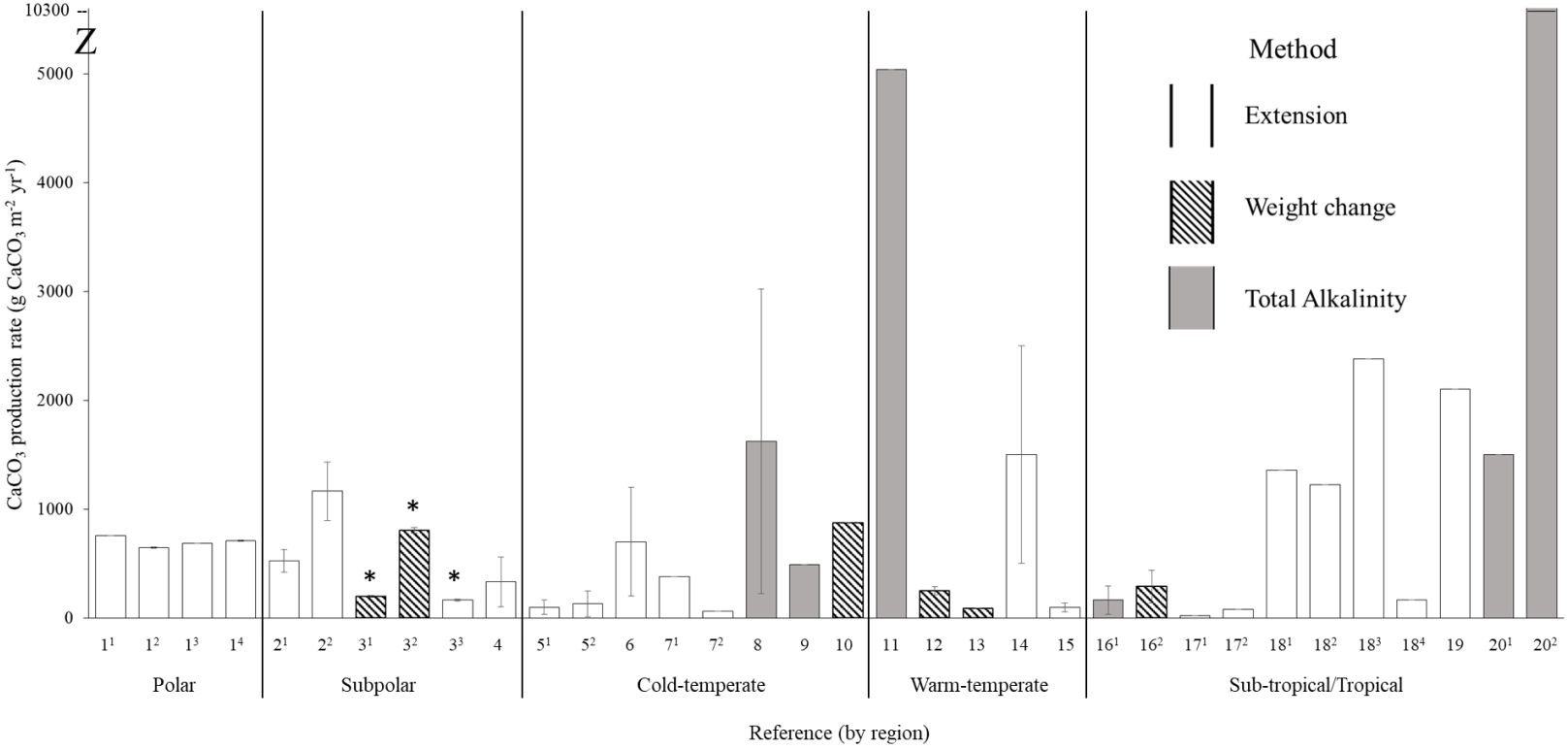

Figure 2.8 Worldwide $CaCO_3$ production rates (± SD) of rhodolith-forming, red coralline algae from polar to tropical regions as estimated with the three most common methods. Estimates from the present study are highlighted by an asterisk (*). Tropical to polar regions are defined as per carbonate realm classifications based on minimum SST by James (1997), and James and Lukasik (2010). Study numbers (references by region) correspond to those in Table 2.3.

and Freiwald, 2014). In oligotrophic tropical waters such as in the Caribbean, Brazil, and Hawaii, $CaCO_3$ production rates of coralline algae are highly variable, ranging from 167 to 2700 g $CaCO_3$ m^{-2} y^{-1} (Amado-Filho et al., 2012; Gherardi, 2004; Riosmena-Rodríguez et al., 2017; Schäfer et al., 2011; Stearn et al., 1977). Such variation may be caused by increased turbidity and sediment cover in some areas (e.g. Brazil), reducing photosynthetic rates by up to 70%, (Amado-Filho et al., 2012; Gherardi, 2004). Indeed, $CaCO_3$ production rates generally decrease with decreasing temperature and light availability, and hence with increasing water depth and turbidity (Bahia et al., 2010; Coletti et al., 2018; dos Reis et al., 2016; Pascelli et al., 2013; Sañé et al., 2016). The study by Freiwald and Henrich (1994) exemplifies this, as *L. glaciale* $CaCO_3$ production rate at greater depths of 18 m (895 g $CaCO_3$ m^{-2} y^{-1}), was just over half that of shallower depth estimates (~7 m, 1423 g $CaCO_3$ m^{-2} y^{-1}). These intra- and inter-regional differences are likely caused by differences in temperature and light regimes and/or the methods used to estimate $CaCO_3$ production (Table 2.3, Figure 2.8).

Our review of published estimates of $CaCO_3$ production rates in rhodolith-forming, red coralline algae revealed high intra- and inter-regional variability, with differences of up to two orders of magnitude in estimates from the same algal species but different methods (Table 2.3). Rhodolith age and extension rates are relatively easy to obtain from the literature, yet there are only a handful of studies which have quantified and used weight change to estimate carbonate production or compared this production from two or more methods of assessment. In the present study, net $CaCO_3$ production rate from the weight change method, 196.16 ± 7.31 g $CaCO_3$ m^{-2} y^{-1}, is similar to that from the apical extension method, 162.83 ± 8.40 g $CaCO_3$ m^{-2} y^{-1}. However, rhodolith age estimated from apical

extension (71.6 ± 10.1 y) was lower than the age derived from net weight change (115.0 ± 21.7 y), and higher than that from measurement of gross weight change (37.9 ± 8.4 y). These differences could be caused by net dry weight loss, including the loss of starch granules (Weykam et al., 1997; Wiencke et al., 2009) and to wet weight change, including absorption of water by organic matter. Short-term weight change (as measured in our study) could then overestimate carbonate loss due to seasonal loss of starch granules being allocated for growth in the low-light winter and spring seasons (Wiencke et al., 2009). Considering that rhodoliths in our study were first collected in April, some stored starch reserves might have been present (Weykam et al., 1997; Wiencke et al., 2009), in which case rhodolith dry weight loss (i.e. the difference between gross and net weight change) may have been greater than strictly inorganic calcium carbonate loss (Hofmann et al., 2018; Weykam et al., 1997; Wiencke et al., 2009).

Our rhodolith age estimates are comparable to those in subarctic *Clathromorphum compactum*, with 93-136 y (Adey et al., 2015, 2013) and *S. durum*, with ≤ 60 y (Goldberg and Heine, 2008). Yet, our different ages among rhodoliths from a same bed indicate that employing different methods, in occurrence apical extension and weight change, can under- or over-estimate age by up to three times. In fact, extension rate and weight change of live-stained rhodoliths were not correlated in the present study. Likewise, the total alkalinity method (which we did not test) yielded consistently higher estimates than the extension and weight change methods, with tropical $CaCO_3$ estimates of up to 10 300 g $CaCO_3$ m^{-2} y^{-1} (Chisholm, 2000). One possible explanation for the typically higher $CaCO_3$ estimates when using the latter method is that measurements from changes in total alkalinity (which are usually short-term) do not account for long-term seasonal variation in addition of carbonate

and sediment to marine systems, particularly in cold-water ones where a large portion of the carbonate that precipitates eventually dissolves (Chisholm, 2000; Smith and Mackenzie, 2016). Therefore, the method chosen largely drives disparity of worldwide rhodolith $CaCO_3$ estimates (Walker and Woelkerling, 1988). More data, gathered with several methods, are required for better assessment and comparison of $CaCO_3$ production rates to inform future rhodolith bed monitoring practices.

A caveat in comparing worldwide estimates is the general assumption that different coralline species and their corresponding thalli deposit $CaCO_3$ at the same rate, which is not often the case (Schäfer et al., 2017). Indeed, many reported species are encrusting (i.e. forming one continuous layer) and grow and calcify at lower rates than branched rhodolith-forming species, with extension rates as low as 0.1 to 0.4 mm y^{-1} (Adey et al., 2013). Slower growth rates of encrusting species lead to lower $CaCO_3$ production rates compared to branched rhodolith-forming species, like *L. glaciale* (Adey et al., 2013; Morgan and Kench, 2018; Steneck and Adey, 1976). Furthermore, a single rhodolith bed may be composed of different growth forms and species (common in warm-temperate to tropical environments), including encrusting and geniculate or non-geniculate coralline algae (Amado-Filho et al., 2012; Morgan and Kench, 2018; Pardo et al., 2017). Therefore, estimating $CaCO_3$ production rate of a multi-species rhodolith bed should consider the varying calcification rates of different morphologies and species.

2.4.3 Rhodolith importance as $CaCO_3$ bio-factories, and conservation implications

Globally, $CaCO_3$ production rate estimates of rhodolith beds are comparable to other large biogenic $CaCO_3$ producers (Andersson and Gledhill, 2013). Because high-

latitude rhodolith extension rates are low, particularly in *L. glaciale*, rhodoliths should be considered non-renewable ecosystem engineers, creating a complex habitat for a high biodiversity of species, similar to tropical coral reefs and cold-water coral forests (Basso et al., 2017; Coletti et al., 2017; Perry et al., 2018; Rossi et al., 2017). The high Mg-calcite skeleton of rhodoliths is more soluble than aragonite or low Mg-calcite, and thus even more vulnerable to ocean acidification (Basso and Granier, 2012; Comeau and Cornwall, 2017; Martin and Hall-Spencer, 2017; McCoy and Kamenos, 2015; Noisette et al., 2013).

Recent studies estimate that rhodoliths and other crustose coralline algae may begin to dissolve by 2040, when calcite saturation is predicted to fall below one (Doney et al., 2009), as calcification declines with increased acidification (Cornwall et al., 2017; James et al., 2014; McCoy and Ragazzola, 2014; Muñoz et al., 2018; Ragazzola et al., 2016). Slow growth of rhodoliths should lead to low resilience and inability to adapt to ocean acidification (Büdenbender et al., 2011; Martin and Gattuso, 2009). Cold-water corals compensate for ocean acidification by supplying metabolic energy to control internal pH (McCulloch et al., 2012), but their skeletons are affected post-mortem without metabolic influence. Williams et al. (2018) suggest a similar compensation may be possible in rhodoliths. Nonetheless, the large difference in gross and net $CaCO_3$ production rates shown in the present study suggest that while rhodoliths may still be able to grow under acidified conditions, this habitat may not be stable because of accelerated rate of dissolution, causing net $CaCO_3$ production rate to approach or exceed zero (Martin and Hall-Spencer, 2017). Future increased $CaCO_3$ dissolution of rhodolith beds may cause severe habitat loss for several species that use such beds for settlement and spawning (Büdenbender et al., 2011; Coletti et al., 2017), including polychaetes, echinoderms,

crustaceans, molluscs and fish (Gagnon et al., 2012; Steller and Foster, 1995). Although the effects of ocean acidification cannot be managed at a small scale, rhodolith beds must be protected (as in New Zealand; Nelson et al., 2012; Riosmena-Rodríguez et al., 2017) from stressors such as trawling, extraction, dredging, etc., to aid in sustaining these $CaCO_3$ bio-factories and biodiversity hotspots.

2.5 LITERATURE CITED

Adey, W.H., 1970. The effects of light and temperature on growth rates in boreal-subarctic crustose corallines. J. Phycol. 6(3): 269-276.

Adey, W.H., Halfar, J., Humphreys, A., Siskiewicz, T., Belanger, D., Gagnon, P., Fox, M., 2015. Subarctic rhodolith beds promote longevity of crustose coralline algal buildups and their climate archiving potential. Palaios 30, 281–293. https://doi.org/10.2110/palo.2014.075.

Adey, W.H., Halfar, J., Williams, B., 2013. The Coralline Genus *Clathromorphum* Foslie emend. Adey Biological, Physiological, and Ecological Factors Controlling Carbonate Production rate in an Arctic-Subarctic Climate Archive. Washington.

Agegian, C., Mackenzie, F., Tribble, J., Sabine, C., 1988. Carbonate production rate and flux from a mid-depth ecosystem, Penguin Back, Hawaii. In: Agegian CR (ed) Biogeochemical cycling and fluxes between the deep euphotic zone and other oceanic realms. National Undersea Research Program Reseach Report 88-1, NOAA, U.S. Dept. of Commerce. Washington, DC, pp 5-32.

Amado-Filho, G.M., Moura, R.L., Bastos, A.C., Salgado, L.T., Sumida, P.Y., Guth, A.Z., Francini-Filho, R.B., Pereira-Filho, G.H., Abrantes, D.P., Brasileiro, P.S., Bahia, R.G., Leal, R.N., Kaufman, L., Kleypas, J.A., Farina, M., Thompson, F.L., 2012. Rhodolith beds are major $CaCO_3$ bio-factories in the tropical south West Atlantic. PLoS One 7. https://doi.org/10.1371/journal.pone.0035171.

Andersson, A.J., Gledhill, D., 2013. Ocean Acidification and Coral Reefs: Effects on Breakdown, Dissolution, and Net Ecosystem Calcification. Ann. Rev. Mar. Sci. 5, 321–348. https://doi.org/10.1146/annurev-marine-121211-172241.

Bahia, R.G., Abrantes, D.P., Brasileiro, P.S., Pereira-Filho, G.H., Amado-Filho, G.M., 2010. Rhodolith bed structure along a depth gradient on the northern coast of Bahia state, Brazil. Brazilian J. Oceanogr. 58, 323–337.

Basso, D., 2012. Carbonate production rate by calcareous red algae and global change. Geodiversitas 34, 13–33. https://doi.org/10.5252/g2012n1a2.

Basso, D., Babbini, L., Ramos-Esplá, A.A., Salomidi, M., 2017. Mediterranean Rhodolith Beds, in: Riosmena-Rodriguez, R., Aquirre, J., Nelson, W. (Eds.), Rhodolith/Maerl

Beds: A Global Perspective. Springer Nature, Florida, pp. 281–298. https://doi.org/10.1007/978-3-319-29315-8_11.

Basso, D., Granier, B., 2012. Calcareous algae in changing environments. Geodiversitas 34, 5–11. https://doi.org/10.5252/g2012n1a1.

Blain, C., Gagnon, P., 2013. Interactions between thermal and wave environments mediate intracellular acidity (H_2SO_4), growth, and mortality in the annual brown seaweed *Desmarestia viridis*. J. Exp. Mar. Bio. Ecol. 440, 176–184. https://doi.org/10.1016/j.jembe.2012.12.013.

Blake, C., Maggs, C.A., 2003. Comparative growth rates and internal banding periodicity of maerl species (Corallinales, Rhodophyta) from northern Europe. Phycologia 42, 606–612. https://doi.org/10.2216/i0031-8884-42-6-606.1.

Bosence, D., Wilson, J., 2003. Maerl growth, carbonate production rates and accumulation rates in the northeast Atlantic. Aquat. Conserv. Mar. Freshw. Ecosyst. 13, S21–S31. https://doi.org/10.1002/aqc.565.

Bosence, D.W.J., 1983. Coralline algal reef frameworks. J. Geol. Soc. London 140, 365–376.

Bosence, D.W.J., 1976. Ecological studies on two unattached coralline algae from Western Ireland. Palaeontology 19, 365−395.

Brasileiro, P.S., Pereira-Filho, G.H., Bahia, R.G., Abrantes, D.P., Guimarães, S.M.P.B., Moura, R.L., Francini-Filho, R.B., Bastos, A.C., Amado-Filho, G.M., 2016. Macroalgal composition and community structure of the largest rhodolith beds in the world. Mar. Biodivers. 46. https://doi.org/10.1007/s12526-015-0378-9.

Büdenbender, J., Riebesell, U., Form, A., 2011. Calcification of the Arctic coralline red algae *Lithothamnion glaciale* in response to elevated CO_2. Mar. Ecol. Prog. Ser. 441, 79–87. https://doi.org/10.3354/meps09405.

Canals, M., Ballesteros, E., 1997. Production rate of carbonate particles by phytobenthic communities on the Mallorca-Menorca shelf, northwestern Mediterranean Sea. Deep Sea Res. Part II Top. Stud. Oceanogr. 44, 611–629. https://doi.org/10.1016/S0967-0645(96)00095-1.

Caragnano, A., Basso, D., Rodondi, G., 2016. Growth rates and ecology of coralline rhodoliths from the Ras Ghamila back reef lagoon, Red Sea. Mar. Ecol. 37, 713–726. https://doi.org/10.1111/maec.12371.

Cavalcanti, G.S., Gregoracci, G.B., Dos Santos, E.O., Silveira, C.B., Meirelles, P.M., Longo, L., Gotoh, K., Nakamura, S., Iida, T., Sawabe, T., Rezende, C.E., Francini-Filho, R.B., Moura, R.L., Amado-Filho, G.M., Thompson, F.L., 2014. Physiologic and metagenomic attributes of the rhodoliths forming the largest $CaCO_3$ bed in the South Atlantic Ocean. Int. Soc. Microb. Ecol. 8, 52–62. https://doi.org/10.1038/ismej.2013.133.

Chave, K.S., Smith, S.V., Roy, K.,1972. Carbonate production rate by coral reefs. Mar. Geol. 12, 123–140.

Chisholm, J.R.M., 2000. Calcification by crustose coralline algae on the northern Great Barrier Reef, Australia. Limnol. Oceanogr. 45, 1476–1484. https://doi.org/10.4319/lo.2000.45.7.1476.

Coletti, G., Basso, D., Corselli, C., 2018. Coralline algae as depth indicators in the Sommières Basin (early Miocene, Southern France). Geobios 51, 15–30. https://doi.org/10.1016/j.geobios.2017.12.002.

Coletti, G., Basso, D., Frixa, A., 2017. Economic Importance of Coralline Carbonates, in: Riosmena-Rodriguez, R., Aguirre, J., Nelson, W. (Eds.), Rhodolith/Maerl Beds: A Global Perspective. Springer Nature, Florida, pp. 87–101. https://doi.org/10.1007/978-3-319-29315-8_4.

Comeau, S., Cornwall, C.E., 2017. Contrasting effects of ocean acidification on coral reef "animal forests" versus seaweed "kelp forests". In: Marine Animal Forests (eds.), 1083-1108. http://doi.org/10.1007/978-3-319-21012-4_29.

Cornwall, C.E., Comeau, S., McCulloch, M.T., 2017. Coralline algae elevate pH at the site of calcification under ocean acidification. Glob. Chang. Biol. 23. https://doi.org/10.1111/gcb.13673.

Darrenougue, N., De Deckker, P., Payi, C., Eggins, S., Fallon, S., 2013. Growth and chronology of the rhodolith-forming, coralline red alga *Sporolithon durum.* Mar. Ecol. Prog. Ser. 474, 105–119. https://doi.org/10.3354/meps10085.

Denny, M.W., 1988. Biology and the mechanics of the wave-swept environment. Princeton University Press, Princeton.

Doney, S.C., Fabry, V.J., Feely, R.A., Kleypas, J.A., 2009. Ocean acidification: The other CO_2 problem. Ann. Rev. Mar. Sci. 1, 169–192. https://doi.org/10.1146/annurev.marine.010908.163834.

dos Reis, V.M., Karez, C.S., Mariath, R., de Moraes, F.C., de Carvalho, R.T., Brasileiro, P.S., Bahia, R. da G., Lotufo, T.M. da C., Ramalho, L.V., de Moura, R.L., Francini-Filho, R.B., Pereira-Filho, G.H., Thompson, F.L., Bastos, A.C., Salgado, L.T., Amado-Filho, G.M., 2016. Carbonate Production rate by Benthic Communities on Shallow Coralgal Reefs of Abrolhos Bank, Brazil. PLoS One 11, e0154417. https://doi.org/10.1371/journal.pone.0154417.

Edyvean, R.G.J., Ford, H., 1987. Growth Rates of *Lithophyllum incrustans* (Corallinales, Rhodophyta) from South West Wales. Br. Phycol. J. 22, 139–146.

El Haïkali, B., Bensoussan, N., Romano, J.C., Bousquet, V., Bousquet, V., 2004. Estimation of photosynthesis and calcification rates of *Corallina elongata* by measurements of dissolved oxygen, pH and total alkalinity. Sci. Mar. 68, 45–56. https://doi.org/10.3989/scimar.2004.68n145

Figueiredo, M.A.O., Coutinho, R., Villas-Boas, A.B., Tâmega, F.T.S., Mariath, R., 2012. Deep-water rhodolith productivity and growth in the southwestern Atlantic. J. Appl. Phycol. 24, 487–193. https://doi.org/10.1007/s10811-012-9802-8.

Foster, M.S., 2001. Rhodoliths: Between rocks and soft places. J. Phycol. 37, 659–667. https://doi.org/10.1046/j.1529-8817.2001.00195.x.

Frantz, B.R., Kashgarian, M., Coale, K.H., Foster, M.S., 2000. Growth rate and potential climate record from a rhodolith using 14C accelerator mass spectrometry. Limnol. Ocean. 45, 1773–1777. https://doi.org/10.4319/lo.2000.45.8.1773.

Freiwald, A., 1998. Microbial maceration and carbonate dissolution on cold-temperate shelves. Historical Biology 13(1), 27-35. https://doi.org/10.1080/08912969809386570.

Gagnon, P., Matheson, K., Stapleton, M., 2012. Variation in rhodolith morphology and biogenic potential of newly discovered rhodolith beds in Newfoundland and Labrador (Canada). Bot. Mar. 55, 85–99. https://doi.org/10.1515/bot-2011-0064.

Gherardi, D.F.M., 2004. Community structure and carbonate production rate of a temperate rhodolith bank from Arvoredo island, Southern Brazil. Brazilian J. Oceanogr. 52, 207–224.

Goldberg, N.A., Heine, J.N., 2008. Age estimates of *Sporolithon durum* (Corallinales, Rhodophyta) from Rottnest Island, Western Australia, based on radiocarbon-dating methods. J. Royal Society of W. Aus. 91(1), 27-30.

Halfar, J., Riegl, B., 2013. From coral framework to rhodolith bed: Sedimentary footprint of the 1982/1983 ENSO in the Galápagos. Coral Reefs 32, 985. https://doi.org/10.1007/s00338-013-1058-5.

Han, G., Ma, Z., Long, Z., Perrie, W., Chassé, J., 2019. Climate change on Newfoundland and Labrador shelves: results from a regional downscaled ocean and sea-ice model under an A1B forcing scenario 2011-2069. Atmospheric Ocean 57(1), 3-17. https://doi.org/10.1080/07055900.2017.1417110.

Harvey, A.S., Harvey, R.M., Merton, E., 2017. The distribution, significance and vulnerability of Australian rhodolith beds: a review. Mar. Freshw. Res. 68, 411–428. https://doi.org/10.1071/MF15434.

Hibino, K., Van Woesik, R., 2000. Spatial differences and seasonal changes of net carbonate accumulation on some coral reefs of the Ryukyu Islands, Japan. J. Exp. Mar. Bio. Ecol. https://doi.org/10.1016/S0022-0981(00)00214-8.

Hofmann, L.C., Schoenrock, K., de Beer, D., 2018. Arctic coralline algae elevate surface pH and carbonate in the dark. Front. Plant Sci. 9(1416), 1-12. https://doi.org/10.3389/fpls.2018.01416.

James, N.P., 1997. The cold-water carbonate depositional realm. In: James, N.P., Clarke, J.A.D. (Eds.), Cool-water Carbonates. Vol. 56. SEPM Special Publication, pp. 1–20.

James, N.P., Lukasik, J., 2010. Cool- and cold-water neritic carbonates. Facies Models 4. 371-399.

James, R.K., Hepburn, C.D., Cornwall, C.E., McGraw, C.M., Hurd, C.L., 2014. Growth response of an early successional assemblage of coralline algae and benthic diatoms to ocean acidification. Mar. Biol. 161. https://doi.org/10.1007/s00227-014-2453-3.

Jørgensbye, H.I.Ø., Halfar, J., 2017. Overview of coralline red algal crusts and rhodolith beds (Corallinales, Rhodophyta) and their possible ecological importance in Greenland. Polar Biol. https://doi.org/10.1007/s00300-016-1975-1.

Joshi, S., Duffy, G.P., Brown, C., 2017. Mobility of maerl-siliciclastic mixtures: Impact of waves, currents and storm events. Estuar. Coast. Shelf Sci. 189: 173-188. https://doi.org/10.1016/j.ecss.2017.03.018.

Kamenos, N., Cusack, M., Moore, P., 2008. Coralline algae are global paleothermometers with bi-weekly resolution. Geochimica et Cosmochimica Acta 72(3): 771-779. https://doi.org/10.1016/j.gca.2007.11.019.

Kamenos, N., Law, A., 2010. Temperature controls on coralline algae skeletal growth. J. Phycol. 46(2): 331-335. https://doi.org/10.1111/j.1529-8817.2009.00780.x.

Kleypas, J.A., Feely, R.A., Fabry, V.J., Langdon, C., Sabine, C.L., Robbins, L.L., 2006. Impacts of ocean acidification on coral reefs and other marine calcifiers: A guide for future research, report of a workshop held 18–20 April 2005, St. Petersburg, FL, sponsored by NSF, NOAA, and the U.S. Geological Survey, 88 pp.

Korczynski, P.C., Logan, J., Faust, J.E., 2002. Mapping monthly distribution of daily light integrals across the contiguous United States. Horttechnology 12(1): 12-16.

Krayesky-Self, S., Richards, J.L., Rahmatian, M., Fredericq, S., 2016. Aragonite infill in overgrown conceptacles of coralline *Lithothamnion* spp. (Hapalidiaceae, Hapalidiales, Rhodophyta): new insights in biomineralization and phylomineralogy. J. Phycol. 52, 161–173. https://doi.org/10.1111/jpy.12392.

Long, M.H., Rheuban, J.E., Berg, P., Zieman, J.C., 2012. A comparison and correction of light intensity loggers to photosynthetically active radiation sensors. Limnol. Oceanogr. Methods 10(6): 416-424. https://doi.org/10.4319/lom.2012.10.416.

Marrack, E.C., 1999. The relationship between water motion and living rhodolith beds in the southwestern Gulf of California, Mexico. Palaios 14, 159–171. https://doi.org/10.2307/3515371.

Martin, S., Castets, M.-D., Clavier, J., 2006. Primary production rate, respiration and calcification of the temperate free-living coralline alga *Lithothamnion corallioides*. Aquat. Bot. 85, 121–128. https://doi.org/10.1016/J.AQUABOT.2006.02.005.

Martin, S., Clavier, J., Chauvaud, L., Thouzeau, G., 2007. Community metabolism in temperate maerl beds. I. Carbon and carbonate fluxes. Mar. Ecol. Prog. Ser. 335, 19–29.

Martin, S., Gattuso, J.-P., 2009. Response of Mediterranean coralline algae to ocean acidification and elevated temperature. Glob. Chang. Biol. 15, 2089–2100. https://doi.org/10.1111/j.1365-2486.2009.01874.x.

Martin, S., Hall-Spencer, J., 2017. Effects of ocean warming and acidification on rhodolith/maërl beds. In: Riosmena-Rodriguez, R., Aquirre, J., Nelson, W. (Eds.), Rhodolith/Maerl Beds: A Global Perspective. Springer Nature, Florida, pp. 55-85. https://doi.org/10.1007/978-3-319-29315-8_11.

Matsuda, S., Iryu, Y., 2011. Rhodoliths from deep fore-reef to shelf areas around Okinawa-jima, Ryukyu Islands, Japan. Mar. Geol. https://doi.org/10.1016/j.margeo.2011.02.013.

McCoy, S.J., Kamenos, N.A., 2015. Coralline algae (Rhodophyta) in a changing world: integrating ecological, physiological, and geochemical responses to global change. J. Phycol. 51, 6–24. https://doi.org/10.1111/jpy.12262.

McCoy, S.J., Ragazzola, F., 2014. Skeletal trade-offs in coralline algae in response to ocean acidification. Nat. Clim. Chang. 4(8), 719-723. https://doi.org/10.1038/NCLIMATE2273.

McCree, K.J., 1973. The measurement of photsynthetically active radiation. Solar Energy 15(1) :83-87. https://doi.org/10.1016/0038-092X(73)90010-8.

McCulloch, M., Falter, J., Trotter, J., Montagna, P., 2012. Coral resilience to ocean acidification and global warming through pH up-regulation. Nat. Clim. Chang. 2(8), 623-627. https://doi.org/10.1038/NCLIMATE1473.

Millar, K.R., Gagnon, P., 2018. Mechanisms of stability of rhodolith beds: sedimentological aspects. Mar. Ecol. Prog. Ser. 594, 65–83. https://doi.org/10.3354/meps12501.

Morgan, K.M., Kench, P.S., 2018. New rates of Indian ocean carbonate production rate by encrusting coral reef calcifiers: periodic expansions following disturbance influence reef-building and recovery. Marine Geology 390, 72-79. https://doi.org/10.1016/J.MARGEO.2017.06.001.

Muñoz, P.T., Sáez, C.A., Martínez-Callejas, M.B., Flores-Molina, M.R., Bastos, E., Fonseca, A., Gurgel, C.F.D., Barufi, J.B., Rörig, L., Hall-Spencer, J.M., Horta, P.A., 2018. Short-term interactive effects of increased temperatures and acidification on the calcifying macroalgae *Lithothamnion crispatum* and *Sonderophycus capensis*. Aquat. Bot. 148, 46–52. https://doi.org/10.1016/j.aquabot.2018.04.008.

Nelson, W.A., Neill, K., Farr, T., Barr, N., Miller, A.S., Stewart, R., 2012. Rhodolith Beds in Northern New Zealand: Characterisation of Associated Biodiversity and Vulnerability to Environmental Stressors New Zealand Aquatic Environment and Biodiversity. Wellington.

New Zealand Department of Conservation, The Ministry of Fisheries, 2011. Coastal marine habitats and marine protected areas in the New Zealand Territorial Sea: a broad scale gap analysis. Wellington.

Nitsch, F., Nebelsick, J.H., Bassi, D., 2015. Constructional and destructional patterns - void classification of rhodoliths from Giglio island, Italy. Palaios 30, 680–691. https://doi.org/10.2110/palo.2015.007.

Noisette, F., Duong, G., Six, C., Davoult, D., Martin, S., 2013. Effects of elevated pCO2 on the metabolism of a temperate rhodolith *Lithothamnion corallioides* grown under different temperatures. J. Phycol. https://doi.org/10.1111/jpy.12085.

Pardo, C., Barbara, I., Barreiro, R., Pena, V., 2017. Insights into species diversity of associated crustose coralline algae (Corallinophycidae, Rhodophyta) with Atlantic Eurpean maerl beds using DNA barcoding. Anales Jard. Bot. Madrid 74(2), e059. https://dx.doi.org/10.3989/ajbm.2459.

Parrish, C.C., Thompson, R.J., Diebel, D., 2005. Lipid classes and fatty acids in plankton and settling matter during the spring bloom in a cold ocean costal environment. Mar. Ecol. Prog. Ser. 286: 57-68. https://doi.org/10.3354/meps286057.

Pascelli, C., Riul, P., Riosmena-Rodríguez, R., Scherner, F., Nunes, M., Hall-Spencer, J.M., Oliveira, E.C. de, Horta, P., 2013. Seasonal and depth-driven changes in rhodolith bed structure and associated macroalgae off Arvoredo island (southeastern Brazil). Aquat. Bot. https://doi.org/10.1016/j.aquabot.2013.05.009.

Pereira-Filho, G.H., Amado-Filho, G.M., de Moura, R.L., Bastos, A.C., Guimarães, S.M.P.B., Salgado, L.T., Francini-Filho, R.B., Bahia, R.G., Abrantes, D.P., Guth, A.Z., Brasileiro, P.S., 2012. Extensive Rhodolith Beds Cover the Summits of Southwestern Atlantic Ocean Seamounts. J. Coast. Res. https://doi.org/10.2112/11T-00007.1.

Perez, D.I., Phinn, S.R., Roelfsema, C.M., Shaw, E., Johnston, L., Iguel, J., 2018. Primary production rate and calcification rates of algae-dominated reef flat and seagrass communities. Journal of Geophysical Research: Biogeosciences 123, 2362-2375. https://doi.org/10.1029/2017JGOD4241.

Perry, C.T., Alvarez-Filip, L., Graham, N.A.J., Mumby, P.J., Wilson, S.K., Kench, P.S., Manzello, D.P., Morgan, K.M., Slangen, A.B.A., Thomson, D.P., Januchowski-Hartley, F., Smithers, S.G., Steneck, R.S., Carlton, R., Edinger, E.N., Enochs, I.C., Estrada-Saldívar, N., Haywood, M.D.E., Kolodziej, G., Murphy, G.N., Pérez-Cervantes, E., Suchley, A., Valentino, L., Boenish, R., Wilson, M., Macdonald, C., 2018. Loss of coral reef growth capacity to track future increases in sea level. Nature 558, 396–400. https://doi.org/10.1038/s41586-018-0194-z.

Perry, C.T., Edinger, E., Kench, P., Murphy, G., Smithers, S., Steneck, R., Mumby, P., 2012. Estimating rates of biologically driven coral reef framework production and erosion: a new census-based carbonate budget methodology and pplication to the reefs of Bonaire. Coral Reefs 31, 853-868. http://doi.org/10.1007/s00338-012-0901-4.

Perry, C.T., Murphy, G.N., Kench, P., Smithers, S., Edinger, E., Steneck, R., Mumby, P., 2013. Caribbean-wide decline in carbonate production threatens coral reef growth. Nature Communications 4(1402). https://doi.org/10.1038/ncomms2409.

Perry, C.T., Spencer, T., Kench, P.S., 2008. Carbonate budgets and reef production rate states: a geomorphic perspective on the ecological phase-shift concept. Coral Reefs 27, 853-866. https://doi.org/10.1007/s00338-008-0418-z.

Potin, P., Floc'h, J.Y., Augris, C., Cabioch, J., 1990. Annual growth rate of the calcareous red alga *Lithothamnion corallioides* (Corallinales, Rhodophyta) in the Bay of Brest, France. Hydrobiologia 204, 263–267. https://doi.org/10.1007/BF00040243.

Quinn, G.P., Keough, M.J., 2002. Experimental design and data analysis for biologists, 1st ed. Cambridge University Press, Cambridge.

Ragazzola, F., Foster, L.C., Form, A., Anderson, P., Hansteen, T., Fietzke, J., 2012. Ocean acidification weakens the structural integrity of coralline algae. Global Change Biology 18 (9): 2804-2812. https://doi.org/10.1111/j.1365-2486-2012.02756x.

Ragazzola, F., Foster, L.C., Jones, C.J., Scott, T.B., Fietzke, J., Kilburn, M.R., Schmidt, D.N., 2016. Impact of high CO_2 on the geochemistry of the coralline algae *Lithothamnion glaciale*. Sci. Rep. 6. https://doi.org/10.1038/srep20572.

Rebelo, A.C., Johnson, M.E., Quartau, R., Rasser, M.W., Melo, C.S., Neto, A.I., Tempera, F., Madeira, P., Avila, S.P., 2018. Modern rhodoliths from the insular shelf of Pico in the Azores (Northeast Atlantic Ocean). Estuar. Coast. Shelf Sci. 210, 7-17. https://doi.org/10.1016/j.ecss.2018.05.029.

Riosmena-Rodríguez, R., López-Calderón, J.M., Mariano-Meléndez, E., Sánchez-Rodríguez, A., Fernández-Garcia, C., 2012. Size and distribution of rhodolith beds in the Loreto Marine Park: their role in coastal processes. J. Coast. Res. 28, 255–260. https://doi.org/10.2112/JCOASTRES-D-11T-00008.1.

Riosmena-Rodríguez, R., Nelson, W., Aguirre, J., 2017. Rhodolith/ Maërl Beds: A Global Perspective, 1st ed. Springer Nature, Florida.

Riul, P., Targino, C.H., Farias, J.D.N., Visscher, P.T., Horta, P.A., 2008. Decrease in *Lithothamnion* sp. (Rhodophyta) primary production rate due to the deposition of a thin sediment layer. J. Mar. Biol. Assoc. UK 88, 17–19. https://doi.org/10.1017/S0025315408000258.

Rossi, S., Bramanti, L., Gori, A., Orejas, C., 2017. Animal forests of the world: an overview. In: Marine Animal Forests (eds.), 1-28. http://doi.org/10.1007/978-3-319-21012-4_1.

Sañé, E., Chiocci, F.L., Basso, D., Martorelli, E., 2016. Environmental factors controlling the distribution of rhodoliths: An integrated study based on seafloor sampling, ROV and side scan sonar data, offshore the W-Pontine Archipelago. Cont. Shelf Res. 129, 10–22. https://doi.org/10.1016/j.csr.2016.09.003.

Savini, A., Basso, D., Alice Bracchi, V., Corselli, C., Pennetta, M., 2012. Maerl-bed mapping and carbonate quantification on submerged terraces offshore the Cilento peninsula (Tyrhenian Sea, Italy). Geodiversitas 34, 77–98. https://doi.org/10.5252/g2012n1a5.

Schäfer, P., Fortunato, H., Bader, B., Liebetrau, V., Bauch, T., Reijmer, J.J.G., 2011. Growth rates and carbonate production rate by coralline red algae in upwelling and non-upwelling settings along the Pacific coast of Panama. PALAIOS 268, 420–432.

Schonberg, C.H.L., Fang, J.K.H., Carreiro-Silva, M., Tribollet, A., Wisshak, M., 2017. Bioerosion: the other ocean acidification problem. ICES J. Mar. Sci. 74(4), 895-925. http://doi.org/10.1093/icesjms/fsw254.

Schwarz, A., Hawes, I., Andrew, N., Mercer, S., Cummings, V., Thrush, S., 2005. Primary production rate potential of non-geniculate coralline algae at Cape Evans, Ross Sea, Antarctica. Mar. Ecol. Prog. Ser. 294, 131–140. https://doi.org/10.3354/meps294131.

Smith, S.V., Mackenzie, F.T., 2016. The role of $CaCO_3$ reactions in the contemporary CO^2 cycle. Aquat. Geochem. 22, 153-175. https://doi.org/10.1007/s10498-015-9282-y.

Snedecor, G.W., Cochran, W.G., 1994. Statistical methods, 8th edition. Iowa State Univeristy Press, Ames, IA.

Sokal, R.R., Rohlf, F.J., 2012. Biometry: the principles and practice of statistics in biological research. 4th edition. W. H. Freeman and Co.: New York. 937 pp.

Stearn, C.W., Scoffin, T.P., Martindale, W., 1977. Calcium Carbonate Budget of a Fringing Reef on the West Coast of Barbados Part I—Zonation and Productivity. Bull. Mar. Sci. 27, 479–510.

Steller, D.L., Foster, M.S., 1995. Environmental factors influencing distribution and morphology of rhodoliths in Bahia Concepcion B.C.S., Mexico. J. Exp. Mar. Bio. Ecol. 194, 201–212.

Steller, D.S., Hernandez-Ayon, J.M., Riosmena-Rodriguez, R., Cabello Pasini, A., 2007. Efecto de la temperatura sobre las tasas de fotosintesis, crecimiento y calcification del alga coralina de vida libre *Lithophyllum margaritae*. Ciencias Marinas 33, 441-456.

Steneck, R.S., Adey, W.H., 1976. The Role of Environment in Control of Morphology in *Lithophyllum congestum*, a Caribbean Algal Ridge Builder. Bot. Mar. 19, 197–216. https://doi.org/10.1515/botm.1976.19.4.197.

Teichert, S., Freiwald, A., 2014. Polar coralline algal $CaCO_3$-production rates correspond to intensity and duration of the solar radiation. Biogeosciences 11, 833–842. https://doi.org/10.5194/bg-11-833-2014.

Vale, N.F., Amado-Filho, G.M., Braga, J.C., Brasileiro, P.S., Karez, C.S., Moraes, F.C., Bahia, R.G., Bastos, A.C., Moura, R.L., 2018. Structure and composition of rhodoliths from the Amazon River mouth, Brazil. J. South Am. Earth Sci. 84. https://doi.org/10.1016/j.jsames.2018.03.014.

Van Der Heijden, L.H., Kamenos, N.A., 2015. Reviews and syntheses: Calculating the global contribution of coralline algae to total carbon burial. Biogeosciences 12, 6429–6441. https://doi.org/10.5194/bg-12-6429-2015.

Villas-Boas, A.B., Riosmena-Rodriguez, R., de Oliveira Figueiredo, M.A., 2014. Community structure of rhodolith-forming beds on the central Brazilian continental shelf. Helgol. Mar. Res. 68, 27–35. https://doi.org/10.1007/s10152-013-0366-z.

Walker, D.I., Woelkerling, W.J., 1988. Quantitative study of sediment contribution by epiphytic coralline red algae in seagrass meadows in Shark Bay, Western Australia. Mar. Ecol. Prog. Ser. 43, 71–77.

Weykam, G., Thomas, D.N., Wiencke, C., 1997. Growth and photosynthesis of the Antarctic red algae *Palmaria decipiens* (Palmariales) and *Iridaea cordata* (Gigartinales) during and following extended periods of darkness. Phycologia 36(5), 395-405. https://doi.org/10.2216/i0031-8884-36-5-395.1.

Wiencke, C., Gomez, I., Dunton, K., 2009. Phenology and seasonal physiological performance of polar seaweeds. Botanica Marina 52, 585-592. https://doi.org/10.1515/BOT.2009.078.

Williams, S., Adey, W., Halfar, J., Kronz, A., Gagnon, P., Bélanger, D., Nash, M., 2018. Effects of light and temperature on Mg uptake, growth, and calcification in the proxy climate archive *Clathromorphum compactum*. Biogeosciences 15, 5745–5759. https://doi.org/10.5194/bg-15-5745-2018.

Wilson, S., Blake, C., Berges, J.A., Maggs, C.A., 2004. Environmental tolerances of free-living coralline algae (maerl): implications for European marine conservation. Biol. Conserv. 120, 279–289. https://doi.org/10.1016/J.BIOCON.2004.03.001.

Yong, Y.S., Yong, W.T.L., Anton, A., 2013. Analysis of formulae for determination of seaweed growth rate. J. Appl. Phycol. 25, 1831-1834. https://doi.org/10.1007/s10811-013-0022-7.

CHAPTER III

SPATIAL VARIATION IN THE STRUCTURE OF A NEWFOUNDLAND RHODOLITH (*Lithothamnion glaciale*) BED ALONG ENVIRONMENTAL GRADIENTS

ABSTRACT

Rhodolith beds are internationally recognized as important benthic ecosystems, harbouring a large biodiversity of organisms. Rhodolith beds typically occur in areas with moderate hydrodynamic forces strong enough to remove sediment from rhodoliths, but not so strong as to cause fragmentation. Factors that drive rhodolith abundance have yet to be studied in Newfoundland rhodolith (*Lithothamnion glaciale*) beds. We quantified with a drop camera system, the abundance and distribution of rhodoliths and dominant bioturbators (*Strongylocentrotus droebachiensis* and *Asterias rubens*), along environmental gradients measuring depth, slope, and bottom type every 20 to 60 m over 3432 m^2 of seabed in southeastern Newfoundland, to gain knowledge about factors controlling distribution and abundance of rhodoliths in, and spatial limits of, rhodolith beds in subpolar systems. Sensors attached to the camera frame or at various locations on the seabed recorded light intensity, water temperature, current velocity, and water flow acceleration. Slope was the most influential factor driving rhodolith abundance, with high rhodolith abundances occurring on slopes below 7°. Rhodolith abundance increased under moderate light and temperature, being highest on bottoms composed of coarse sand, gravel, and dead rhodolith fragments. Flow acceleration did not vary significantly along a depth gradient, yet increased along a 610-m transect traversing the bed longitudinally at a depth of ~15 m. However, rhodolith abundance did not increase with flow acceleration. Bioturbator abundance was generally low throughout the bed and unrelated to rhodolith abundance. Results challenge the long-standing paradigm that water motion is a main factor determining the spatial limits of rhodolith beds.

3.1 INTRODUCTION

Local distribution of habitat-forming benthic communities such as kelp beds, coral reefs and rhodolith beds is determined by the interaction of several abiotic and biotic factors (McArthur et al., 2010; Peterson et al., 2018). Rhodolith beds are an important habitat-forming benthic community in coastal waters, as rhodoliths form structurally complex habitats that house a large diversity of species (Foster et al., 2013; Gabara et al., 2018; Harvey et al., 2017; Matsuda and Iryu, 2011). Rhodolith beds consist of lattices of living and dead unattached thalli of crustose coralline algae that contribute significantly to the global carbonate budget by sequestering carbon while forming their Mg-calcite skeletons (Amado-Filho et al., 2012; Bahia et al., 2010; Copeland et al., 2013; Jørgensbye and Halfar, 2017). Rhodolith beds have a worldwide distribution, and are generally found in the sub-tidal zone to depths exceeding 200 m, in areas of coarse sand, gravel or shell debris (Amado-Filho et al., 2012; Foster, 2001; Gagnon et al., 2012; Moura et al., 2016; Nelson et al., 2012). In tropical environments, rhodolith beds can be found at depths exceeding 200 m, while in temperate and polar areas, such as Europe and Eastern Canada, rhodoliths are mainly distributed at depths less than 30 m (Basso et al., 2017; Dutertre et al., 2015; Pereira-Filho et al., 2012; Teichert et al., 2014). Rhodolith beds can contain several different rhodolith species that are adapted to specific environmental conditions (Dutertre et al., 2015; Wilson et al., 2004). However, few studies have investigated the main drivers of rhodolith distribution and abundance within a bed (Dutertre et al., 2015; Foster, 2001; Melbourne et al., 2018; Steller and Foster, 1995). Limited knowledge on the subject has resulted in diverse and sometimes conflicting interpretations about rhodolith ecosystems.

The upper and lower bathymetric limits of rhodolith beds are thought to be driven by hydrodynamic forces, such as waves and currents. Hydrodynamic forces have substantial influence on the dynamics of shallow benthic communities, driving the zonation and distribution of subtidal species assemblages (Blain and Gagnon, 2013; Gaylord, 1999; Kraufvelin et al., 2010). Some species cannot withstand intense water motion, and can be dislodged or fragmented (Miller et al., 2007; Rebelo et al., 2018), while other species rely on fragmentation for transport and dispersal to enhance asexual reproduction (Freiwald, 1998). Within a rhodolith bed, it is assumed that moderate water motion is required to move/turn rhodoliths, to give the entire rhodolith equal access to light energy (Foster, 2001; Joshi et al., 2017; Marrack, 1999). Hydrodynamic forces would then limit the upper boundary of a rhodolith bed, as rhodoliths occurring in very shallow, high wave action areas would not survive the frequent fragmentation and dislodgement (Marrack, 1999; Rebelo et al., 2018; Savini et al., 2012).

Millar and Gagnon (2018) challenged the importance of current-driven water motion in the centre of a rhodolith bed through their study of sedimentation patterns in a *Lithothamnion glaciale* bed located in St. Philip's, Conception Bay, southeastern Newfoundland (Canada). They concluded that hydrodynamic forces were insufficient to move rhodoliths and that resident bioturbators, namely the brittle star, *Ophiopholus aculeata*, common sea star, *Asterias rubens*, and the green sea urchin, *Stronglyocentrotus droebachiensis*, contributed to dislodgement of sediment from rhodoliths, and therefore to the stability of the bed (Millar and Gagnon, 2018). Bioturbation is broadly defined as sediment transport processes executed by animals that stir and mix sediments, allowing for ventilation (Kristensen et al., 2012; Marrack, 1999; Riosmena-Rodríguez et al., 2017).

Bioturbators therefore prevent burial or smothering of rhodoliths (Adler et al., 2001; Ceccarelli et al., 2005; Chen et al., 2016; Pereira-Filho et al., 2015).

The lower rhodolith bed boundary is indirectly thought to be driven by hydrodynamic forces, through the process of sedimentation, combined with light attenuation. Wave-driven oscillatory water motion becomes diminished as depth increases, which causes sediment to settle on the seabed (Campos and Dominguez, 2010; Foster, 2001; Steller and Foster, 1995; Villas-Bôas et al., 2014). If such sediment falls onto rhodoliths, they become smothered and buried. Grall and Hall-Spencer (2003) showed that re-suspended sediment from dredging practices smothered rhodoliths and led them to die from lack of light penetration through the sediment. Suspended sediment can cloud sea water, blocking light that these autotrophic organisms need to photosynthesize (Campos and Dominguez, 2010; Griffin et al., 2008; Steller and Foster, 1995; Villas-Boas et al., 2014). Dense layers of fine sediment can also limit gaseous exchange occurring within rhodoliths, reducing their fitness (Riul et al., 2008; Wilson et al., 2004). Even though hydrodynamic forces, bioturbation, and sedimentation are thought to be the main drivers of vitality and boundaries of rhodolith beds, only a few studies have actually examined the relationships between abiotic and biotic factors and rhodolith bed structure (Dutertre et al., 2015; Foster, 2001; Martin et al., 2014; Melbourne et al., 2018; Steller and Foster, 1995).

To date, several abiotic and biotic factors other than hydrodynamic forces and sedimentation have been studied on how they affect different rhodolith species. For example, temperature often drives a rhodolith species' distribution as high temperatures often accelerate growth until a threshold is reached, which is dependent on the species observed (McCoy and Kamenos, 2015; Muñoz et al., 2018; Short et al., 2015). Light is also

an important species distribution driver, especially in photosynthetic organisms that need access to light energy (Coletti et al., 2018; Sañé et al., 2016). However, too much light, often in shallow, coastal areas, can cause UV damage to photosynthetic tissue (Drollet et al., 1993). Temperature and light often interact to determine species distribution as they co-vary with depth, where temperature and light diminish with increasing water depth. Characterized substrate or bottom type also varies with depth, with finer substrates like silt and mud often found at deeper depths, while bedrock and boulders are found in shallow depths (Brown et al., 2011; Copeland et al., 2013; Misiuk et al., 2018). Rhodoliths usually occur on finer substrates such as gravel, sand or mud, where the gravel is made up of live and dead rhodolith fragments (Sañé et al., 2016; Wilson et al., 2004). It is important to understand the factors that drive distribution and abundance as increasing climate change will highly influence rhodolith distribution in the near-future (Gabara et al., 2018; Melbourne et al., 2015; Perry et al., 2018; Peterson et al., 2018).

From the increasing influence of climate change, rhodolith beds will be subject to more frequent storm events that will increase hydrodynamic forces and therefore, re-suspend more sediment (Gunderson et al., 2016; Harborne et al., 2017; Nelson et al., 2012). In turn, stronger wave action would cause higher rates of abrasion and destruction of rhodoliths and rhodolith thalli, resulting in the deterioration or disappearance of rhodolith beds (Gabara et al., 2018; Hinojosa-Arango et al., 2009; Melbourne et al., 2018). Moreover, re-suspended sediment from storms will limit rhodolith access to light energy, leading them to die (Grall and Hall-Spencer, 2003; Hinojosa-Arango et al., 2009; Martin et al., 2014). As marine calcifiers, rhodoliths also face the challenge of ocean acidification, which could lead to high rates of dissolution in the future, as their Mg-calcite skeleton is relatively

soluble and thus highly vulnerable to ocean acidification (Basso and Granier, 2012; Büdenbender et al., 2011; McCoy and Ragazzola, 2014; Noisette et al., 2013). Future expedited rhodolith dissolution will destroy rhodolith habitats and the diversity among them (Doney et al., 2009; dos Reis et al., 2016; Kleypas et al., 2006; Nitsch et al., 2015).

Another challenge rhodolith beds face is destructive fishing practices, such as dredging and trawling (Barbera et al., 2003; Grall and Hall-Spencer, 2003). Dredging and trawling along beds for economically important organisms like scallops and fish causes re-suspension of sediments, which could lead to mass rhodolith death in areas where wave action and bioturbator presence is not sufficient enough to clear rhodoliths of sediment (Riosmena-Rodriguez et al., 2017). Studies that monitor rhodolith beds consistently subjected to dredging practices have shown little to no recovery over time, resulting in rhodolith bed loss (Barbera et al., 2003; Grall and Hall-Spencer, 2003; Riul et al., 2008; Sheehan et al., 2015). It is necessary for scientists to understand what drives rhodolith bed distribution to determine how climate change and destructive fishing practice stressors will impact these diverse ecosystems in the future.

Rhodoliths in Canada have been scarcely examined to date, with knowledge of the location and extent of beds incomplete. The rhodolith bed off St. Philip's, Conception Bay, southeastern Newfoundland has been studied intensively, using SCUBA-based detailed surveys over relatively small areas, but has yet to be mapped (Belanger and Gagnon, pers. comm.; Gagnon et al., 2012; Millar and Gagnon, 2018). The present study uses a drop camera survey, flow acceleration and temperature/illuminance loggers within and beyond the rhodolith bed in St. Philip's to (1) test the hypothesis that hydrodynamic forces, water temperature and light are the main factors influencing rhodolith abundance; and (2)

examine other abiotic and biotic factors, as well as factor interaction, that may also play a key role in influencing rhodolith abundance. It also (3) presents rhodolith distribution within and beyond known bed limits.

3.2 MATERIALS AND METHODS

3.2.1 Study Site

The study was carried out from March to November 2018 in a rhodolith bed (consisting of *Lithothamnion glaciale*) thought to occur at depths ranging from ~8 to 25 m off St. Philip's, in Conception Bay, Newfoundland, Canada (47.592° N, 52.893° W) (Figure 3.1). The boreal coastal Newfoundland climate is characterized by cool surface water temperatures (reaching <0°C in the late winter, and a maximum of ~ 14°C in the late summer), with high rainfall, and strongest storm conditions associated with occasional post-tropical storms in fall (Environment and Climate Change Canada, 2018). St. Philip's experiences moderate tidal currents and small amounts of fluvial discharge to the bay from the mouth of a river ~300 m away from the rhodolith bed. Conception Bay (Figure 3.1) is sheltered from south and east winds, however partially exposed to limited fetch northerly and westerly winds that demonstrate high variability over short time periods (Environment and Climate Change Canada, 2018; Millar and Gagnon, 2018). High wind variability makes Conception Bay an interesting site to investigate drivers of rhodolith distribution. Green sea urchins (*Stronglyocentrotus droebachiensis* [Figure 3.2A-B]), common sea stars (*Asterias rubens* [Figure 3.2C]), brittle stars (*Ophiopholus aculeata* and *Ophiura robusta* [Figure 3.2D]), and mottled red chitons (*Tonicella marmorea*) are common across the surface of the bed (Gagnon et al., 2012).

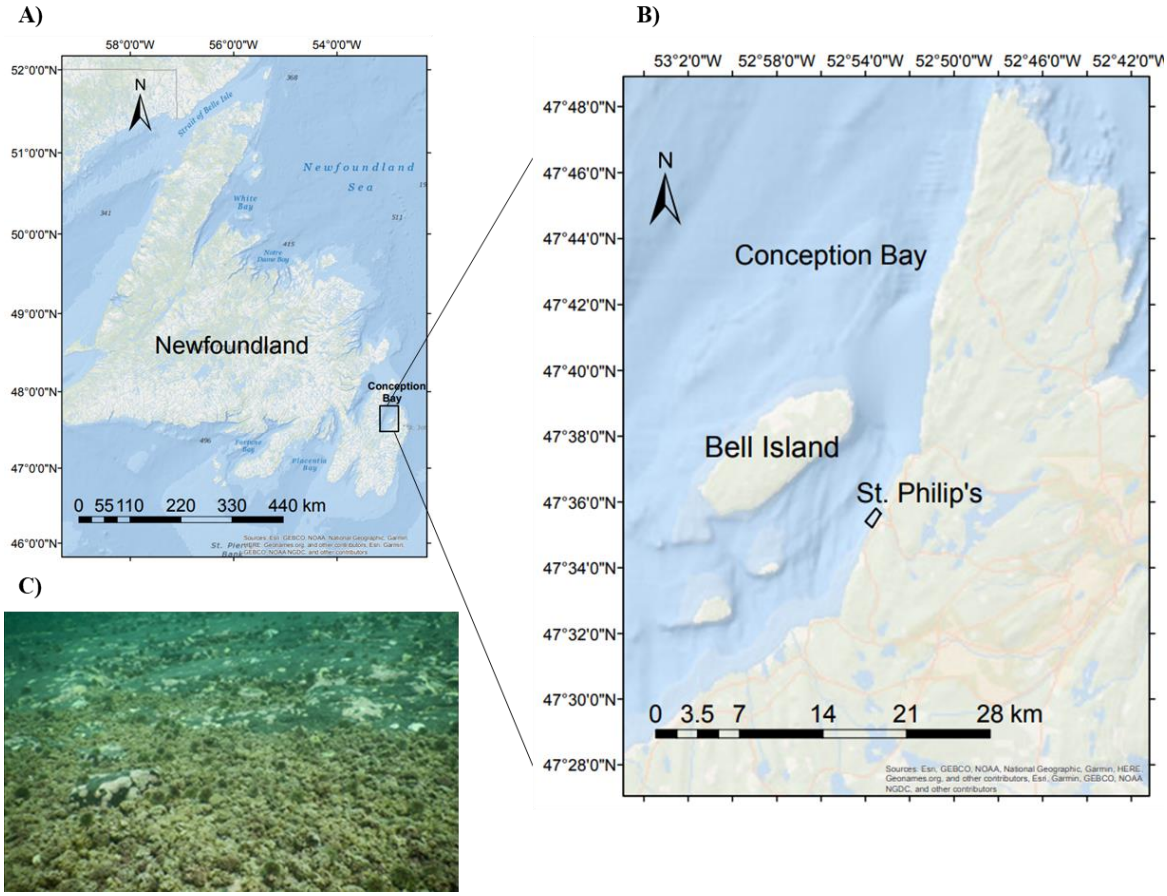

Figure 3.1 Map of a Newfoundland (**A**) rhodolith bed in St. Philip's, Conception Bay (**B**). Rhodolith bed location is indicated with the black outlined polygon in **B**. **C** displays rhodoliths within the St. Philip's rhodolith bed (photo by David Bélanger). Base maps obtained from GEBCO.

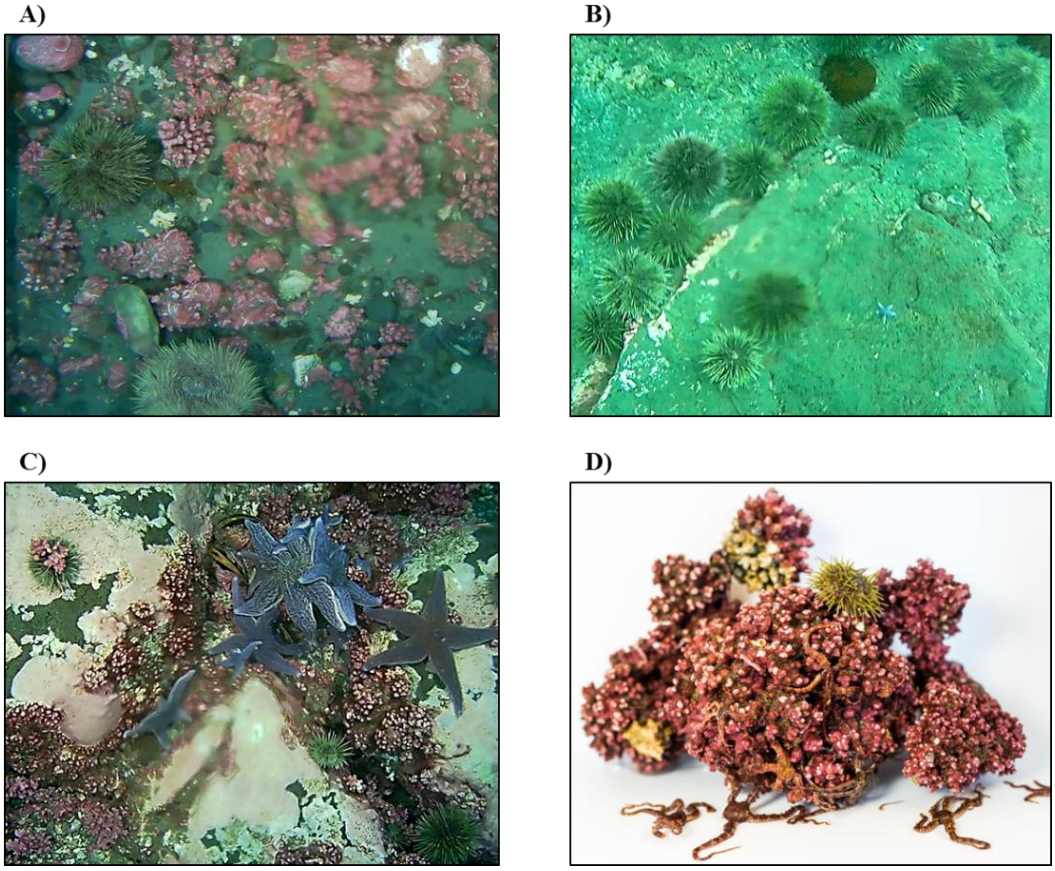

Figure 3.2 Dominant bioturbators in the St. Philip's study area, including the green sea urchin (*Stronglyocentrotus droebachiensis*) within the rhodolith bed (**A**) and on bedrock (**B**), sea stars (*Asterias rubens*) on top of rhodoliths and encrusted boulders (**C**), and brittle stars (*Ophiopholus aculeata* and *Ophiura robusta*) embedded within a rhodolith (**D**). Image **D** is courtesy of Sean Hacker-Teper, all other images by Laura Teed. Any blurriness in the centre of the imagery (**A-C**) is due to condensation.

3.2.2 Factors driving rhodolith abundance

3.2.2.1 Seafloor video

Drop camera surveys of the study area were conducted in Fall 2018 (October - November) with a surface-based GitUp Git2 drop video camera positioned in a stainless steel 50 cm x 50 cm x 97 cm frame, in which the camera was positioned ~52 cm from the bottom of the frame (Figure 3.3). On the upper corners of the frame (~61 cm above the bottom of the frame), three marine grade Kraken LED torches, outputting 650 lumens, were installed and positioned at a ~32° angle towards the center of the frame (Figure 3.3). Latex gloves were wrapped around each Kraken light in order to diffuse the light equally across the 50 x 50 cm quadrat at the bottom of the camera frame. Weights of 0.9 kg were also installed on the outside of each bottom corner of the metal frame to prevent tipping and to help maintain the frame's position once on the seafloor (Figure 3.3). The drop video camera was attached to a 121-m long cable reel (Shark Marine Technologies Inc.) attached to the boat and operated at the surface. The cable reel was then attached to the camera power source consisting of a 10-inch screen to observe video in real time. Seafloor video surveys were conducted from a 6-m rigid inflatable boat (RIB) vessel. Position of the survey vessel during linear transects was recorded at every drop of the camera to the seafloor via a Garmin eTrex-30 hand-geld GPS with an estimated horizontal accuracy of <3 m. This method assumes the camera system remains directly under the vessel, which limited data collection to calm wind/weather conditions.

Across the pre-determined polygon survey area (~3432 m^2), 497 sample stations were identified (Figure 3.4). This polygon was drawn to sample known areas of the

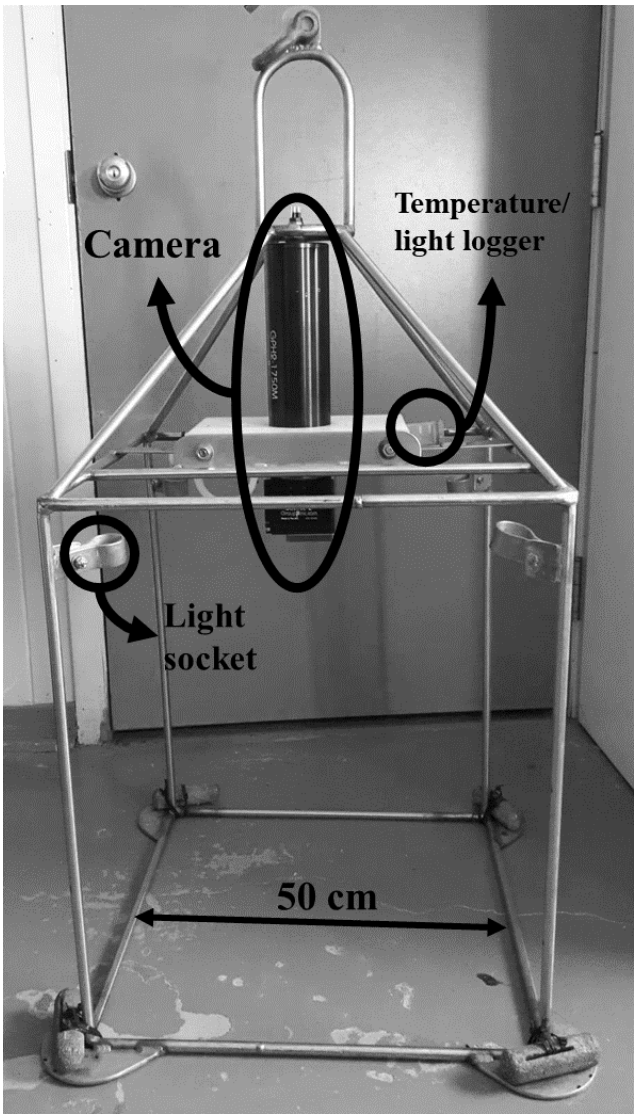

Figure 3.3 Drop camera stainless steel frame (50 cm x 50 cm x 97 cm) equipped with a GitUp Git2 camera suspended ~52 cm above the base of the frame. A temperature and light logger is located directly beside the suspended camera. Light sockets are located in each upper frame corner to house LED Kraken lights, and 0.9 kg weights are attached to each bottom frame corner to help the camera frame remain upright.

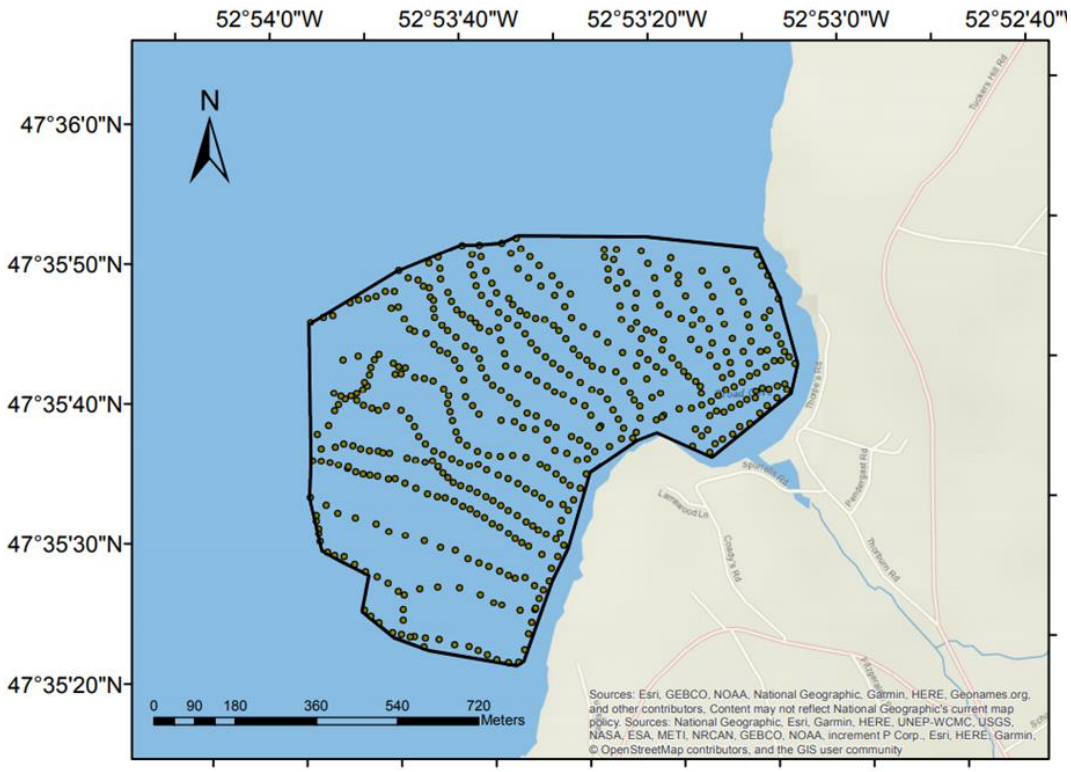

Figure 3.4 Area sampled during drop camera survey in and beyond known limits of the St. Philip's, Newfoundland rhodolith bed (~3432 m^2). Each point within the polygon represents a location where the camera system was lowered to the seabed, where a still image was extracted (n = 497).

rhodolith bed off St. Philip's (based on previous diver observations of rhodolith patches), as well as to explore beyond known rhodolith bed areas to determine if rhodoliths occur at greater depths and lateral gradients than previously observed. Linear transects ranged from ~250 (corners of polygon) to 1000 m in length (full width of polygon) with ~60 m between adjacent transects. Along any given transect, 2 to 10 second video samples (allowing time for sediment to settle) were collected approximately every 20 m (Figure 3.4).

From each underwater video segment where the camera frame was on the seafloor, a still image (.jpg) was extracted using Microsoft Photos at each sampling location. From each image, visible organisms were identified into groups for analysis including live rhodolith, dead rhodolith, encrusting coralline algae, urchin and sea star (combined to represent 'bioturbator' cover), as well as other not used in analysis (including bivalve, gastropod, crab, fish, as well as brown, red and green seaweed). Encrusting coralline algae was chosen to analyze effect on rhodolith abundance as the rhodolith form of *L. glaciale* often occurs from encrusting forms breaking off hard substrates to form rhodoliths. Therefore, an area of high encrusting *L. glaciale* abundance should correlate with high rhodolith abundance of the same species. Percent (%) cover was estimated using the point intercept method. A 7 x 7 grid was overlaid onto each bottom photo in ImageJ and the biotic or abiotic element present underneath each grid intercept was recorded. Using the 7 x 7 grid, 49 intercepts were recorded for each image, with each intercept accounting for ~2.04% cover. The outline of the 50 x 50 cm stainless steel frame was referenced for scale. There was ~6.18 cm between each point-intercept, corresponding to previously measured sizes of rhodoliths (~6 cm) in the St. Philip's bed (Gagnon et al., 2012). Dominant substrate of each image was also recorded for the seven most prevalent bottom types including:

bedrock, boulder, cobble, pebble, gravel, sand/silt (indistinguishable on seafloor video), and live rhodolith (patch so dense that underlaying substrate could not be differentiated) (Figure 3.5A-G). Percent cover of live rhodoliths, dead rhodoliths, bioturbators (urchins, sea stars), and encrusting coralline algae was determined for each sampling station and input into ArcGIS 10.5 according to the corresponding GPS coordinates matching the timestamp of each still image to characterize the sampling area.

3.2.2.2 Characterization of benthic habitats

Temperature and light loggers (Onset HOBO UA-002-64 Pendant Data Logger) were attached to the camera frame (at a height of ~70 cm from the seafloor, directly to the right and left of where the camera was suspended; Figure 3.3), and recorded temperature (°C) and illuminance (lux) every 2 s. Temperature and light readings were then extracted at each sampling location according to the time of the still image taken from the recorded underwater video. Temperature and light were averaged between the two HOBO pendant loggers, and input into ArcGIS 10.5 according to the corresponding GPS coordinate of each sampling station in order to help characterize the sampling polygon.

The reel cable attached to the camera was marked every meter in order to approximate depth at each sampling location. Depth measurements were then input into ArcGIS 10.5 across the polygon sampling area to estimate seafloor bathymetry. Seafloor bathymetry of the entire study area (~3432 m^2) was interpolated using the Empirical Bayesian Kriging tool (r^2 = 0.99) under the Geostatistical Analyst extension in ArcGIS 10.5. Geomorphometric variables (slope, and BPI – Bathymetric Position Index: inner

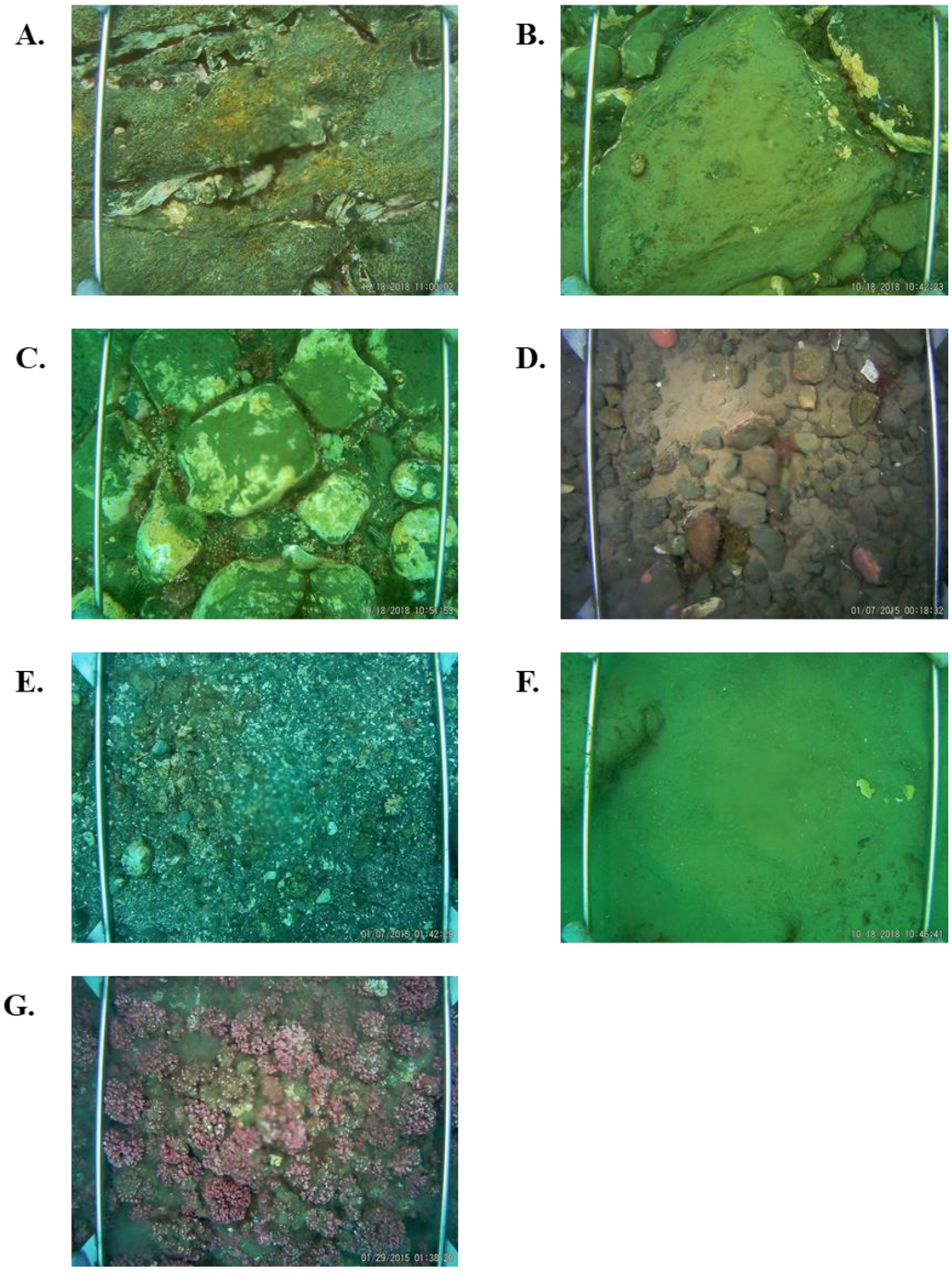

Figure 3.5 Bottom types observed in the St. Philip's study area. Quantified bottom types include bedrock (**A**), boulder (**B**), cobble (**C**), pebble (**D**), gravel (**E**), sand (**F**) and live rhodolith (**G**); where rhodoliths were so densely packed that the underlying bottom type could not be determined. Gravel and sand were often seen mixed with live and dead rhodolith fragments. Any blurriness in the centre of the imagery is due to condensation.

radius of 1m and outer radius of 5m, given the small spatial scale of the study area) were calculated from interpolated bathymetry using the Benthic Terrain Modeler extension. Geomorphometric variables were chosen for inclusion to capture relevant terrain attributes and assist in classifying rhodolith patches. BPI is derived from Topographic Position Index on land which recognizes crests (BPI > 0) and troughs (BPI < 0) in a landscape and defines them by measuring differences in surrounding areas (Secomandi et al., 2017; Weiss, 2001). In the marine environment, crests and troughs found on the seafloor using BPI can be indicative of sediment transport (Downie et al., 2016; Misiuk et al., 2018). BPI should therefore be considered when observing abiotic influence on rhodolith abundance, as rhodolith distribution is known to be influenced by sedimentation (Joshi et al., 2017, 2014; Wilson et al., 2004).

3.2.2.3 Waves and currents

To measure hydrodynamic forces at various locations in St. Philip's, modified underwater relative swell kinetic instruments (URSKIs) were used (Figurski et al. 2011; Figure 3.6). An URSKI is composed of a submersible accelerometer logger (Onset HOBO UA-004-64 Pendant G Data Logger) contained in a perforated cylindrical, 8-cm-long container positioned at one end of a sealed, positively buoyant, 90 cm ABS pipe (8 cm in diameter). The bottom end of the pipe was tethered with 18 cm twine to cinderblocks sitting on the rhodolith bed surface at depths of approximately 7 m, 15 m, and 22 m (approximately the upper, middle and lower limits of the St. Philip's rhodolith bed; Figure 3.6). URSKIs were also deployed across a lateral gradient of ~ 15m at the four following locations: south

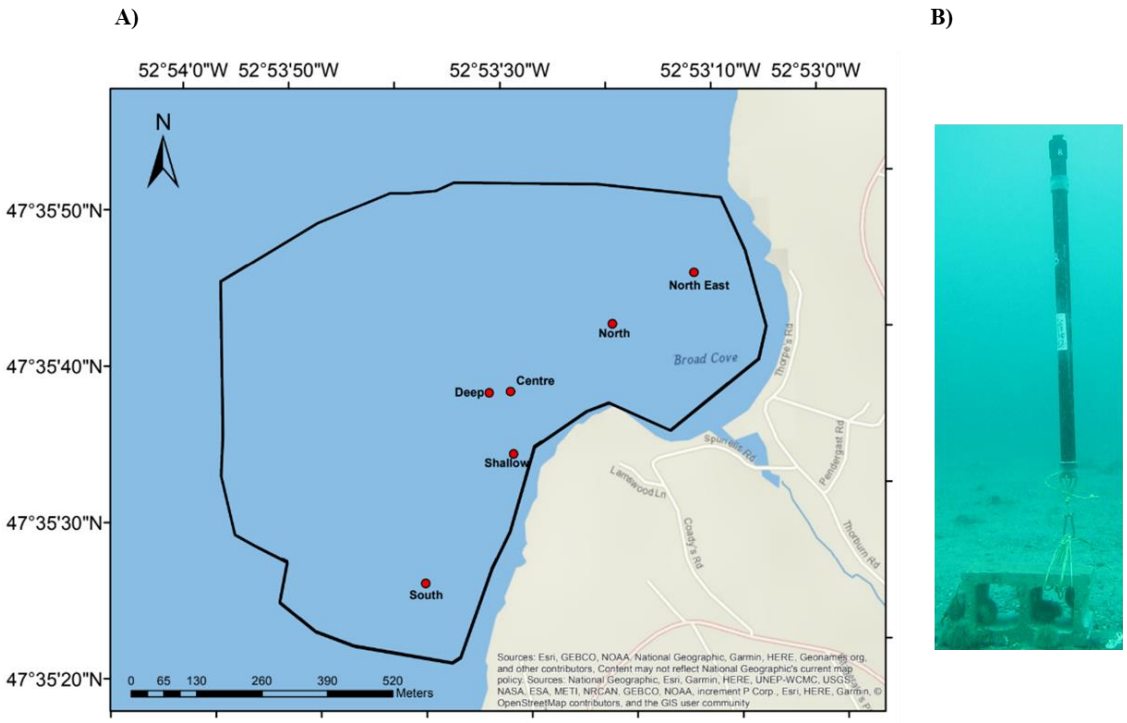

Figure 3.6 Location of deployed URSKIs (**A**) across lateral and depth gradients. **B** shows an URSKI deployed within the polygon (at the northeast location) attached to a cinderblock (photo by Patrick Gagnon).

of estimated rhodolith bed limits (i.e., beyond known bed limits), the previously estimated centre of the rhodolith bed, and north and northeast of bed limits (beyond known bed limits; Figure 3.6A). URSKI positions along the lateral gradient were determined using previously mapped near-shore bathymetry in St. Philip's during a small-scale multibeam survey (courtesy of K. Regular, unpublished data). In still water, URSKIs stand vertically in the water column with the accelerometer logger at the upper end, approximately 1.6 m above the seabed (19 cm-tall cinderblock, 18 cm twine, 1.25 m URSKI). If water is flowing, the upper/free end of the buoyant instrument (i.e. the accelerometer) will tilt at a speed, direction, and angle consistent with current water flow (Figure 3.6B). The accelerometer logger recorded instantaneous acceleration (m s^{-2}) in the x- (vertical), y- (horizontal) and z- (horizontal) directions every 2 min. The y- and z-direction data were used to calculate, by trigonometry, instantaneous acceleration vectors indicative of the horizontal (parallel to seabed) flow acceleration to which rhodoliths were exposed. The vertical axis (x) was not included in the analysis because of lack of vertical movement. Instantaneous flow accelerations were calculated using the following formula:

$$\text{Flow acceleration (m s}^{-2}) = \sqrt{y^2 + z^2}$$

From this data, mean hourly flow accelerations were calculated at each depth from 9 March to 17 July 2018. Laterally across the bed at a depth of ~15 m, mean hourly flow accelerations were calculated at each location (south, centre, north and northeast) from 12 October to 11 November 2018.

Accelerometer loggers were switched out monthly until 17 July 2018, and then again from 12 October to 11 November 2018 as each accelerometer only contained 30.1 days of memory (64 GB), recording at a 2-minute frequency. Due to weather and time constraints, accelerometer loggers across a depth gradient did not record continuously from 9 March to 17 July 2018. Instead, data was collected from 9 March to 8 April in the first deployment, 18 April to 18 May in the second deployment, 28 May to 19 June for the third deployment, and 19 June to 19 July 2018 for the fourth deployment. On 12 October 2018, three URSKIs were relocated across a lateral gradient at a depth of ~15 m and recorded continuously from 12 October to 11 November 2018.

Loggers were switched out with empty memory loggers by SCUBA divers. New loggers were attached to a second set of URSKI caps using a zip tie. The original set of URSKI caps with old loggers attached, were unscrewed from the URSKIs underwater, and collected in a plastic bag, labelled based on depth location (i.e., Shallow, Centre, and Deep). New caps, equipped with new loggers, were then removed from their respective plastic bags (labelled based on location), and screwed into the top of the URSKI. Once old loggers were removed, they were brought back to the Ocean Science Centre (OSC), where they were detached from URSKI logger caps and rinsed. Accelerometer data from the loggers was then acquired using HOBOwarePro, where data was readout in m s^{-2} and transferred into Microsoft Excel.

Since accelerometer loggers were >1 m above the rhodolith-covered seabed, rhodoliths may have been affected by weaker water flows than those recorded by the URSKIs (Denny, 1988; Denny and Wethey, 2001). Any difference in flow regimes was deemed insignificant because the current study was concerned with relative effects of

hydrodynamic forces (not absolute). As well, all rhodoliths were on the seabed, and therefore under the influence of similar flow patterns. Lunar cycles (tidal) and storm events (bidirectional wave motion from high winds) were reported to examine causes of high flow acceleration (Environment and Climate Change Canada, 2018).

To determine actual near-bottom current velocity, an Aquadrop acoustic Doppler current profiler (ADCP) was deployed in the previously identified center of the St. Philip's rhodolith bed from 16 February to 18 April 2018 (with slight movement in location on 9 March 2018 to match the centre URSKIS [Figure 3.6]). The ADCP recorded current velocity every 10 minutes for a 3-minute interval. ADCP data was extracted using MatLab. Current velocities (m s^{-1}) were extracted at 1.5 m from the seabed (bin 3), to match with position of underwater accelerometers in the water column. Current velocity was filtered to only include data from 9 March to 7 April 2018, the days correlating with the centre URSKI logger in order to perform a regression analysis and determine if current velocity could be predicted based on flow acceleration (Appendix C). Daily mean current velocities were recorded in the North and East directions (Appendix C).

3.2.3 Statistical analysis

With proven high accuracy (Diesing and Stephens, 2015; Downie et al., 2016; Redding et al., 2017; Stock et al., 2018), machine learning techniques can be used to determine which abiotic and biotic factors drive rhodolith abundance. The machine learning technique of Boosted Regression Tree (BRT) was used to determine the influence of predictor variables of depth, temperature, illuminance, bioturbator abundance, encrusting algae abundance, slope, and BPI on the response variable, rhodolith abundance.

This analysis was chosen based on BRT's ability to handle spatially autocorrelated data, which occurred in preliminary analyses based on a high number of data observations (497) occurring over a small spatial scale (~3432 m^2). BRT is able to reduce variance by combining many regression trees (1000 – 50 000 trees), approximating the function to be learned (response variable). BRT often outperforms other modelling methods by being insensitive to outliers, removing the assumption of independent observations (spatial autocorrelation), and removing unimportant variables (Elith et al., 2008; Misiuk et al., 2018; Stock et al., 2018). For live rhodolith abundance models, BRT models with a tree complexity of 5 were used, with a learning rate set to 0.005 and the bag fraction set to 0.5, as per recommended settings (Elith et al., 2008). All analyses were completed in RStudio Desktop 1.2 (R Core Team, 2014).

Rhodolith abundance models were built from the drop camera data of 497 sampling sites. The full model for BRT analyses of rhodolith cover included depth, temperature, illuminance, substrate class, encrusting algae abundance, bioturbator abundance, slope, and bathymetric position index (BPI). If variables contributed little influence (<10%) in explaining rhodolith abundance, a simplified model analysis was conducted, where variables contributing <10% influence were dropped from the model and the change in predicted deviance was calculated. If BRT results indicated that certain variables could be removed from the model, such variables were removed, and the model was re-run. If the resultant simplified model was less accurate than the original/full model (higher deviance), then the full model (which could explain more of the variance) was used. The R packages *gbm* (Ridgeway, 2006) and *dismo* (Elith and Leathwick, 2009) were used for BRT modeling.

For hourly means of flow acceleration (m s^{-2}) across a depth gradient, a two-way ANOVA with the fixed factor Depth (three Depth treatments: shallow, centre, and deep) and the continuous factor Date/Time (across 4-5-month deployment) was conducted to test the effect of Depth on the response variable, flow acceleration. The same analysis was conducted for flow acceleration across a lateral gradient, with the fixed factor Location (four Location treatments: south, centre, north, and northeast) and the continuous factor Date/Time (across a one-month deployment). In all ANOVAs, homogeneity of the variance, independence, and normality of residuals were verified by observing the distribution of residuals and the normal probability plot of the residuals. In ANOVAs, Tukey HSD post-hoc comparisons were conducted to detect significant differences among levels of depth and location factors. A significance level of 0.05 was used in all analyses. All analyses were carried out in RStudio Desktop 1.2 (R Core Team, 2014). All means were presented with 95% confidence intervals (means ± 95% CI), unless otherwise stated.

3.3 RESULTS

3.3.1 Characterization of benthic habitats

Images extracted from the drop camera survey totaled 497, with rhodolith cover, bottom type, bioturbator cover, encrusting algae cover, depth, temperature, light, slope and BPI estimated for each image. Rhodolith cover varied from 0% cover to 92%, across depths ranging from 6 to 46 m (maximum depth). However, rhodolith cover observed at shallow (6 m) and deep (46 m) depths was less than 20%. Any rhodolith abundance above or equal to 10% cover (yellow and red map area, with the blue map area representing rhodolith cover <10%) was deemed as part of the rhodolith bed (as per Basso et al. 2015; Nelson et al.

2012). The resultant map (Figure 3.7A) showed rhodoliths to be mostly distributed from 13.7 to 31.2 m depth (Figure 3.7B), with temperatures ranging from 6.22 to 9.76 °C (Figure 3.7C), and moderate to high illuminance (300 to 1500 lx) (Figure 3.7D), in areas with slope ranging from a 1.5 to 7.3° angle (Figure 3.7E). BPI within the rhodolith bed ranged from -22 to +10, with an average BPI of -2, indicating flat seabed (Figure 3.7F). Higher rhodolith cover was seen in areas with finer substrates, and encrusting algae seen in coarser substrates such as bedrock and boulders (Figure 3.7G). Encrusting coralline algae cover ranged from 4 to 67% within the rhodolith bed, predominantly in the southern portion of the sample area (Figure 3.7H). Dominant bioturbators observed on the surface of the seafloor included the green sea urchin (*Stronglyocentrotus droebachiensis*) and the common sea star (*Asterias rubens*) (Figure 3.2A-C). Other known bioturbators such as brittle stars (*Ophiopholus aculeata* and *Ophiura robusta*), could not be seen/accounted for in the images, as they embed themselves into rhodoliths and blend in (Figure 3.2D and 3.7I).

Rhodolith cover extended much further south than previously recorded, suggesting two separate rhodolith patches within the bed, with areas of moderate rhodolith cover in the south covering a 996 m^2 area (Figure 3.7A). The estimated size of the previously studied rhodolith patch off the coast of St. Philip's was 1005 m^2, with rhodolith cover reaching as high as 92% (Figure 3.7A). Areas outside of the rhodolith bed (less than 10% rhodolith cover, encompassing ~1431 m^2) extended from 4 to 114 m depth (Figure 3.7B), slope ranging from 0.004 to 63.37° (Figure 3.7E) temperatures ranging from 0.23 to 13.17 °C (Figure 3.7C), and illuminance approaching 0 at deep depths (Figure 3.7D).

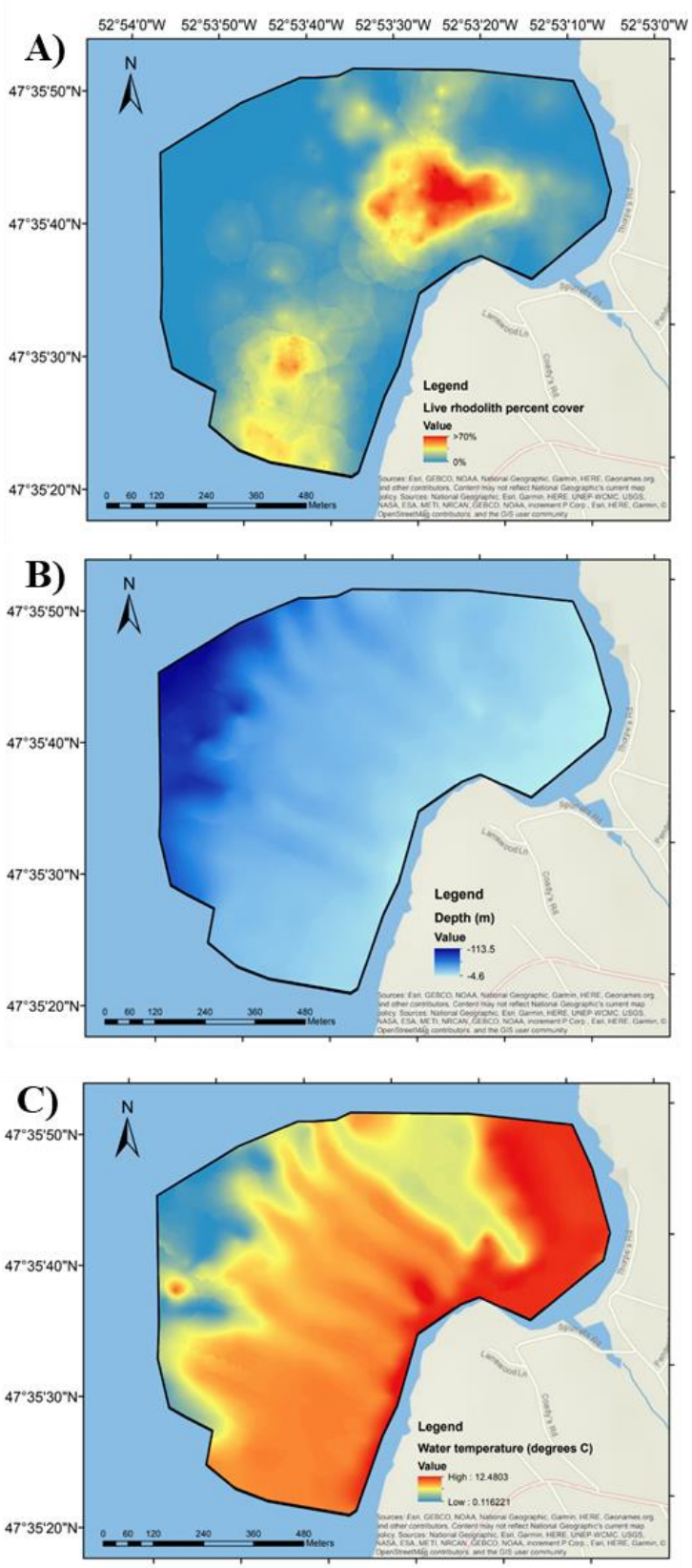
A)
52°54'0"W
52°53'50"W
52°53'40"W
52°53'30"W
52°53'20"W
52°53'10"W
52°53'0"W
47°35'50"N
47°35'40"N
47°35'30"N
47°35'20"N
N
Legend
Live rhodolith percent cover
Value
>70%
0%
0 60 120 240 360 480
Meters
B)
Legend
Depth (m)
Value
-113.5
-4.6
C)
Legend
Water temperature (degrees C)
Value
High : 12.4803
Low : 0.116221

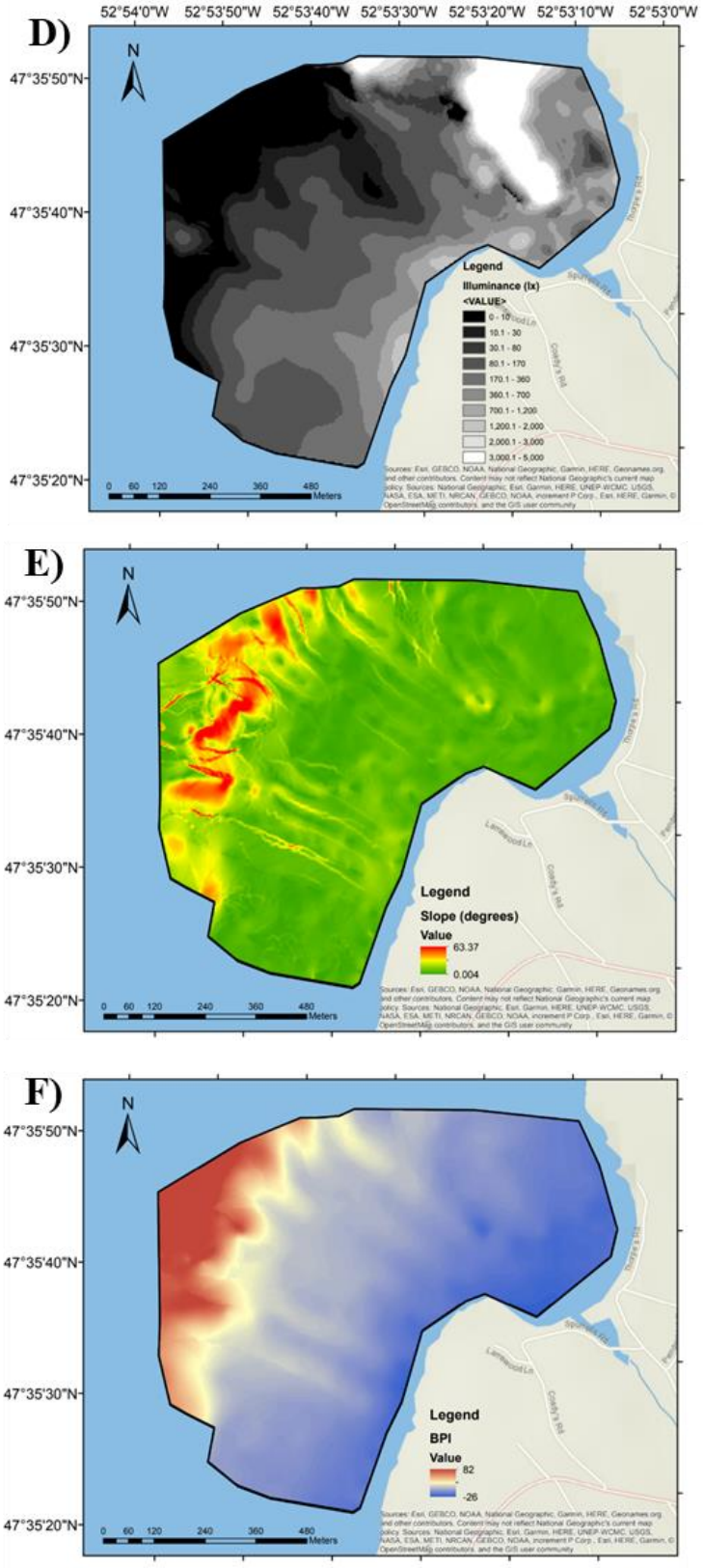
D)
52°54'0"W
52°53'50"W
52°53'40"W
52°53'30"W
52°53'20"W
52°53'10"W
52°53'0"W
47°35'50"N
47°35'40"N
47°35'30"N
47°35'20"N
N
Legend
Illuminance (lx)
<VALUE>
0 - 10
10.1 - 30
30.1 - 80
80.1 - 170
170.1 - 360
360.1 - 700
700.1 - 1,200
1,200.1 - 2,000
2,000.1 - 3,000
3,000.1 - 5,000
0 60 120 240 360 480
Meters
E)
Legend
Slope (degrees)
Value
63.37
0.004
F)
Legend
BPI
Value
82
-26

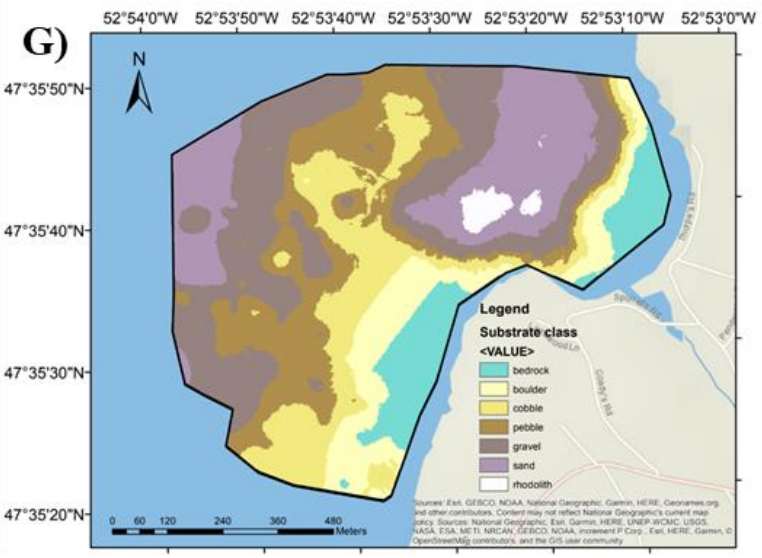
G)
52°54'0"W
52°53'50"W
52°53'40"W
52°53'30"W
52°53'20"W
52°53'10"W
52°53'0"W
47°35'50"N
47°35'40"N
47°35'30"N
47°35'20"N
N
Legend
Substrate class
<VALUE>
bedrock
boulder
cobble
pebble
gravel
sand
rhodolith
0 60 120 240 360 480
Meters

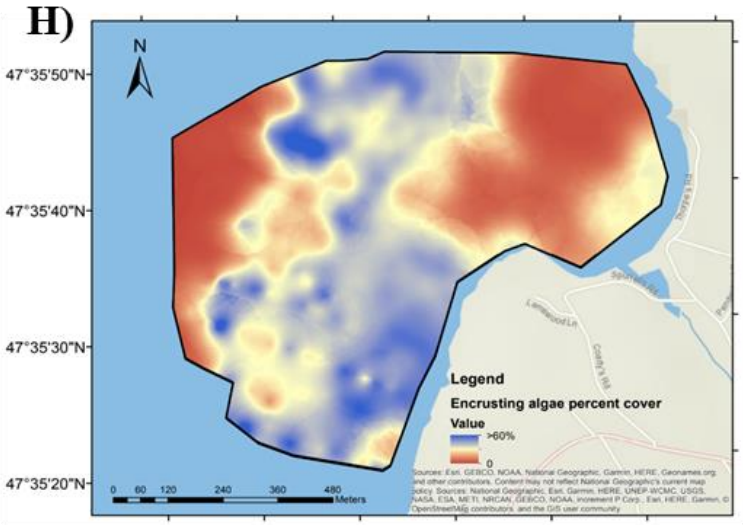
H)
47°35'50"N
47°35'40"N
47°35'30"N
47°35'20"N
N
Legend
Encrusting algae percent cover
Value
>60%
0
0 60 120 240 360 480
Meters

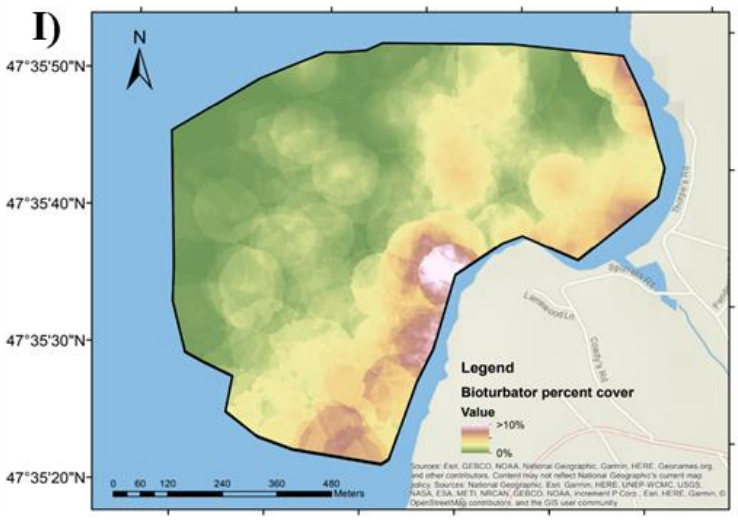
I)
47°35'50"N
47°35'40"N
47°35'30"N
47°35'20"N
N
Legend
Bioturbator percent cover
Value
>10%
0%
0 60 120 240 360 480
Meters

Figure 3.7 Distribution of rhodoliths across the St. Philip's survey area (3432 m^2), showing rhodolith abundance (in percent cover: **A**), water temperature (**C**), illuminance (**D**), slope of the seafloor (**E**), BPI (**F**), substrate/bottom type (**G**), encrusting coralline algae abundance (**H**), and bioturbator abundance (**I**). BPI interpretation at deeper depths was grainy, and therefore deemed untrustworthy at deep depths. Interpolated data completed using the Empirical Bayesian Kriging tool in ArcMap 10.5.

BRT results show that slope had the highest relative influence on live rhodolith cover (22.4%), followed by temperature (20.5%) and light (16.9%), both highly correlated with depth (Figure 3.8). The original model included depth, however the final model removed depth due to high co-linearity and correlation with temperature and light ($R^2 >$ 0.80; see Appendix D for temperature-depth profile as well as rhodolith abundance-depth profile). Furthermore, to reduce co-linearity of temperature and light, the residuals of temperature and illuminance were used. This increased model accuracy from 80 to 82%. As slope increased, rhodolith abundance decreased (Figure 3.9). Rhodolith abundance was highest in areas of moderate water temperature and illuminance. Rhodolith abundance increased in areas with negative BPI (indicating troughs), and as BPI approached 0 (indicating a gentle slope) (Figure 3.9). Rhodolith abundance decreased as encrusting coralline algae cover reached above 80% (Figure 3.9). In terms of substrate class, rhodoliths were most abundant in areas of finer sediment; i.e., in rounded gravel (2-4 mm in size) and sandy (<2 mm grain size) areas as well as in areas where no other substrate except live rhodoliths were observed. Bioturbator cover (the percent cover of bioturbators that could be observed on the surface of the rhodolith bed) was found to have the lowest relative influence on rhodolith abundance with 4.5% influence (Figure 3.8). Rhodolith abundance increased with low cover of bioturbators and then levelled off as bioturbator cover exceeded 13% (Figure 3.9). Even though bioturbator cover influence was low, it was kept in the model as the change in deviance once it was removed was high.

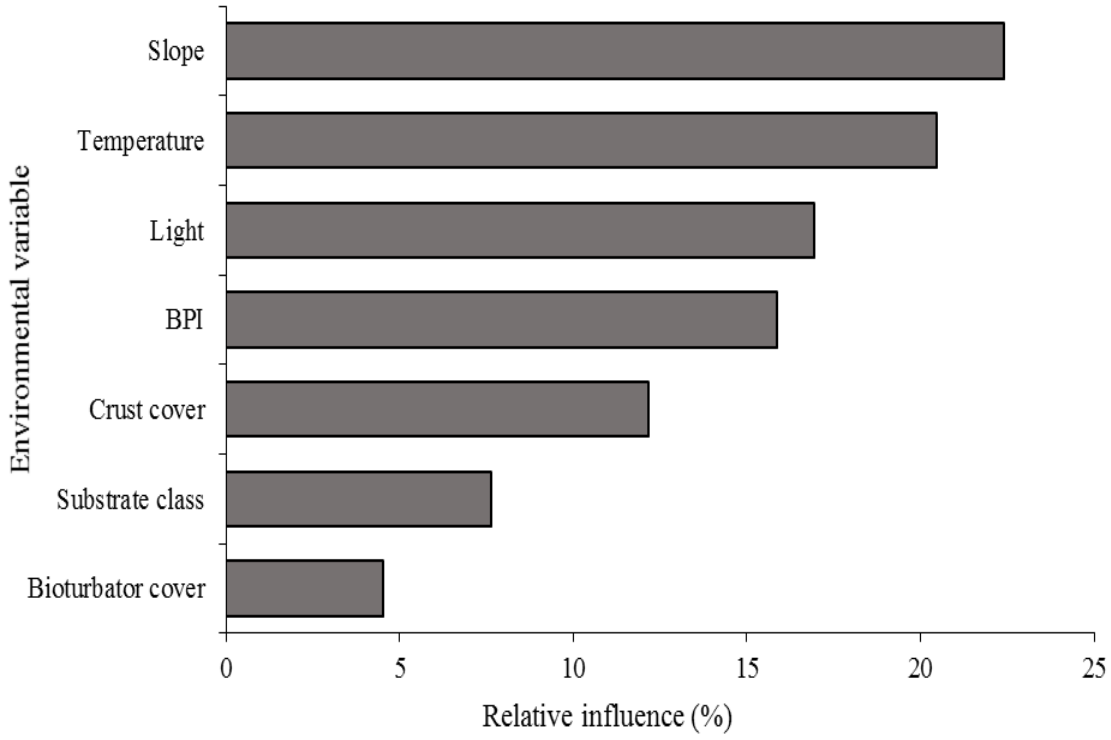

Figure 3.8 Relative influence (%) that each environmental variable (slope, temperature, light, BPI, encrusting algae percent cover, substrate class, and bioturbator percent cover) contributed to predicting live rhodolith cover. Model accuracy as presented by BRT is 82%.

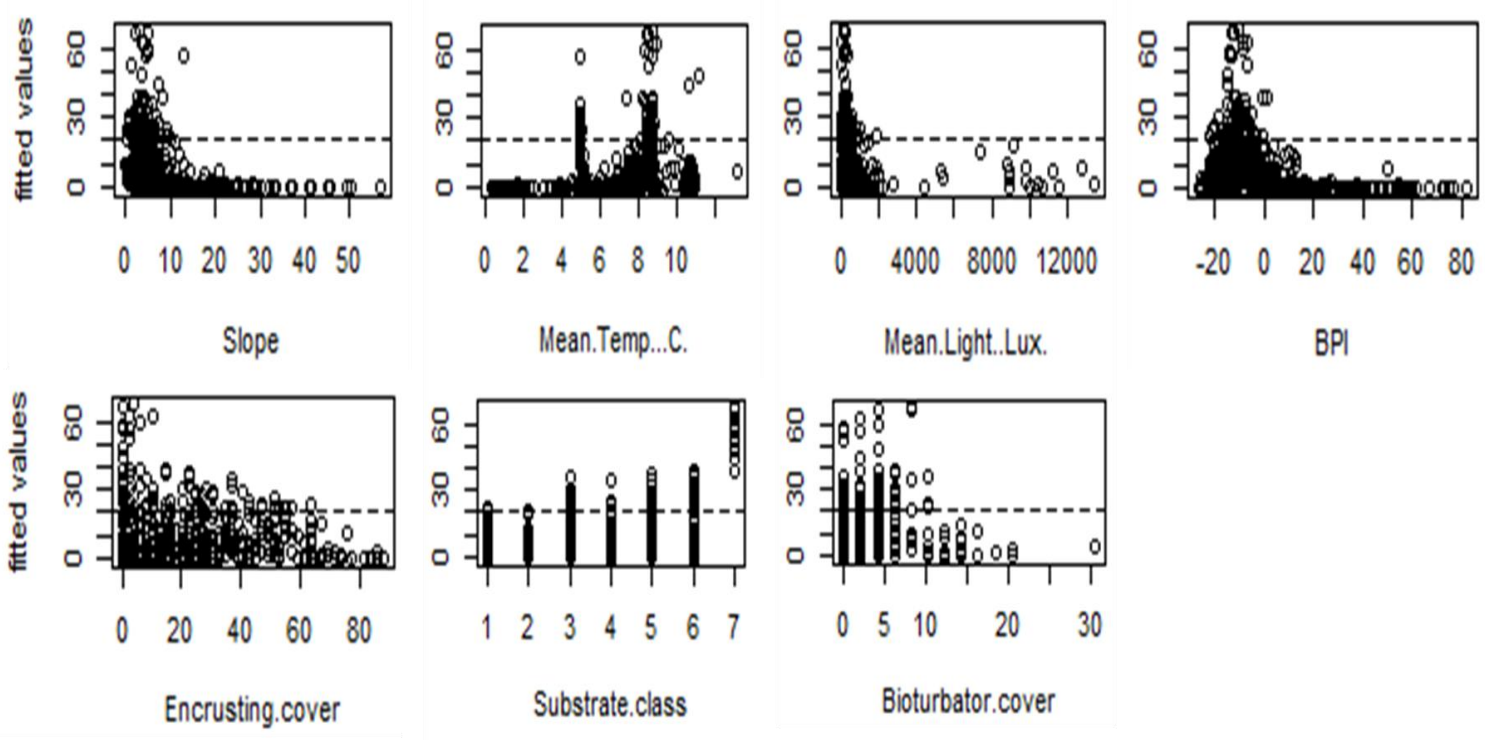

Figure 3.9 Trends of each explanatory variable's (slope, temperature, light, BPI, encrusting algae percent cover, substrate class, and bioturbator percent cover) influence on the fitted values of live rhodolith cover. Fitted values pertain to the distribution of response variable (rhodolith cover) values caused by each environmental variable.

Several environmental parameters were found to highly interact, with the most prominent interaction between BPI and temperature (1530.78; Table 3.1), suggesting co-linearity. Other notable interactions include BPI and light (948.89) as well as BPI and encrusting algae cover (533.98; Table 3.1).

3.3.2 Waves and currents

Flow acceleration did not vary with depth; however, flow acceleration did show a slight increase over time, peaking at 16.88 m s^{-2} on 26 July (Figure 3.10). Otherwise, flow acceleration remained consistent across depths with mean hourly flow acceleration mostly ranging from 0.1 to 1.3 m s^{-2} (Figure 3.10). Times of high flow acceleration were often due to lunar cycles (i.e., full and new moons). Other peaks of high flow acceleration were due to storm events causing high winds (Figure 3.10).

Flow acceleration did vary with location across a 15 m lateral gradient, as well as over time (Figure 3.11). Flow acceleration was consistently higher at the south location, peaking at 16.04 m s^{-2} on 04 November. This was followed by the centre URSKI logger location which peaked at 9.72 m s^{-2} also on 04 November. Flow acceleration at the north and northeast URSKI did not significantly vary from each other but were weaker than flow acceleration at the south and centre location, peaking at 2.19 m s^{-2} on 04 November (Figure 3.11). Regarding time, flow acceleration displayed peaks on 16 October and 04 November in the south and centre location. These peaks of high flow acceleration are due to storm events causing high winds. Lunar cycles did not influence flow acceleration laterally (Figure 3.11). Other than these peaks, flow acceleration mostly ranged from 0.1 to 3.2 m s^{-2} over the course of the field deployment (Figure 3.11).

Table 3.1 Pairwise interactions (from BRT) of all environmental variable influence on live rhodolith cover. Numbers approaching 0 indicate no interaction of variables, while numbers approaching or above 1000 indicate very high interaction. The three most important pairwise interactions are presented in bold.

Variable	Temp	Light	BPI	Crust	Substrate	Bioturbator
Slope	176.98	9.01	23.04	71.43	34.91	26.50
Temp	-	416.7	**1530.78**	161.69	279.91	160.05
Light		-	**948.89**	21.92	194.76	0.96
BPI			-	**533.98**	484.67	20.25
Crust				-	38.21	31.89
Substrate					-	30.76

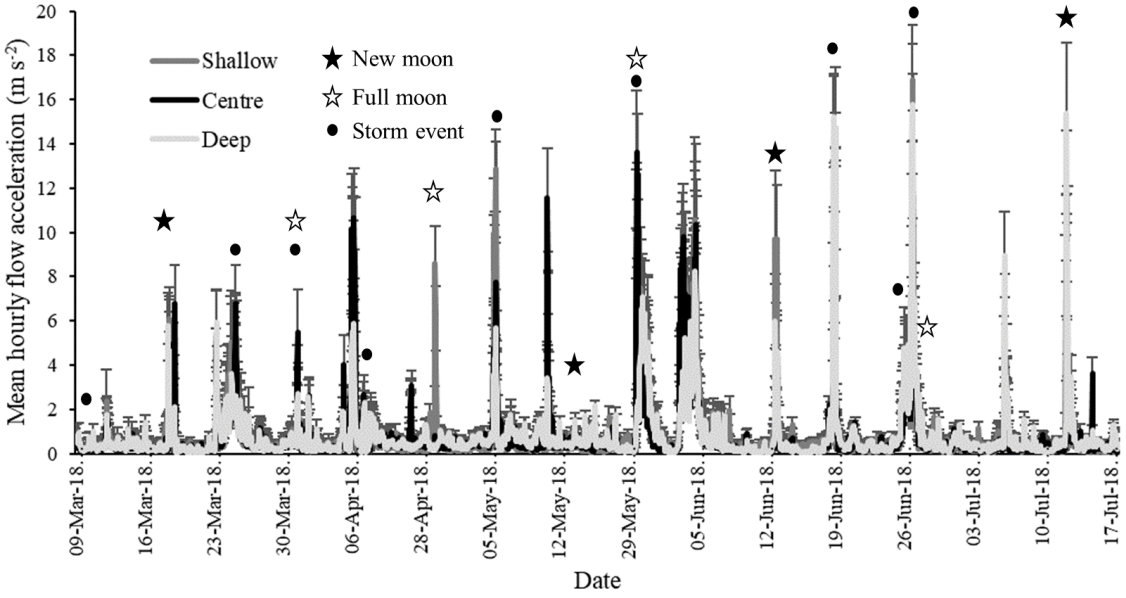

Figure 3.10 Hourly mean flow acceleration (m s^{-2} ±95% C.I.) in the rhodolith bed off the coast of St. Philip's across three depths: shallow (~8m, dark grey), centre (~15m, black) and deep (~20m, light grey), from March to July, 2018. New moons are marked by black stars and full moons are marked by white stars above error bars. Major storm events with high winds and precipitation are marked with closed circles.

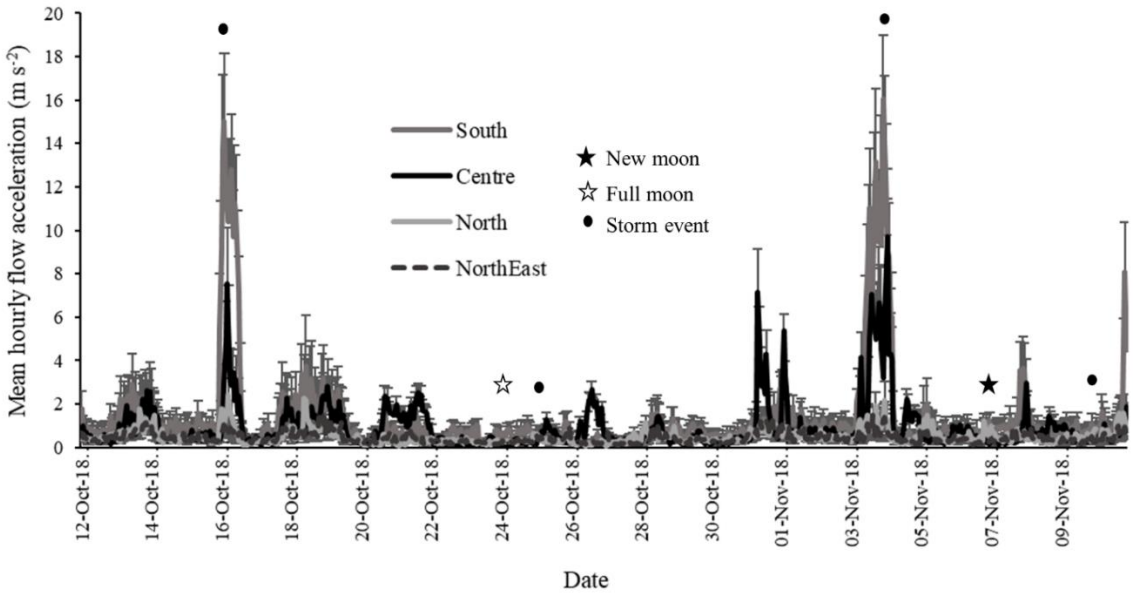

Figure 3.11 Hourly mean flow acceleration (m s^{-2} ±95% C.I.) across a lateral gradient of ~15m in the rhodolith bed off the coast of St. Philip's at four locations: south (dark grey), centre (black), north (light grey) and northeast (dashed), from October to November, 2018. New moons are marked by black stars and full moons are marked by white stars above error bars. Major storm events with high winds and precipitation are marked with closed circles.

Depth and date displayed no interactive effects on mean hourly flow accelerations ($p = 0.143$, Table 3.2A). However, flow acceleration did vary significantly according to date (across five months) ($p < 0.001$, Table 3.2A). Flow acceleration did not vary across the three measured depths ($p = 0.499$, Table 3.2A). Comparatively, lateral location (four locations across a lateral gradient at 15 m depth) and date did display interactive effects on mean hourly flow accelerations over the course of one month ($p < 0.001$, Table 3.2B).

3.4 DISCUSSION

The objectives of this study were to characterize a Newfoundland rhodolith bed to (1) test the hypothesis that hydrodynamic forces, water temperature and light are the main factors influencing rhodolith abundance; and (2) examine other abiotic and biotic factors that may also play a key role in influencing rhodolith abundance. Rhodoliths were found further south than anticipated, suggesting that the rhodolith bed present along the coast of St. Philip's is larger than previously thought. Slope, temperature, and illuminance were the most influential factors explaining variation in rhodolith distribution and abundance, while flow acceleration did not vary across depths. Our results challenge the long-standing paradigm that hydrodynamic forces are a main driver of rhodolith abundance.

3.4.1 Factors driving rhodolith abundance in St. Philip's

Slope of the seafloor had the highest influence on rhodolith abundance at 22.4%, where rhodolith abundance decreased with increasing slope. Increasingly sloped ridges are likely the cause of separation between the northern and southern rhodolith patches (patches of high rhodolith abundance; >10%) that make up the rhodolith bed off the coast of St.

Table 3.2 Summary of a two-way ANOVA with interaction (applied to hourly means of flow acceleration), testing the effects of depth location **(A)** (shallow, centre and deep), lateral location **(B)** across 15m depth (south, centre, north and northeast), and date (continuous variable) on mean hourly flow acceleration (m s^{-2}). N=2542 for depth gradient analysis, α=5%. N=716 for lateral gradient analysis, α=5%.

A. Depth gradient

Source	df	SS	MS	F	p-value
Depth	2	2.7	1.325	0.696	0.499
Date	1	19.4	19.407	10.192	**<0.001**
Depth*Date	2	7.4	3.706	1.946	0.143

B. Lateral gradient

Source	df	SS	MS	F	p-value
Location	3	375.5	125.158	88.250	**<0.001**
Date	1	140.3	140.327	98.946	**<0.001**
Location*Date	3	72.9	24.309	17.140	**<0.001**

Philip's. The relationship between rhodolith abundance and seafloor slope has scarcely been examined to date, however, in Italy, *L. valens* and *L. minervae* rhodoliths were absent on slopes exceeding 6° (Sañé et al., 2016). Furthermore, only encrusting growth forms of the same species were found on steeper slopes (Sañé et al., 2016). In the Tyrrhenian Sea, *L. coralloides* were only present on gentle slopes, with the highest rhodolith abundance from 0 to 2°, and low abundance from 6 to 8° (Savini et al., 2012). In Svalbard, only encrusting coralline algae (*L. glaciale*) was found on steeper slopes up to 32°, while rhodolith forms occurred on gentle slopes (Teichert et al., 2012). Similar trends were observed in St. Philip's, where rhodoliths (*L. glaciale*) were scarcely found in areas with slopes larger than 7°. It is likely that because rhodoliths are free-living, they would roll down steep slopes to deeper depths where temperature and light are diminished, and burial is enhanced (Pascelli et al., 2013; Sañé et al., 2016; Savini et al., 2012). Moreover, highly sloped areas are usually correlated with hard substrates in which rhodoliths do not often associate (Riosmena-Rodríguez et al., 2017). If this is the case, rhodoliths would indeed not be found on steep slopes.

Water temperature was the second most influential factor in driving rhodolith abundance, followed by illuminance, where rhodolith abundance was highest in areas of moderate water temperature (6.2 to 9.8°C) and illuminance (300 to 1500 lx). *L. glaciale* are known to occur from cold-temperate to polar realms on both sides of the North Atlantic and in the Northwest Pacific (Adey, 1970; Adey et al., 1976; Bosence and Wilson, 2003). *L. glaciale* is therefore confined to cold-water temperatures, were reproductive conceptacles are only produced in temperatures less than 9°C (Hall-Spencer, 1994; Teichert et al., 2012; Wilson et al., 2004). The St. Philip's site exhibited temperatures approaching

0°C, however rhodoliths were not found abundantly in temperatures below 6°C, likely due to the interaction of other factors such as slope, illuminance or sedimentation. Rhodolith growth has been found to respond to seasonal variations in water temperature and light cycles by accelerating growth in the warmer summer temperatures coupled with longer periods of daylight (Adey, 1970; Kamenos and Law, 2010). Rhodoliths can still grow throughout the winter however, relying on stored starch and photosynthates (Hofmann et al., 2018; Weykam et al., 1997; Wiencke et al., 2009; Williams et al., 2018). High illuminance can induce photodamage and increase photoinhibition of rhodoliths (Wilson et al., 2004). This could explain why rhodoliths in St. Philip's are not found in areas of illuminance above 1500 lux.

Illuminance and sea temperature co-vary with depth. *L. glaciale* has been found in polar and subpolar seas at depths exceeding 60 m (Adey et al., 1976). However, *L. glaciale* can only occur at this depth in clear waters (i.e., deeper photic limit), allowing access to light energy. Indeed, in more turbid environments such as off the coast of Brittany, France (which is not as limited by temperature), where rhodolith beds are subjected to dredging activities, rhodoliths are most abundant at depths less than 30 m (Barbera et al., 2003; Dutertre et al., 2015; Grall and Hall-Spencer, 2003). This is reflected in the St. Philip's site of the present study, where rhodolith abundance was highest at depths ranging from 13 to 31 m. Rhodoliths are likely uncommon at depths exceeding 31 m because of the interaction of abiotic factors such as slope, light, and sedimentation.

Bathymetric position index (BPI) was the fourth most influential factor influencing rhodolith abundance, at 15.9%. Research has yet to be conducted on BPI influence on rhodolith abundance, yet it should be considered as BPI can identify small- and large-scale

crests and troughs on the seafloor indicative of bottom currents and sediment transport that could hinder rhodolith growth (Downie et al., 2016; Martin et al., 2014; Misiuk et al., 2018; Secomandi et al., 2017). In St. Philip's, rhodoliths occurred in areas with negative BPI values, approaching 0 indicating higher rhodolith abundance in slight trough/depression areas on gentle slopes (Secomandi et al., 2017; Weiss, 2001). Rhodoliths observed in troughs and depressions were seen in shallower depths, likely between coarser substrates of boulders and cobbles. *L. glaciale* at deeper bed depths (up to ~31 m) occurred on a gentle slope, resulting in BPI values approaching 0. BPI highly interacted with water temperature and light, where temperature and light decreased with increasing BPI. This suggests that low BPI values were correlated with warmer, well-lit areas along with higher rhodolith abundance. No conclusions could be drawn on BPI at deeper depths within the study area, as BPI results here were likely influenced by interpolation artefacts and deemed untrustworthy.

Encrusting coralline algae cover was responsible for 12.2% influence on rhodolith abundance, displaying a negative relationship (i.e., as rhodolith cover increased, encrusting algae cover decreased). In St. Philip's, encrusting algae consists of the same species that forms rhodoliths, *L. glaciale*. As such, rhodoliths often form via fragmentation of encrusting forms (Foster, 2001; Wilson et al., 2004). Likewise, high rhodolith abundance should correlate with high cover of encrusting algae that would break off and form rhodoliths. Indeed, rhodoliths in St. Philip's were found abundantly with moderate crust cover, up to ~55%. However, this could be an underestimate as encrusting algae could be obscured by overlaying rhodoliths. Areas containing above 55% encrusting algae cover occurred in shallow, near-shore areas. Rhodoliths likely do not occur so close to shore due

to higher temperatures, illuminance, and wave action (Foster, 2001; Melbourne et al., 2018; Steller and Foster, 1995). Furthermore, encrusting algae commonly occur on coarse, hard substrates, and reports of rhodoliths on hard bottoms are rare because they easily roll away and are more subject to abrasion and competition with kelp, seaweeds, bryozoans and encrusting algae (Foster, 2001; Foster et al., 2013). Indeed, rhodoliths are known to be distributed across finer sediments/bottom types including sand and gravel substrates (De Grave, 1999; Joshi et al., 2017; Martin et al., 2014). This trend is also observed in St. Philip's with higher rhodolith abundance across finer substrates, resulting in a 7.6% substrate influence on rhodolith abundance.

Bioturbator cover had the lowest influence on rhodolith abundance, at 4.5%, where rhodoliths were mostly distributed in areas of low bioturbator cover (up to 13% cover). Rhodolith abundance within a bed is thought to be heavily influenced by the presence of bioturbators that aid in rhodolith movement/rolling and sediment eradication when currents and waves are too weak to do so (Foster, 2001; Foster et al., 2013; Marrack, 1999; Millar and Gagnon, 2018). Indeed, resident bioturbators in St. Philip's such as *O. aculeata*, *A. rubens*, and *S. droebachiensis*, have been shown to contribute to the dislodgement of sediment from rhodoliths (Millar and Gagnon, 2018). However, in the current study, bioturbator estimation was limited by what could be observed on the surface of rhodoliths, in this case, only larger *A. rubens*, and *S. droebachiensis*. Therefore, influence of bioturbators on rhodolith abundance in the current study could be underestimated. Moreover, this underestimation could also be related to the fact that *A. rubens*, and *S. droebachiensis* were abundant in near-shore bedrock outcrops where rhodoliths were absent (i.e., bioturbators were also abundant beyond rhodolith bed limits).

A key factor thought to influence rhodolith abundance (not included in the BRT model) is hydrodynamic forces. Rhodolith beds are commonly found in areas with moderate wave action and currents strong enough to prevent burial of rhodoliths, but not so strong as to cause fragmentation or abrasion (Dutertre et al., 2015; Foster, 2001; Hall-Spencer, 1998). Rhodolith beds in Brittany (France) commonly occur in areas where mean current velocity ranges from 0.02 to 0.73 m s^{-1}, with rhodolith cover decreasing in current velocities exceeding 0.5 m s^{-1} (Dutertre et al., 2015). In the Gulf of California, current velocities estimated between 0.2 and 0.8 m s^{-1} were required to move *L. coralloides*, *L. margaritae* and *P. calcareum*, as they were found to have a high drag coefficient (Melbourne et al., 2018). Current velocity in St. Philip's was considerably lower than this, peaking at 0.09 m s^{-1} (Appendix C), within range of those in European rhodolith beds (Dutertre et al., 2015; Foster, 2001; Joshi et al., 2017). Occurrences of high flow accelerations in St. Philip's were caused by lunar cycles and storm events, indicating bidirectional oscillatory wave motion (Harris et al., 1996; Nelson et al., 2012). In the Gulf of California, maximum oscillatory motion was not strong enough to move rhodoliths (Harris et al., 1996; Marrack, 1999). Likewise, in our study, flow acceleration only varied across a lateral gradient, but is not thought to influence rhodolith abundance (which was highest at the centre and north URSKI location) as currents are likely not strong enough to remove sediments or cause fragmentation. Bioturbator influence is likely more important in the removal of sediments (Marrack, 1999; Millar and Gagnon, 2018; Rebelo et al., 2018). However, previously reported sedimentation rates in St. Philip's were low, ranging from 0.19 to 2 mg cm^{-2} day^{-1}, likely too low to bury rhodoliths even in the absence of bioturbators (Millar and Gagnon, 2018).

Other factors could be at work in driving rhodolith abundance that are not mentioned in the current study including salinity and nutrient concentration (Dutertre et al., 2015; Martin et al., 2014; Savini et al., 2012; Schoenrock et al., 2018). Metabolic processes in *L. glaciale* have been shown to be negatively influenced by low salinity, caused by close proximity to freshwater input (Dutertre et al., 2015; Schoenrock et al., 2018). As well, increases in nutrient concentration from river input/land-based discharge has been found to inhibit productivity and calcification (McConnico et al., 2017; Schubert et al., 2019). However, even though the St. Philip's rhodolith bed is located approximately 300 m from a river mouth, salinity and nutrient concentration does not significantly differ (S. Hacker-Teper and P. Gagnon, unpublished data).

3.4.2 Challenging rhodolith bed driver paradigms

Growth of benthic communities is thought to be driven by light and temperature while community stability is driven by hydrodynamic forces and sedimentation (Kostylev and Hannah, 2007). Indeed, temperature and light drive growth and species distribution of rhodoliths, where growth often increases with temperature and light until a threshold is reached (Bosence and Wilson, 2003; Foster et al., 2013). Temperature and illuminance were the second and third most influential factors influencing rhodolith distribution and abundance in the current study, supporting the hypothesis and long-standing paradigm that temperature and light are two of the main factors driving rhodolith abundance.

The other long-standing paradigm is the influence of hydrodynamic forces driving rhodolith bed limits and the stability of beds. High currents and wave action dislodge and fragment rhodoliths, inhibiting abundance in shallow, intertidal areas, while low currents

permit sediments to settle on rhodoliths (Foster, 2001; Steller and Foster, 1995). The current study challenges this hypothesis and paradigm, as current velocity was consistently low, and there was no difference in flow acceleration between upper and lower rhodolith bed limits. Instead, this study introduces the significance of slope as a main driver, where rhodolith abundance increases with decreasing slope. Moreover, factors examined in this study are not independent, signifying the importance of examining how factors interact to drive rhodolith abundance. Furthermore, it is crucial to examine rhodolith drivers at regional scales because small, sheltered bays may be more influenced by factors such as temperature and slope, whereas rhodolith beds located elsewhere may be subject to stronger hydrodynamic forces or nutrient input/turbidity from nearby rivers.

3.4.3 Conclusions

The research presented here demonstrates the effectiveness of using drop camera surveys to characterize nearshore habitats. Moreover, the present study can act as a baseline assessment of conditions in which Newfoundland rhodolith beds thrive and can help define environmental conditions correlated with rhodolith presence in Newfoundland, aiding in predicting other Newfoundland regions that likely contain rhodoliths.

Although degradation of Newfoundland rhodolith beds via dredging and land-based pollution is low, spatial variation can occur from climatic events such as increased water temperatures, ocean acidification, and more intense storm events (Büdenbender et al., 2011; Kamenos et al., 2013; McCoy and Kamenos, 2015; Nelson et al., 2012). Continued efforts to locate and better understand rhodolith habitats that house a high diversity of ecologically

and economically important species are crucial to developing successful conservation and management strategies.

3.5 LITERATURE CITED

Adey, W.H., Masaki, T., Akjoka, H., 1976. The distribution of crustose corallines in Eastern Hokkaido and biogeographic relationships of the flora. Bull. Fac. Fish. Hokkaido Univ. 26(4), 303-313.

Adler, P., Raff, D., Lauenroth, W., 2001. The effect of grazing on the spatial heterogeneity of vegetation. Oecologia 128, 465–479. https://doi.org/10.1007/s004420100737

Amado-Filho, G.M., Moura, R.L., Bastos, A.C., Salgado, L.T., Sumida, P.Y., Guth, A.Z., Francini-Filho, R.B., Pereira-Filho, G.H., Abrantes, D.P., Brasileiro, P.S., Bahia, R.G., Leal, R.N., Kaufman, L., Kleypas, J.A., Farina, M., Thompson, F.L., 2012. Rhodolith beds are major $CaCO_3$ bio-factories in the tropical south West Atlantic. PLoS One 7. https://doi.org/10.1371/journal.pone.0035171

Bahia, R.G., Abrantes, D.P., Brasileiro, P.S., Pereira-Filho, G.H., Amado-Filho, G.M., 2010. Rhodolith bed structure along a depth gradient on the northern coast of Bahia state, Brazil. Brazilian J. Oceanogr. 58, 323–337.

Barbera, C., Bordehore, C., Borg, J.A., Glémarec, M., Grall, J., Hall-Spencer, J.M., de la Huz, C., Lanfranco, E., Lastra, M., Moore, P.G., Mora, J., Pita, M.E., Ramos-Espla, A.A., Rizzo, M., Sanchez-Mata, A., Seva, A., Schembri, P.J., Valle, C., 2003. Conservation and management of northeast Atlantic and Mediterranean maerl beds. Aquat. Conserv. Mar. Freshw. Ecosyst. 13, S65–S76. https://doi.org/10.1002/aqc.569

Basso, D., Babbini, L., Ramos-Esplá, A.A., Salomidi, M., 2017. Mediterranean Rhodolith Beds, in: Riosmena-Rodriguez, R., Aquirre, J., Nelson, W. (Eds.), Rhodolith/Maerl Beds: A Global Perspective. Springer Nature, Florida, pp. 281–298. https://doi.org/10.1007/978-3-319-29315-8_11

Basso, D., Granier, B., 2012. Calcareous algae in changing environments. Geodiversitas 34, 5–11. https://doi.org/10.5252/g2012n1a1

Blain, C., Gagnon, P., 2013. Interactions between thermal and wave environments mediate intracellular acidity (H_2SO_4), growth, and mortality in the annual brown seaweed *Desmarestia viridis*. J. Exp. Mar. Bio. Ecol. 440, 176–184. https://doi.org/10.1016/j.jembe.2012.12.013

Bosence, D., Wilson, J., 2003. Maerl growth, carbonate production rates and accumulation rates in the northeast Atlantic. Aquat. Conserv. Mar. Freshw. Ecosyst. 13, S21–S31. https://doi.org/10.1002/aqc.565

Brown, C.J., Smith, S.J., Lawton, P., Anderson, J.T., 2011. Benthic habitat mapping: A review of progress towards improved understanding of the spatial ecology of the seafloor using acoustic techniques. Estuar. Coast. Shelf Sci. 92, 502–520. https://doi.org/10.1016/j.ecss.2011.02.007

Büdenbender, J., Riebesell, U., Form, A., 2011. Calcification of the Arctic coralline red algae *Lithothamnion glaciale* in response to elevated CO_2. Mar. Ecol. Prog. Ser. 441, 79–87. https://doi.org/10.3354/meps09405

Campos, R.H.S., Dominguez, J.M.L., 2010. Mobility of sediments due to wave action on the continental shelf of the Northern coast of the state of Bahia. Brazilian J. Oceanogr. 58, 57–63. https://doi.org/10.1590/S1679-87592010000600007

Ceccarelli, D.M., Jones, G.P., McCook, L.J., 2005. Foragers versus farmers: contrasting effects of two behavioural groups of herbivores on coral reefs. Oecologia 145, 445–453. https://doi.org/10.1007/s00442-005-0144-y

Chen, M., Ding, S., Liu, L., Xu, D., Gong, M., Tang, H., Zhang, C., 2016. Kinetics of phosphorus release from sediments and its relationship with iron speciation influenced by the mussel (*Corbicula fluminea*) bioturbation. Sci. Total Environ. 542, 833–840. https://doi.org/10.1016/j.scitotenv.2015.10.155

Coletti, G., Basso, D., Corselli, C., 2018. Coralline algae as depth indicators in the Sommières Basin (early Miocene, Southern France). Geobios 51, 15–30. https://doi.org/10.1016/j.geobios.2017.12.002

Coletti, G., Basso, D., Frixa, A., 2017. Economic Importance of Coralline Carbonates, in: Riosmena-Rodriguez, R., Aguirre, J., Nelson, W. (Eds.), Rhodolith/Maerl Beds: A Global Perspective. Springer Nature, Florida, pp. 87–101. https://doi.org/10.1007/978-3-319-29315-8_4

Copeland, A., Edinger, E., Devillers, R., Bell, T., LeBlanc, P., Wroblewski, J., 2013. Marine habitat mapping in support of Marine Protected Area management in a subarctic fjord: Gilbert Bay, Labrador, Canada. J. Coast. Conserv. https://doi.org/10.1007/s11852-011-0172-1

De Grave, S., 1999. The influence of sedimentary heterogeneity on within maerl bed differences in infaunal crustacean community. Estuar. Coast. Shelf Sci. 49, 153–163. https://doi.org/10.1006/ECSS.1999.0484

Denny, M.W., 1988. Biology and the mechanics of the wave-swept environment. Princeton University Press, Princeton.

Denny, M.W., Wethey, D., 2001. Physical processes that generate patterns in marine communities. In: Bertness MD, Gaines SD, Hay ME (eds) Marine community ecology. Sinauer Associates, Sunderland, pp. 3-37.

Diesing, M., Stephens, D., 2015. A multi-model ensemble approach to seabed mapping. J. Sea Res. 100, 62–69. https://doi.org/10.1016/J.SEARES.2014.10.013

Doney, S.C., Fabry, V.J., Feely, R.A., Kleypas, J.A., 2009. Ocean acidification: The other CO_2 problem. Ann. Rev. Mar. Sci. 1, 169–192. https://doi.org/10.1146/annurev.marine.010908.163834

dos Reis, V.M., Karez, C.S., Mariath, R., de Moraes, F.C., de Carvalho, R.T., Brasileiro, P.S., Bahia, R. da G., Lotufo, T.M. da C., Ramalho, L.V., de Moura, R.L., Francini-Filho, R.B., Pereira-Filho, G.H., Thompson, F.L., Bastos, A.C., Salgado, L.T., Amado-Filho, G.M., 2016. Carbonate Production by Benthic Communities on Shallow Coralgal Reefs of Abrolhos Bank, Brazil. PLoS One 11, e0154417. https://doi.org/10.1371/journal.pone.0154417

Downie, A.L., Dove, D., Green, S.L., Cooper, R., 2016. Semi-automated mapping of rock in the North Sea. JNCC. Peterborough. 26 pp.

Drollet, J.H., Glaziou, P., Martin, P.M.V., 1993. A study of mucus from the solitary coral *Fungia fungites* (Scleractinia: Fungiidae) in relation to photobiological UV adaptation. Mar. Biol. 115, 263–266. https://doi.org/10.1007/BF00346343

Dutertre, M., Grall, J., Ehrhold, A., Hamon, D., 2015. Environmental factors affecting maerl bed structure in Brittany (France). Eur. J. Phycol. 50, 371–383. https://doi.org/10.1080/09670262.2015.1063698

Elith, J., Leathwick, J.R., 2009. Species Distribution Models: Ecological Explanation and Prediction Across Space and Time. Annu. Rev. Ecol. Evol. Syst. 40, 677-697. https://doi.org/10.1146/annurev.ecolsys.110308.120159

Elith, J., Leathwick, J.R., Hastie, T., 2008. A working guide to boosted regression trees. J. Anim. Ecol. 77, 802–813. https://doi.org/10.1111/j.1365-2656.2008.01390.x

Environment and Climate Change Canada, 2018. Daily data report for 2018 – Climate. Accessed from: https://www.climate.weather.gc.ca/climate_data/daily_data_e.html?StationID=50089.

Evans, S., Abdo, D., 2010. A cost-effective technique for measuring relative water movement for studies of benthic organisms. Mar. Fresh. Res. 61, 1327-1335. https://doi.org/10.1071/MF10007.

Figurski, J., Malone, D., Lacy, J., Denny, M., 2011. An inexpensive instrument for measuring wave exposure and water velocity. Limnol. Ocean. Methods 9, 201-214. https://doi.org/10.4319/lom.2011.9.204.

Foster, M.S., 2001. Rhodoliths: Between rocks and soft places. J. Phycol. 37, 659–667. https://doi.org/10.1046/j.1529-8817.2001.00195.x

Foster, M.S., Amado-Filho, G.M., Kamenos, N.A., Riosmena-Rodríguez, R., Steller, D.L., 2013. Rhodoliths and Rhodolith Beds. Smithson. Contrib. Mar. Sci. 39, 143–155.

Freiwald, A., 1998. Modern Nearshore Cold-Temperate Calcareous Sediments in the

Troms dsitrict, Northern Norway. J. Sediment. Res. 68, 763–776.

Gabara, S.S., Hamilton, S.L., Edwards, M.S., Steller, D.L., 2018. Rhodolith structural loss decreases abundance, diversity, and stability of benthic communities at Santa Catalina Island, CA. Mar. Ecol. Prog. Ser. 595, 71-88. https://doi.org/10.3354/meps12528

Gagnon, P., Matheson, K., Stapleton, M., 2012. Variation in rhodolith morphology and biogenic potential of newly discovered rhodolith beds in Newfoundland and Labrador (Canada). Bot. Mar. 55, 85–99. https://doi.org/10.1515/bot-2011-0064

Gaylord, B., 1999. Detailing agents of physical disturbance: wave-induced velocities and accelerations on a rocky shore. J. Exp. Mar. Bio. Ecol. 239, 85–124. https://doi.org/10.1016/S0022-0981(99)00031-3

Grall, J., Hall-Spencer, J.M., 2003. Problems facing maerl conservation in Brittany. Aquat. Conserv. Mar. Freshw. Ecosyst. 13, S55–S64. https://doi.org/10.1002/aqc.568

Griffin, J.D., Hemer, M.A., Jones, B.G., 2008. Mobility of sediment grain size distributions on a wave dominated continental shelf, southeastern Australia. Mar. Geol. 252, 13–23. https://doi.org/10.1016/J.MARGEO.2008.03.005

Gunderson, A.R., Armstrong, E.J., Stillman, J.H., 2016. Multiple Stressors in a Changing World: The Need for an Improved Perspective on Physiological Responses to the Dynamic Marine Environment. Ann. Rev. Mar. Sci. 8, 357–378. https://doi.org/10.1146/annurev-marine-122414-033953

Hall-Spencer, J., 1998. Conservation issues relating to maerl beds as habitats for molluscs. J. Conchol. Sepcial Publ. 2, 271–285.

Hall-Spencer, J.M., 1994. Biological studies on non-geniculate Corallinaceae. PhD thesis, University of London.

Harborne, A.R., Rogers, A., Bozec, Y.-M., Mumby, P.J., 2017. Multiple Stressors and the Functioning of Coral Reefs. Ann. Rev. Mar. Sci. 9, 445–468. https://doi.org/10.1146/annurev-marine-010816-060551

Harris, P.T., Tsuji, Y., Marshall, J.F., Davies, P.J., Honda, N., Matsuda, H., 1996. Sand and rhodolith-gravel entrainment on the mid- to outer-shelf under a western boundary current: Fraser Island continental shelf, eastern Australia. Mar. Geol. 129, 313–330. https://doi.org/10.1016/0025-3227(96)83350-0

Harvey, A.S., Harvey, R.M., Merton, E., 2017. The distribution, significance and vulnerability of Australian rhodolith beds: A review. Mar. Freshw. Res. 68, 411–428. https://doi.org/10.1071/MF15434

Hinojosa-Arango, G., Maggs, C.A., Johnson, M.P., 2009. Like a rolling stone: the mobility of maerl (Corallinaceae) and the neutrality of the associated assemblages. Ecology 90, 517–528. https://doi.org/10.1890/07-2110.1

Hofmann, L.C., Schoenrock, K., de Beer, D., 2018. Arctic Coralline Algae Elevate Surface pH and Carbonate in the Dark. Front. Plant Sci. 9, 1–12. https://doi.org/10.3389/fpls.2018.01416

Jørgensbye, H.I.Ø., Halfar, J., 2017. Overview of coralline red algal crusts and rhodolith beds (Corallinales, Rhodophyta) and their possible ecological importance in Greenland. Polar Biol. 40, 517-531. https://doi.org/10.1007/s00300-016-1975-1

Joshi, S., Duffy, G.P., Brown, C., 2017. Mobility of maerl-siliciclastic mixtures: Impact of waves, currents and storm events. Estuar. Coast. Shelf Sci. 189, 173–188. https://doi.org/10.1016/j.ecss.2017.03.018

Joshi, S., Duffy, G.P., Brown, C., 2014. Settling velocity and grain shape of maerl biogenic gravel. J. Sediment. Res. 84, 718–727. https://doi.org/10.2110/jsr.2014.51

Kamenos, N.A., Burdett, H.L., Aloisio, E., Findlay, H.S., Martin, S., Longbone, C., Dunn, J., Widdicombe, S., Calosi, P., 2013. Coralline algal structure is more sensitive to rate, rather than the magnitude, of ocean acidification. Glob. Chang. Biol. 19, 3621–3628. https://doi.org/10.1111/gcb.12351

Kleypas, J., Feely, R., Fabry, V., Langdon, C., Sabine, C., Robbins, L., 2006. Impacts of ocean acidification on coral reefs and other marine calcifiers: A guide for future research. St. Petersburg, FL.

Kostylev, V.E., Hannah, C.G., 2007. Mapping the seafloor for habitat characterization and mapping of seabed habitats. In: Todd, B.J., Greene, H.G., eds., Mapping the seafloor for habitat characterization: geological association of Canada, Special paper. 47, 171-184.

Kraufvelin, P., Lindholm, A., Pedersen, M.F., Kirkerud, L.A., Bonsdorff, E., 2010. Biomass, diversity and production of rocky shore macroalgae at two nutrient enrichment and wave action levels. Mar. Biol. 157, 29–47. https://doi.org/10.1007/s00227-009-1293-z

Kristensen, E., Penha-Lopes, G., Delefosse, M., Valdemarsen, T., Quintana, C.O., Banta, G.T., 2012. What is bioturbation? The need for a precise definition for fauna in aquatic sciences. Mar. Ecol. Prog. Ser. 446, 285–302. https://doi.org/10.3354/meps09506

Marrack, E.C., 1999. The relationship between water motion and living rhodolith beds in the southwestern Gulf of California, Mexico. Palaios 14, 159–171. https://doi.org/10.2307/3515371

Martin, C.S., Giannoulaki, M., De Leo, F., Scardi, M., Salomidi, M., Knittweis, L., Pace, M.L., Garofalo, G., Gristina, M., Ballesteros, E., Bavestrello, G., Belluscio, A., Cebrian, E., Gerakaris, V., Pergent, G., Pergent-Martini, C., Schembri, P.J., Terribile, K., Rizzo, L., Souissi, J. Ben, Bonacorsi, M., Guarnieri, G., Krzelj, M., Macic, V., Punzo, E., Valavanis, V., Fraschetti, & S., 2014. Coralligenous and maërl habitats: predictive modelling to identify their spatial distributions across the

Mediterranean Sea. Sci. Rep. 4. https://doi.org/10.1038/srep05073

Matsuda, S., Iryu, Y., 2011. Rhodoliths from deep fore-reef to shelf areas around Okinawa-jima, Ryukyu Islands, Japan. Mar. Geol. 282, 215-230. https://doi.org/10.1016/j.margeo.2011.02.013

McArthur, M.A., Brooke, B.P., Przeslawski, R., Ryan, D.A., Lucieer, V.L., Nichol, S., McCallum, A.W., Mellin, C., Cresswell, I.D., Radke, L.C., 2010. On the use of abiotic surrogates to describe marine benthic biodiversity. Estuar. Coast. Shelf Sci. 88, 21-32. https://doi.org/10.1016/j.ecss.2010.03.003

McConnico, L.A., Carmona, G.H., Morales, J.S.M., Rodríguez, R.R., 2017. Temporal variation in seaweed and invertebrate assemblages in shallow rhodolith beds of Baja California Sur, México. Aquat. Bot. 139, 37–47. https://doi.org/10.1016/j.aquabot.2017.02.007

McCoy, S.J., Kamenos, N.A., 2015. Coralline algae (Rhodophyta) in a changing world: integrating ecological, physiological, and geochemical responses to global change. J. Phycol. 51, 6–24. https://doi.org/10.1111/jpy.12262

McCoy, S.J., Ragazzola, F., 2014. Skeletal trade-offs in coralline algae in response to ocean acidification. Nat. Clim. Chang. 4, 719-723. https://doi.org/10.1038/nclimate2273

Melbourne, L.A., Denny, M.W., Harniman, R.L., Rayfield, E.J., Schmidt, D.N., 2018. The importance of wave exposure on the structural integrity of rhodoliths. J. Exp. Mar. Bio. Ecol. 503, 109–119. https://doi.org/10.1016/j.jembe.2017.11.007

Melbourne, L.A., Griffin, J., Schmidt, D.N., Rayfield, E.J., 2015. Potential and limitations of finite element modelling in assessing structural integrity of coralline algae under future global change. Biogeosciences 12, 5871–5883. https://doi.org/10.5194/bg-12-5871-2015

Millar, K.R., Gagnon, P., 2018. Mechanisms of stability of rhodolith beds: sedimentological aspects. Mar. Ecol. Prog. Ser. 594, 65–83. https://doi.org/10.3354/meps12501

Miller, L.P., O'Donnell, M.J., Mach, K.J., 2007. Dislodged but not dead: survivorship of a high intertidal snail following wave dislodgement [WWW Document]. J. Mar. Biol. Assoc. United Kingdom. 87(3).

Misiuk, B., Lecours, V., Bell, T., 2018. A multiscale approach to mapping seabed sediments. PLoS One 13, e0193647. https://doi.org/10.1371/journal.pone.0193647

Moura, R.L., Amado-Filho, G.M., Moraes, F.C., Brasileiro, P.S., Salomon, P.S., Mahiques, M.M., Bastos, A.C., Almeida, M.G., Silva, J.M., Araujo, B.F., Brito, F.P., Rangel, T.P., Oliveira, B.C.V., Bahia, R.G., Paranhos, R.P., Dias, R.J.S., Siegle, E., Figueiredo, A.G., Pereira, R.C., Leal, C. V., Hajdu, E., Asp, N.E., Gregoracci, G.B., Neumann-Leitão, S., Yager, P.L., Francini-Filho, R.B., Fróes, A., Campeão, M.,

Silva, B.S., Moreira, A.P.B., Oliveira, L., Soares, A.C., Araujo, L., Oliveira, N.L., Teixeira, J.B., Valle, R.A.B., Thompson, C.C., Rezende, C.E., Thompson, F.L., 2016. An extensive reef system at the Amazon River mouth. Sci. Adv. 2, e150125. https://doi.org/10.1126/sciadv.1501252

Muñoz, P.T., Sáez, C.A., Martínez-Callejas, M.B., Flores-Molina, M.R., Bastos, E., Fonseca, A., Gurgel, C.F.D., Barufi, J.B., Rörig, L., Hall-Spencer, J.M., Horta, P.A., 2018. Short-term interactive effects of increased temperatures and acidification on the calcifying macroalgae *Lithothamnion crispatum* and *Sonderophycus capensis*. Aquat. Bot. 148, 46–52. https://doi.org/10.1016/j.aquabot.2018.04.008

Neill, K.F., Nelson, W.A., D'Archino, R., Leduc, D., Farr, T.J., 2015. Northern New Zealand rhodoliths: assessing faunal and floral diversity in physically contrasting beds. Mar. Biodivers. 45(1), 63-75. https://doi.org/10.1007/s12526-014-0229-0

Nelson, W.A., Neill, K., Farr, T., Barr, N., Miller, A.S., Stewart, R., 2012. Rhodolith Beds in Northern New Zealand: Characterisation of Associated Biodiversity and Vulnerability to Environmental Stressors New Zealand Aquatic Environment and Biodiversity. Wellington.

Nitsch, F., Nebelsick, J.H., Bassi, D., 2015. Constructional and destructional patterns - void classification of rhodoliths from Giglio island, Italy. Palaios 30, 680–691. https://doi.org/10.2110/palo.2015.007

Noisette, F., Duong, G., Six, C., Davoult, D., Martin, S., 2013. Effects of elevated pCO_2 on the metabolism of a temperate rhodolith *Lithothamnion corallioides* grown under different temperatures. J. Phycol. https://doi.org/10.1111/jpy.12085

Pascelli, C., Riul, P., Riosmena-Rodríguez, R., Scherner, F., Nunes, M., Hall-Spencer, J.M., Oliveira, E.C. de, Horta, P., 2013. Seasonal and depth-driven changes in rhodolith bed structure and associated macroalgae off Arvoredo island (southeastern Brazil). Aquat. Bot. 111, 62-65. https://doi.org/10.1016/j.aquabot.2013.05.009

Pereira-Filho, G., Veras, P., Francini-Filho, R., Moura, R., Pinheiro, H., Gibran, F., Matheus, Z., Neves, L., Amado-Filho, G., 2015. Effects of the sand tilefish *Malacanthus plumieri* on the structure and dynamics of a rhodolith bed in the Fernando de Noronha Archipelago, tropical West Atlantic. Mar. Ecol. Prog. Ser. 541, 65–73. https://doi.org/10.3354/meps11569

Pereira-Filho, G.H., Amado-Filho, G.M., de Moura, R.L., Bastos, A.C., Guimarães, S.M.P.B., Salgado, L.T., Francini-Filho, R.B., Bahia, R.G., Abrantes, D.P., Guth, A.Z., Brasileiro, P.S., 2012. Extensive Rhodolith Beds Cover the Summits of Southwestern Atlantic Ocean Seamounts. J. Coast. Res. 28, 261–269. https://doi.org/10.2112/11T-00007.1

Perry, C.T., Alvarez-Filip, L., Graham, N.A.J., Mumby, P.J., Wilson, S.K., Kench, P.S., Manzello, D.P., Morgan, K.M., Slangen, A.B.A., Thomson, D.P., Januchowski-Hartley, F., Smithers, S.G., Steneck, R.S., Carlton, R., Edinger, E.N., Enochs, I.C.,

Estrada-Saldívar, N., Haywood, M.D.E., Kolodziej, G., Murphy, G.N., Pérez-Cervantes, E., Suchley, A., Valentino, L., Boenish, R., Wilson, M., Macdonald, C., 2018. Loss of coral reef growth capacity to track future increases in sea level. Nature 558, 396–400. https://doi.org/10.1038/s41586-018-0194-z

Peterson, A., Herkül, K., Torn, K., 2018. Modeling Coastal Benthic Biodiversity Using Georeferenced Environmental Data: Mapping Present and Predicting Future Changes. J. Coast. Res. 85, 376–380. https://doi.org/10.2112/SI85-076.1

R Core Team, 2014. R: A language and environment for statistical computing. R Foundation for Statistical Computing, Vienna.

Rebelo, A.C., Johnson, M.E., Quartau, R., Rasser, M.W., Melo, C.S., Neto, A.I., Tempera, F., Madeira, P., Ávila, S.P., 2018. Modern rhodoliths from the insular shelf of Pico in the Azores (Northeast Atlantic Ocean). Estuar. Coast. Shelf Sci. 210, 7–17. https://doi.org/10.1016/j.ecss.2018.05.029

Redding, D., Lucas, T., Blackburn, T., Jones, K., 2017. Evaluating Bayesian spatial methods for modelling species distributions with clumped and restricted occurrence data. PLoS One 12, e0187602. https://doi.org/10.1371/journal.pone.0187602

Ridgeway, G., 2006. Generalized boosted regression models. Documentation on the R Package 'gbm', version 1·5–7. Accessed from: http://www.i-pensieri.com/gregr/gbm.shtml.

Riosmena-Rodríguez, R., Nelson, W., Aguirre, J., 2017. Rhodolith/ Maërl Beds: A Global Perspective, 1st ed. Springer Nature, Florida.

Riul, P., Targino, C.H., Farias, J.D.N., Visscher, P.T., Horta, P.A., 2008. Decrease in *Lithothamnion* sp. (Rhodophyta) primary production due to the deposition of a thin sediment layer. J. Mar. Biol. Assoc. UK 88, 17–19. https://doi.org/10.1017/S0025315408000258

Sañé, E., Chiocci, F.L., Basso, D., Martorelli, E., 2016. Environmental factors controlling the distribution of rhodoliths: An integrated study based on seafloor sampling, ROV and side scan sonar data, offshore the W-Pontine Archipelago. Cont. Shelf Res. 129, 10–22. https://doi.org/10.1016/j.csr.2016.09.003

Savini, A., Basso, D., Alice Bracchi, V., Corselli, C., Pennetta, M., 2012. Maerl-bed mapping and carbonate quantification on submerged terraces offshore the Cilento peninsula (Tyrrhenian Sea, Italy). Geodiversitas 34, 77–98. https://doi.org/10.5252/g2012n1a5

Schoenrock, K.M., Bacquet, M., Pearce, D., Rea, B.R., Schofield, J.E., Lea, J., Mair, D., Kamenos, N., 2018. Influences of salinity on the physiology and distribution of the Arctic coralline algae, *Lithothamnion glaciale* (Corallinales, Rhodophyta). J. Phycol. 54, 690–702. https://doi.org/10.1111/jpy.12774

Schubert, N., Salazar, V.W., Rich, W.A., Vivanco Bercovich, M., Almeida Saá, A.C.,

Fadigas, S.D., Silva, J., Horta, P.A., 2019. Rhodolith primary and carbonate production in a changing ocean: The interplay of warming and nutrients. Sci. Total Environ. 676, 455–468. https://doi.org/10.1016/j.scitotenv.2019.04.280

Secomandi, M., Jones, E., Terente, V., Comrie, R., Owen, M., 2017. Application of the Bathymetric Position Index method (BPI) for the purpose of defining a reference seabed level for cable burial, in: Offshore Site Investigation Geotechnics 8th International Conference Proceedings. Society of Underwater Technology, pp. 904–913. https://doi.org/10.3723/osig17.904

Sheehan, E.V., Bridger, D., Cousens, S., Attrill, M., 2015. Testing the resilience of dead maerl infaunal assemblages to the experimental removal and re-lay of habitat. Mar. Ecol. Prog. Ser. 535, 117–128. https://doi.org/10.3354/meps11400

Short, J., Foster, T., Falter, J., Kendrick, G.A., McCulloch, M.T., 2015. Crustose coralline algal growth, calcification and mortality following a marine heatwave in Western Australia. Cont. Shelf Res. 106, 38-44. https://doi.org/10.1016/j.csr.2015.07.003

Steller, D.L., Foster, M.S., 1995. Environmental factors influencing distribution and morphology of rhodoliths in Bahia Concepcion B.C.S., Mexico. J. Exp. Mar. Bio. Ecol. 194, 201–212.

Stock, A., Haupt, A.J., Mach, M.E., Micheli, F., 2018. Mapping ecological indicators of human impact with statistical and machine learning methods: Tests on the California coast. Ecol. Inform. 48, 37–47. https://doi.org/10.1016/j.ecoinf.2018.07.007

Teichert, S., Woelkerling, W., Rüggeberg, A., Wisshak, M., Piepenburg, D., Meyerhöfer, M., Form, A., Büdenbender, J., Freiwald, A., 2012. Rhodolith beds (Corallinales, Rhodophyta) and their physical and biological environment at 80°31′N in Nordkappbukta (Nordaustlandet, Svalbard Archipelago, Norway). Phycologia 51, 371–390. https://doi.org/10.2216/11-76.1

Teichert, S., Woelkerling, W., Rüggeberg, A., Wisshak, M., Piepenburg, D., Meyerhöfer, M., Form, A., Freiwald, A., 2014. Arctic rhodolith beds and their environmental controls (Spitsbergen, Norway). Facies. 60, 15-37. https://doi.org/10.1007/s10347-013-0372-2

Villas-Boas, A.B., Riosmena-Rodriguez, R., de Oliveira Figueiredo, M.A., 2014. Community structure of rhodolith-forming beds on the central Brazilian continental shelf. Helgol. Mar. Res. 68, 27–35. https://doi.org/10.1007/s10152-013-0366-z

Villas-Bôas, A.B., Tâmega, F.T.D.S., Andrade, M., Coutinho, R., Figueiredo, M.A.D.O., 2014. Experimental Effects of Sediment Burial and Light Attenuation on Two Coralline Algae of a Deep Water Rhodolith Bed in Rio de Janeiro, Brazil. Cryptogam. Algol. 35, 67–76. https://doi.org/10.7872/crya.v35.iss1.2014.67

Weiss, A.D., 2001. Topographic position and landforms analysis. Seattle.

Weykam, G., Thomas, D.N., Wiencke, C., 1997. Growth and photosynthesis of the

Antarctic red algae *Palmaria decipiens* (Palmariales) and *Iridaea cordata* (Gigartinales) during and following extended periods of darkness. Phycologia 36, 395–405. https://doi.org/10.2216/i0031-8884-36-5-395.1

Wiencke, C., Gómez, I., Dunton, K., 2009. Phenology and seasonal physiological performance of polar seaweeds. Bot. Mar. 52, 585–592. https://doi.org/10.1515/BOT.2009.078

Williams, S., Adey, W., Halfar, J., Kronz, A., Gagnon, P., Bélanger, D., Nash, M., 2018. Effects of light and temperature on Mg uptake, growth, and calcification in the proxy climate archive *Clathromorphum compactum*. Biogeosciences 15, 5745–5759. https://doi.org/10.5194/bg-15-5745-2018

Wilson, S., Blake, C., Berges, J.A., Maggs, C.A., 2004. Environmental tolerances of free-living coralline algae (maerl): implications for European marine conservation. Biol. Conserv. 120, 279–289. https://doi.org/10.1016/J.BIOCON.2004.03.001

CHAPTER IV

SUMMARY

4.1 Overall objective of the study

Rhodolith beds are globally distributed benthic ecosystems that house a large diversity of flora and fauna (Foster, 2001). Yet, few studies examine carbonate production of these beds, with no studies comparing methods used to do so. As well, it is thought that hydrodynamic forces and sedimentation delineate upper and lower bed limits, respectively. However, few studies examine slope influence on rhodolith abundance, or the interaction of several factors that together determine distribution and abundance of rhodoliths.

The present study estimated $CaCO_3$ production in the presence and absence of bioturbators, as well as factors driving rhodolith abundance in southeastern Newfoundland. Specifically, (1) net and gross $CaCO_3$ production rate of *L. glaciale* was estimated in the presence and absence of bioturbators using the varying approaches of weight change and extension rate; and (2) abiotic and biotic factor influence on rhodolith abundance was determined through a drop camera survey covering areas of known rhodolith cover, and beyond. The study took place in a rhodolith bed off the coast of St. Philip's, Newfoundland.

4.2 Significance of the study

Chapter II demonstrated that carbonate production of a Newfoundland rhodolith bed was similar to other beds occurring from cold-temperate to polar seas (Bosence and Wilson, 2003; Teichert and Freiwald, 2014). Any large differences in carbonate production estimates was likely caused by the method chosen to do so. Estimating carbonate production and factors that may influence this production of a *Lithothamnion glaciale* rhodolith bed further exemplifies the importance of rhodolith bed contribution to the global carbon budget. Moreover, examining discrepancies among methodologies of estimating

carbonate production demonstrates the necessity of introducing a more universal approach. The present study is the first to directly compare weight change and extension rate methods used in calculating carbonate production, as well as the first to demonstrate the lack of bioturbator effect on rhodolith extension and carbonate production.

Chapter III demonstrated that abiotic factors, namely slope of the seafloor, water temperature and illuminance, play key roles in determining rhodolith abundance and distribution in southeastern Newfoundland. *L. glaciale* displayed the highest abundance in gently sloped areas (<7°), with moderate temperatures (6.2 to 9.8 °C) and illuminance (300 to 1500 lux). Water flow acceleration did not vary across a depth gradient, with current velocities too low to cause rhodolith movement. By challenging the importance of hydrodynamic forces and bioturbation as main drivers regulating *Lithothamnion glaciale* abundance, and introducing that of seafloor slope, the present study fuels the debate on abiotic and biotic factors influencing rhodolith bed abundance and function. The present study provides the first demonstration of slope importance in regulating rhodolith abundance, as well as examining the interaction of key abiotic and biotic drivers in determining *L. glaciale* distribution in Newfoundland rhodolith systems. This study questions previous assumptions about factors influencing rhodolith beds and introduces questions as to how drivers interact and may change on temporal and spatial scales.

4.3 Future directions

The present study provides a framework for further research into the $CaCO_3$ production of rhodoliths beds, and the environmental components that drive rhodolith distribution. Future studies should focus on predicting rhodolith bed occurrences in

Newfoundland based on the environmental conditions described here. Water flow acceleration in this study gave a good indication of conditions above the surface of the rhodolith bed, as well as beyond bed limits, however, using equipment able to distinguish between oscillatory and unidirectional flows would aid in understanding the insignificance of water flow acceleration in this study, since rhodoliths are more easily displaced under oscillatory movement. Additional factors such as seasonality, salinity, and nutrient content should also be evaluated as they may influence rhodolith abundance and distribution. Furthermore, once rhodolith presence is detected, methodology outlined in this study can be employed to determine each rhodolith bed's contribution to the global carbon budget.

Most of what we know about the distribution and stability of rhodolith beds is a 'snapshot' through time, derived from short-term research. These 'snapshots' lack continuity that could aid in managing and monitoring the stability of rhodolith beds. Research of rhodolith beds should move from short-term studies to long-term studies in order to better understand factors influencing rhodolith bed distribution and dynamics, as this work has done. The current study, while also a 'snapshot', can act as a baseline assessment of environmental conditions in which Newfoundland rhodolith beds thrive, informing future monitoring practices observing declines in rhodolith carbonate production and abundance with increasing climate change. Repeated surveys over many years within the same rhodolith system will expand our knowledge of how environmental conditions may change over time and under the influence of climate change.

Because rhodoliths are comprised of a Mg-calcite skeleton, they are at high risk of dissolution under current ocean acidification conditions and those predicted for the future (McCoy and Ragazzola, 2014). Moreover, increasing storm events derived from climate

change could cause mass destruction of rhodolith beds from high fragmentation or abrasion under high wave action conditions, as well as smothering or burial of rhodoliths from resuspended sediments (Grall and Hall-Spencer, 2003). As rhodoliths become buried and increasingly dissolve from climate change conditions, rhodoliths will no longer be able to grow and deposit calcium carbonate needed to form their complex three-dimensional skeleton. Without their complex structure, rhodoliths will not be able to support such a high biodiversity of ecologically and economically important species that use rhodolith beds to spawn and settle. Future long-term management and monitoring of vulnerable rhodolith habitats is necessary, as resilience capability of rhodolith beds under changing ocean climate conditions is limited by baseline knowledge.

4.4 LITERATURE CITED

Bosence, D., Wilson, J., 2003. Maerl growth, carbonate production rates and accumulation rates in the northeast Atlantic. Aquat. Conserv. Mar. Freshw. Ecosyst. 13, S21–S31. https://doi.org/10.1002/aqc.565

Foster, M.S., 2001. Rhodoliths: Between rocks and soft places. J. Phycol. 37, 659–667. https://doi.org/10.1046/j.1529-8817.2001.00195.x

Grall, J., Hall-Spencer, J.M., 2003. Problems facing maerl conservation in Brittany. Aquat. Conserv. Mar. Freshw. Ecosyst. 13, S55–S64. https://doi.org/10.1002/aqc.568

McCoy, S.J., Ragazzola, F., 2014. Skeletal trade-offs in coralline algae in response to ocean acidification. Nat. Clim. Chang. 4(8), 719-723. https://doi.org/10.1038/NCLIMATE2273

Teichert, S., Freiwald, A., 2014. Polar coralline algal $CaCO_3$-production rates correspond to intensity and duration of the solar radiation. Biogeosciences 11, 833–842. https://doi.org/10.5194/bg-11-833-2014

APPENDIX A

Experiment Timeline

Figure A.1 Timeline from collection of rhodoliths to the end of the calcium carbonate production experiment (Chapter II) in the rhodolith bed studied (off the coast of St. Philip's, Newfoundland) and final rhodolith weighing (see 2.2 for details of experiment).

APPENDIX B

Determination of lux to PAR conversion factor

The following procedure was applied to convert the illuminance values (in lux) of sunlight recorded in the field experiment to irradiance (PAR) values (in µmol photons m^{-2} s^{-1}). Illuminance and irradiance were recorded simultaneously for 15 min at a depth of 15 m on a partly cloudy day, with low winds in April and August, when phytoplankton density was respectively high (during spring bloom) and low (after spring bloom) (Parrish et al., 2005). Illuminance was recorded once per second with the same model of temperature and light logger (HOBO Pendant; Onset Computer Corporation) used in field experiment. Irradiance was recorded 240 times min^{-1} with a quantum sensor (LI-192; LI-COR). Both instruments were mounted next to each another on a metal frame placed on the surface of the rhodolith bed with the light sensor of each instrument pointing towards the sea surface. One conversion factor was calculated for each sampling day by averaging illuminance and irradiance data for each of the 15 min that each trial lasted, and then by dividing each mean illuminance by corresponding mean irradiance. Means of the resulting 15 conversion factors (one per minute for each day) were averaged, yielding one overall conversion factor of 23.5 (Table B.1).

Table B.1 Mean (±SD) illuminance to PAR conversion factors (in lux/µmol photons m^{-2} s^{-1}) at a depth of 15 m on a partly cloudy day with low winds in both April and August, when phytoplankton density was respectively high and low (n=15 for each factor per day, and 30 for the overall factor pooled across days). *Overall factor used to convert sunlight illuminance values to PAR values during field deployment.

Sampling day	Conversion factor
1 (April)	25.0 (0.1)
2 (August)	21.9 (0.5)
Days pooled	*23.5 (1.6)

APPENDIX C

Regression analysis of flow acceleration and current velocity

Flow acceleration variance of the centre URSKI logger from 9 March to 7 April 2018 was extracted to match the timestamp of ADCP current velocities (as in Figurski et al., 2011). To determine if current velocity could be predicted based on flow acceleration, a regression analysis was conducted. Standard deviation of daily flow acceleration resultant vector was used against daily average ADCP current velocity to perform the regression. Standard deviation was used in order to highlight differences in URSKI accelerometer locations, as was recommended by Figurski et al. (2011) and Evans and Abdo (2010). If the overall relationship was significant (high r^2, and $p<0.05$), then the equation of the regression line would be used to estimate the current velocity for all collected URSKI data across depth and lateral gradients. If regression was not significant, current velocity could not be determined for URSKI logger data, and only flow acceleration could be used for relative differences in hydrodynamic forces across depth and lateral gradients.

Mean hourly current velocity from the ADCP at depth and time matching the URSKI deployment in the centre of the St. Philip's rhodolith bed, ranged from -0.092 m s^{-1} east velocity on 2 March to 0.056 m s^{-1} north velocity on 05 April 2018 (Figure C.1). Mean daily current velocity and the mean daily vector standard deviation of flow acceleration from the centre URSKI were weakly negatively correlated (r=0.37) (Figure C.1), and the regression analysis was not highly significant, implying a weak predictive power (p=0.04; Table C.1). This suggests that the equation of the line of the regression analysis should not be used in order to infer current velocity of all URSKI loggers at all deployments. Furthermore, current velocity and flow acceleration in the centre of rhodolith

bed did not align in time; peaks of high current velocity did not match in time with those seen in flow acceleration (Figure C.1). This suggests that URSKIs recorded wave-driven oscillatory motion rather than unidirectional currents as measured by the ADCP.

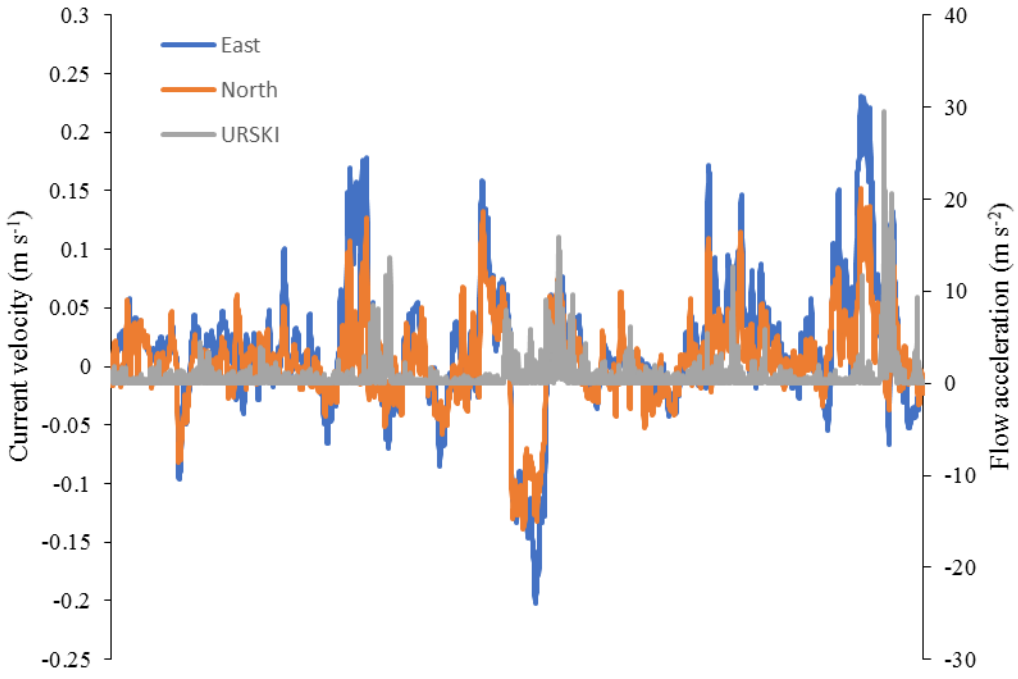

Figure C.1 Mean hourly current velocity (m s^{-1}) in the east (blue) and north (orange) direction recorded from ADCP at approximately 15m depth (left axis), and flow acceleration (m s^{-2}; right axis, grey) in the centre of the St. Philip's rhodolith bed. Current velocities were extracted at a depth of 1.5m from the seabed to match height of URSKI accelerometer loggers. Velocities from 09 March to 07 April, 2018.

Table C.1 Summary of regression analysis, testing if mean daily current velocity (m s^{-1}, from ADCP) can be predicted by the standard deviation of the mean daily resultant vector (data from URSKI flow accelerometer loggers). $R^2 = 0.1395$. N = 29, α=5%.

Source	df	SS	MS	F	p-value
Regression	1	0.0016	0.0016	4.634	**0.041**
Residual	27	0.0093	0.0003		

APPENDIX D

Temperature, depth, and rhodolith abundance profiles

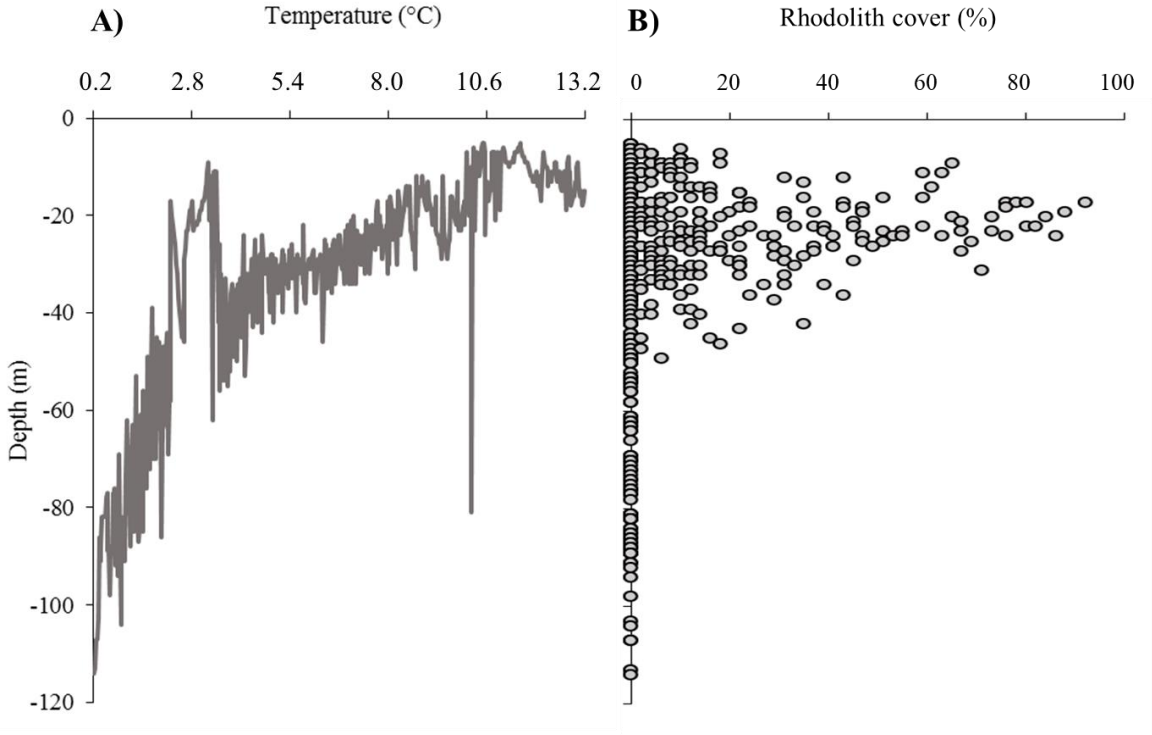

Figure D.1 Temperature (**A**) and rhodolith abundance (**B**) profiles of all 497 sample stations off the coast of St. Philip's according to depth.